# MODEL STUDY OF C-5A LANDINGS ON AM2 LANDING MAT

Fred W. Kiefer, et al

Utah State University

Prepared for:

Air Force Weapons Laboratory

August 1973

AFWL-TR-
72-210



# MODEL STUDY OF C-5A LANDINGS ON AM2 LANDING MAT

Fred W. Kiefer
Paul T. Blotter
Vance T. Christiansen

Utah State University

TECHNICAL REPORT NO. AFWL-TR-72-210

August 1973



AIR FORCE WEAPONS LABORATORY
Air Force Systems Command
Kirtland Air Force Base
New Mexico

Reproduced by
NATIONAL TECHNICAL
INFORMATION SERVICE
U S Department of Commerce
Springfield VA 22151

AIR FORCE WEAPONS LABORATORY
Air Force Systems Command
Kirtland Air Force Base
New Mexico 87117

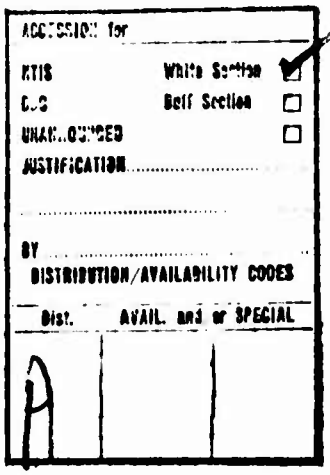

UNCLASSIFIED
Security Classification

AD-767231

## DOCUMENT CONTROL DATA - R & D

*(Security classification of title, body of abstract and indexing annotation must be entered when the overall report is classified)*

| | |
|---|---|
| 1 ORIGINATING ACTIVITY (Corporate author)<br>Utah State University<br>Logan, Utah 84321 | 2a. REPORT SECURITY CLASSIFICATION<br>Unclassified<br>2b. GROUP |

3 REPORT TITLE

MODEL STUDY OF C-5A LANDINGS ON AM2 LANDING MAT

4 DESCRIPTIVE NOTES (Type of report and inclusive dates)
9 June 1971 through 1 February 1973

5 AUTHOR(S) (First name, middle initial, last name)

Fred W. Kiefer, Paul T. Blotter, Vance T. Christiansen

| | | |
|---|---|---|
| 6 REPORT DATE<br>August 1973 | 7a. TOTAL NO. OF PAGES<br>~~136~~ 133 | 7b. NO. OF REFS<br>5 |
| 8a. CONTRACT OR GRANT NO. F29601-71-C-0129<br>b. PROJECT NO. 683M<br>c. Task 4E<br>d. | 9a. ORIGINATOR'S REPORT NUMBER(S)<br>AFWL-TR-72-210<br>9b. OTHER REPORT NO(S) (Any other numbers that may be assigned this report) | |

10. DISTRIBUTION STATEMENT

Approved for public release; distribution unlimited.

| | |
|---|---|
| 11. SUPPLEMENTARY NOTES | 12. SPONSORING MILITARY ACTIVITY<br>AFWL (DEZ)<br>Kirtland AFB, NM 87117 |

13. ABSTRACT

(Distribution Limitation Statement A)

After a buckling failure in a section of AM2 landing mat runway during a test landing of a C-5A at Dyess AFB, Texas, in August 1970, a model testing program was initiated. This report presents the results of the development and testing of an analytical model and a 1/7-scale physical model AM2 mat runway subjected to C-5A loadings. The analytical model represents the landing mat as a series of discrete rigid elements interconnected and suspended by springs and dashpots subjected to external forces simulating Coulomb friction, shear, and the action of the aircraft. Results from the computer program developed include a simulation of the Dyess failure and an evaluation of various mat modifications. The 1/7-scale physical model of the C-5A landing gear produced buckling failures in the model AM2 mat runway similar to the failure that occurred at Dyess AFB. Five runway modifications were tested: (1) restraint by pretensioned bands riveted to the mat at intervals along the runway length, (2) diagonal laying pattern, (3) increased friction on the underside of the mat, (4) cleats attached to the underside of every sixth row of mats to provide shearing-type resistance to movement, (5) three lines of mat units attached longitudinally to the top of the runway to prevent joint rotation. The use of bands and the diagonal laying pattern prevented buckling failure of the mat. Increasing the coefficient of friction made little or no improvement in mat behavior. Cleats delayed the buckling failure. The longitudinal mat stiffners did not prevent buckling failure.

DD FORM 1 NOV 68 1473

1a

UNCLASSIFIED
Security Classification

| 14. KEY WORDS | LINK A | | LINK B | | LINK C | |
|---|---|---|---|---|---|---|
| | ROLE | WT | ROLE | WT | ROLE | WT |
| Expedient surfaces | | | | | | |
| AM2 landing gear | | | | | | |
| Aircraft operations | | | | | | |
| Landing mat repair | | | | | | |
| C-5A aircraft | | | | | | |

## FOREWORD

This report was prepared by the Utah State University, Logan, Utah, under Contract F29601-71-C-0129. The research was performed under Program Element 63723F, Project 683M, Task 4E.

Inclusive dates of research were 9 June 1971 through 1 February 1973. The report was submitted 18 June 1973 by the Air Force Weapons Laboratory Project Officer, Mr. Harry R. Marien (DEZ).

The authors wish to acknowledge the efforts of Dr. R. K. Watkins for the pilot model study and other assistance during the preparation of this report. The assistance of K. Daftarian with the analytical model and M. A. Crafts and L. E. Beuer with design and operation of the physical model is also gratefully acknowledged.

This report has been reviewed and is approved.

HARRY R. MARIEN
Project Officer

OREN G. STROM
Lt Colonel, USAF
Chief, Aerospace Facilities Branch

WILLIAM B. LIDDICOET
Colonel, USAF
Chief, Civil Engineering Research Division

## ABSTRACT

After a buckling failure in a section of AM2 landing mat runway during a test landing of a C-5A at Dyess AFB, Texas, in August 1970, a model testing program was initiated. This report presents the results of the development and testing of an analytical model and a 1/7-scale physical model AM2 mat runway subjected to C-5A loadings. The analytical model represents the landing mat as a series of discrete rigid elements interconnected and suspended by springs and dashpots subjected to external forces simulating Coulomb friction, shear, and the action of the aircraft. Results from the computer program developed include a simulation of the Dyess failure and an evaluation of various mat modifications. The 1/7-scale physical model of the C-5A landing gear produced buckling failures in the model AM2 mat runway similar to the failure that occurred at Dyess AFB. Five runway modifications were tested: (1) restraint by pretensioned bands riveted to the mat at intervals along the runway length, (2) diagonal laying pattern, (3) increased friction on the underside of the mat, (4) cleats attached to the underside of every sixth row of mats to provide shearing-type resistance to movement, (5) three lines of mat units attached longitudinally to the top of the runway to prevent joint rotation. The use of bands and the diagonal laying pattern prevented buckling failure of the mat. Increasing the coefficient of friction made little or no improvement in mat behavior. Cleats delayed the buckling failure. The longitudinal mat stiffeners did not prevent buckling failure.

(Distribution Limitation Statement A)

TABLE OF CONTENTS

TABLE OF CONTENTS (CONTINUED)

TABLE OF CONTENTS (CONTINUED)

LIST OF FIGURES

LIST OF FIGURES (CONTINUED)

LIST OF FIGURES (CONTINUED)

LIST OF TABLES

# SECTION I

# INTRODUCTION

## 1.1 Comments on the Dyess Tests

One acceptance test of the C-5A aircraft requires the successful landing on AM2 landing mat. This test was performed at Dyess Air Force Base near Abilene, Texas, in August, 1970. During the Dyess test the C-5A landed four times. After the aircraft came to rest following one of the earlier landings, a vertical bow wave or buckle was observed in front of the main landing gears; that is, the mats in front of the landing gears were humped up an estimated 4 in. (Ref. 4). Also a serious in-plane bowing of the mat had been caused by the braking aircraft (5 to 7.5 in.). On the fourth landing two areas of landing mat were destroyed, with considerable damage to the aircraft. The failure was unexpected because the C-5A has a greater flotation capability than the C-141, and C-141 landings had caused no apparent problem. Testing was stopped and a model study was initiated as an expedient and economical means of answering certain questions concerning landing mat behavior (Ref. 3).

## 1.2 Objectives of the Model Study

The objectives of the study were to develop both analytical and physical models which could be used to duplicate the conditions of the Dyess failure and to evaluate the effectiveness of various mat alterations in preventing failure of the AM2 mat runways with C-5A landings. The analytical results were to be correlated with the physical model results

and used to evaluate mat response for conditions beyond the limitations of the physical model.

## 1.3 Work Performed

(1) Existing literature pertaining to the response of AM2 mat and aircraft landing characteristics was reviewed.

(2) A pilot model was constructed and tested prior to construction of a more detailed model. The initial similitude conditions were based upon equating the modulus of material stiffness of the model and the prototype. This resulted in a relatively heavy model weighing $1/n^2$ the prototype weight, where n is the linear scale factor. Also, this model required high material stresses, high tire pressures, and soil density 1/n that of the prototype. Because these conditions were difficult to achieve, an alternative similitude criteria was adopted for the detailed physical model described in Section IV.

(3) An analytical model was developed and programmed for a digital computer to permit simulation of mat behavior under various mat conditions and loadings. The model relates the overall mat response to several conditions and loadings, such as joint modifications, changes in friction coefficients, surface irregularities, mat geometry, aircraft deceleration rates, and horizontal thrust.

(4) A detailed 1/7-scale physical model of the AM2 landing mat and the C-5A landing gear was constructed and tested. The similitude condition adopted was based upon equating material densities of the model and prototype. This criteria leads to a weight ratio of $1/n^3$ and thus a lighter model. Material stresses and tire pressure are 1/n those of the

prototype. Because it was possible to meet these criteria reasonably well, a reliable model was obtained.

(5) Five modifications of the model landing mat were tested and evaluated as follows: (a) restraint by pretensioned bands riveted to the mat at intervals along the runway length, (b) diagonal laying pattern, (c) increased coefficient of friction on the underside of the mat, (d) every sixth row of a landing field was cleated across the full width of a field with 3/4-in. cleats to provide shearing resistance between mat and subgrade, (e) three longitudinal lines of mat units were riveted to the top surface of a landing field to provide moment resistance across mat joints.

## 1.4 Summary of Results

Testing of the model AM2 landing mat included 79 landings. Two failures similar to the Dyess failure were produced under controlled conditions. Each buckling failure occurred about 3/4 the way down the 120-ft runway as the model moved a few feet into a section of mats that had been tightly compressed together by previous landings.

Pretensioned bands stretched the length of the runway and fastened at intervals to the mat runway proved an effective means of preventing mat movement and buckling failure.

A mat runway placed in a 45-degree pattern was not susceptible to buckling. However, a small forward displacement occurs with every landing. Sliding along the 45-degree joint was also a problem.

Increasing friction on the underside of the mat was not effective in preventing a buckling failure.

Cleats under the runway did not prevent movement and buckling. The cleats bent under the weight of the aircraft as the mat units tipped in two-panel waves, and the subgrade deformed slightly near the cleats allowing some sliding movement.

The longitudinal stiffeners were not effective in preventing failure. With continued longitudinal movement a region of compressed mat developed and a buckling failure occurred on the fourth test landing.

## SECTION II

## DEVELOPMENT OF THE PHYSICAL MODEL

Before designing the physical model, a pilot model was constructed to minimize problems with similitude, construction and operation of a small-scale model. Details of the pilot study are reported as Appendix B. The general conclusion was that a small-scale model study was feasible.

Following the pilot model study, a more carefully analyzed scale model of the C-5A landing gear and the AM2 landing mat was constructed and tested.

### 2.1 Dimensional Analysis

The more important variables influencing mat behavior are listed in Table 2.1.

These 11 fundamental variables can be reduced to 8 pi-terms (or dimensionless parameters). A useful set of pi-terms are included in the following functional relationship:

$$(\psi) = \text{function}\left(\frac{W}{\rho g \lambda^3}\right), \left(\frac{a}{g}\right), \left(\frac{\rho g \lambda}{E}\right), \left(\frac{v^2}{g\lambda}\right), \left(\frac{p}{\rho g \lambda}\right), (f), (N)$$

Performance $\psi$ is the dependent term and is a function of the independent pi-terms on the right side of the equation. To establish similitude between the model and the prototype, each independent pi-term must be the same for both model and prototype. Thus, the dependent variable $\psi$ will be the same for both model and prototype, meaning that performance observed in the model can be expected in the prototype. The prediction equation is:

Table 2.1. Fundamental Variables Considered in the Physical Model.*

| Symbol | Definition | Basic Dimensions-FLT |
|---|---|---|
| $\psi$ | Performance (bow wave, failure, etc.) | - |
| W | Weight of aircraft (up to 571 Kips) | F |
| $\lambda$ | All other distances or lengths | L |
| $\rho$ | Density of materials | $FT^2L^{-4}$ |
| E | Stiffness modulus of all materials | $FL^{-2}$ |
| g | Acceleration of gravity | $LT^{-2}$ |
| a | Other acceleration | $LT^{-2}$ |
| v | All velocities | $LT^{-1}$ |
| f | All coefficients of friction | $FL^{-2}$ |
| N | Number of landings or coverages | - |
| P | Pressure—tire and soil | $FL^{-2}$ |

*Other fundamental variables undoubtedly affect the model performance but their influence is not significant. For example the strength S of all materials could easily be included. But critical performance (performance limit) occurs long before any materials fail. Critical performance is a bow wave, mat movement with each coverage, or in-plane bowing that increases with each coverage.

$\psi = (\psi)_m$—identical performance of model and prototype

Mat failure is defined as the condition where an initial mat irregularity continues to increase in height ahead of the approaching aircraft to such a height that the passing aircraft cannot restore the mat to its normal position. Instead the deflected mats are broken apart. In contrast failure has not occurred when the aircraft crosses two-panel waves of limited height pushing the mats down to a normal position without disconnecting or damaging the panels or joints.

## 2.2 Design for Similitude

For the pilot model study, similitude conditions were based upon setting the stiffness modulus ratio $E_r$ equal to unity. The resulting similitude criteria indicated several conditions that would be difficult to achieve for the model; (1) a weight ratio $W_r$ equal to $n^2$ and a heavy model (10,000 lb to model the complete C-5A landing gear), (2) equal pressures and material stress in the model and prototype requiring more costly wheels and tires, (3) model soil density $1/n^{th}$ that of the prototype. By adopting an alternate similitude criteria the above problems were avoided.

For the adopted similitude criteria, the density ratio $\rho_r$ was set equal to unity. Table 2.2 shows the scale relationships which result using $\rho_r = 1$ as a set condition, and includes scale relationships for additional variables necessary in comparing model and prototype behavior. Note in Table 2.2 that the weight ratio $W_r$ equals $n^3$ which allows a much lighter model. Elastic stiffness, pressures and stresses in the model are 1/n those of the prototype, which can be achieved easily in cases such

Table 2.2. Similitude Conditions for the Physical Model.

| | Variable and Scale Factor | | Comments |
|---|---|---|---|
| set conditions | $g_r = 1^*$ | | same gravitational field for model and prototype |
| | $\lambda_r = n$ | | linear scale ratio-geometric similarity |
| | $\rho_r = 1$ | | same material densities in model and prototype |
| resulting conditions | $W_r = n^3$ | $\left(\frac{W}{\rho g \lambda^3}\right) = \left(\frac{W}{\rho g \lambda^3}\right)_m$ | lighter weight model, model weight $1/n^3$ that of the prototype |
| | $a_r = 1$ | $\left(\frac{a}{g}\right) = \left(\frac{a}{g}\right)_m$ | accelerations the same in model and prototype |
| | $f_r = 1$ | $(f) = (f)_m$ | same coefficient of friction in model and prototype |
| | $N_r = 1$ | $(N) = (N)_m$ | same number of coverages in model and prototype |
| | $V_r = \sqrt{n}$ | $\left(\frac{V^2}{g\lambda}\right) = \left(\frac{V^2}{g\lambda}\right)_m$ | model velocities $1/\sqrt{n}$ that of prototype |
| | $E_r = n$ | $\left(\frac{\rho g \lambda}{E}\right) = \left(\frac{\rho g \lambda}{E}\right)_m$ | stiffness modulus of materials in model 1/n that of prototype |
| | $p_r = n$ | $\left(\frac{p}{\rho g \lambda}\right) = \left(\frac{p}{\rho g \lambda}\right)$ | pressure and stress in model 1/n that of prototype |
| | $t_r = \sqrt{n}$ | | time in model $1/\sqrt{n}$ that of prototype |
| | $k_r = 1$ | $FL^{-3}$ | modulus of soil reaction the same in model and prototype (plate bearing test) |
| | $I_r = n^5$ | $FLT^2$ | mass moment of inertia of model landing mat about longitudinal axis $1/n^5$ that of prototype mat |

*The subscript m refers to the model, no subscript indicates the prototype and the subscript r indicates the prototype to model ratio.

as tire pressures and spring moduli. Soil stiffness can be varied by using more compressible soil in the model. However, this was attempted only in the pilot model study. It was concluded that soil compression was not pertinent to the Dyess failure (Ref. 3).

In the construction and operation of the model the similitude conditions for the variables shown in Table 2.2 have been closely maintained. This has resulted in a reliable model and better correlation between model and prototype.

The last two similitude conditions in Table 2.2, $k_r = 1$ and $l_r = n^5$, are derived from the definitions which are expressed dimensionally as follows:

$$k = p/\lambda \quad \text{and}$$
$$I = \lambda^3 \rho \lambda^2$$

## 2.3 The Model Landing Gear

A 1/7 model scale was selected after consideration of the sizes of commercially available tires, wheels and brakes, as well as problems of modeling the AM2 mat. Either a larger or smaller model would have increased costs and added to the difficulty of constructing a useful model.

A scale model of the main landing gear and nose landing gear of the C-5A was constructed to 1/7 scale. Figure 2.1 is a photograph of the model landing gear.

The basic weight of the model was 1000 lbs which represents a prototype weight of 343,000 lbs. (From Table 2.2, $W = W_m n^3 = 1000 (7)^3 = 343{,}000$ lbs.) With the additional weight of operating gear and a

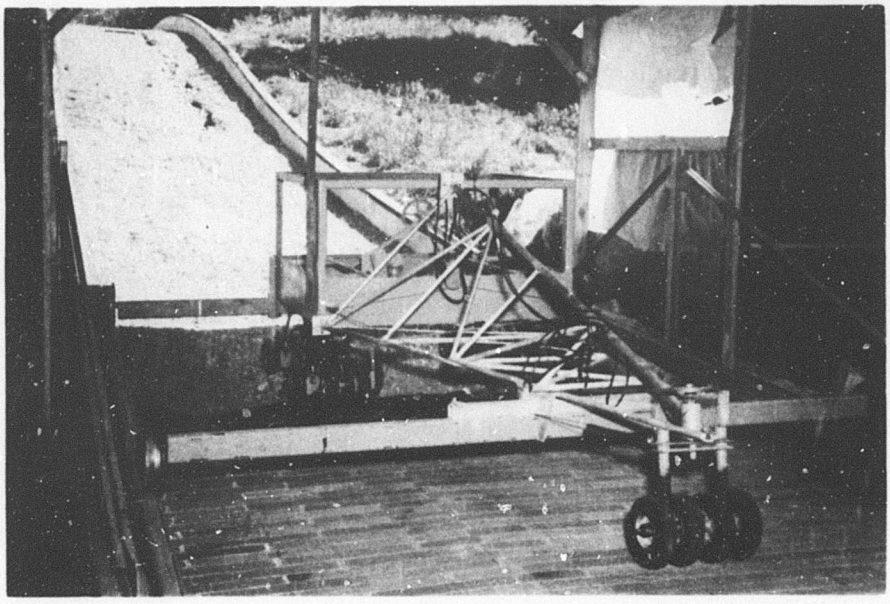

Figure 2.1. Model C-5A Landing Gear.

''pilot,'' the operating weight varied between 1220 lb (419,000 lb prototype) and 1500 lb (515,000 lb prototype). This compares with the 470,000 lb weight of the C-5A which caused the Dyess failure.

Each bogie of the main gear consists of three pairs of wheels, each pair attached to a rotating axle (see Figure 2.2 for a plan of the wheel pattern). A brake disk is welded to each axle and located between the two wheels (see Figure 2.3). A hydraulically-operated caliper-type disk brake mounted between each pair of wheels grips the upper part of the brake disk attached to the rotating axle. On the front pair of wheels the caliper disk brake is supported by a pin connector to the bogie strut. This arrangement acts as a compensator by lifting the front wheels during


Figure 2.2. Footprint of C-5A Aircraft, Model and Prototype.

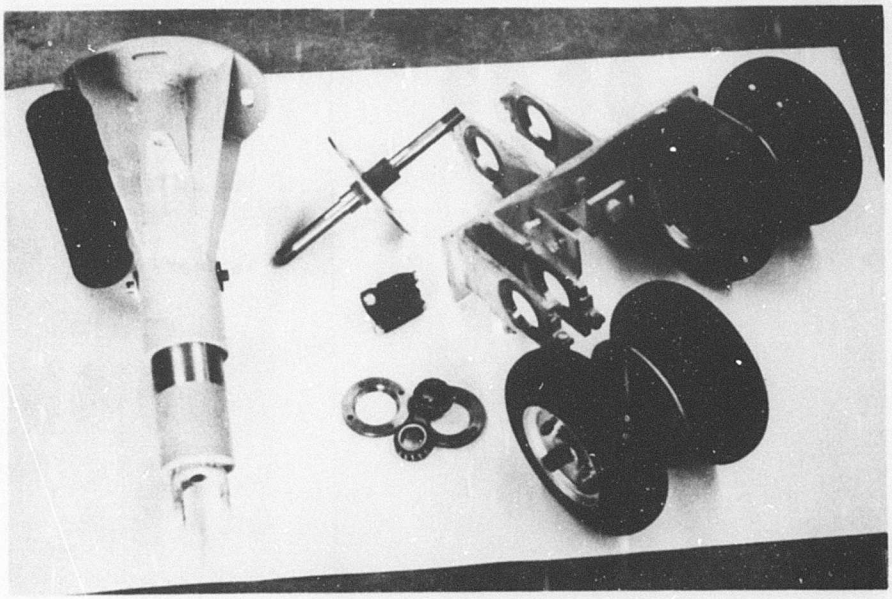

Figure 2.3. Components of Main Bogie, C-5A Model Landing Gear.

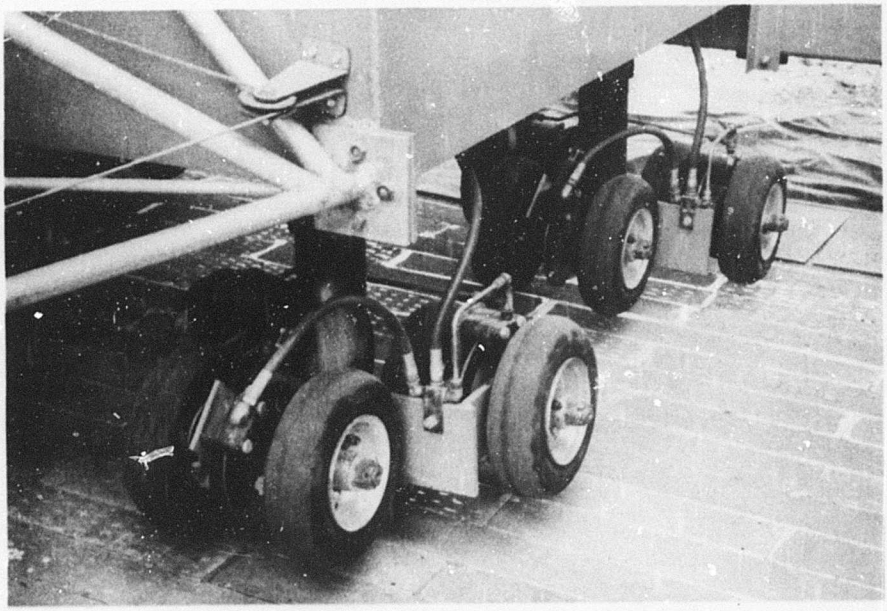

Figure 2.4. Main Bogies of C-5A Model Landing Gear.

braking to provide a more uniform weight distribution to all wheels of the bogie (see Figure 2.4).

The six wheels have 4-in. rims on which are mounted standard 2.5/2.8 x 4-in. pneumatic tires with just under an 8-in. outside diameter. The tread rubber was ground off the tires to make them more flexible and to better simulate the prototype tires. Similitude requires that the tire pressure be 1/nth that of the prototype, or based on the Dyess test 82/7 ≈ 12 psi. However, because of extra stiffness of the model tires, only 5-psi tire pressure was used to obtain correct tire contact area.

The main frame of the model landing gear is constructed of steel channels and angles. The nose landing gear is attached to a frame of aluminum tubing which is mounted on the front of the main frame. The nose gear is mounted on a rotating axis to steer the model when it is moving on the rubber tires. The main frame contains a place for an operator to sit and control the steering and braking of the model.

Also attached to the frame are two 10-ft long steel axles with steel-flanged track wheels. The landing approach was simulated by suspending the model between two steel rails using the steel wheels.

A spring suspension system in the main struts and on the nose gear simulates the suspension system of the prototype.

## 2.4 Acceleration Track

The acceleration track is a 375-ft long pair of rails. For 272 ft the track is nearly level, then it descends vertically about 20 ft through a double vertical curve (Figure 2.5). At the approach to the runway the last 17 ft of rail is cantilevered out over the model runway. The rail at this point has a slope of 3 degrees simulating the specified glide

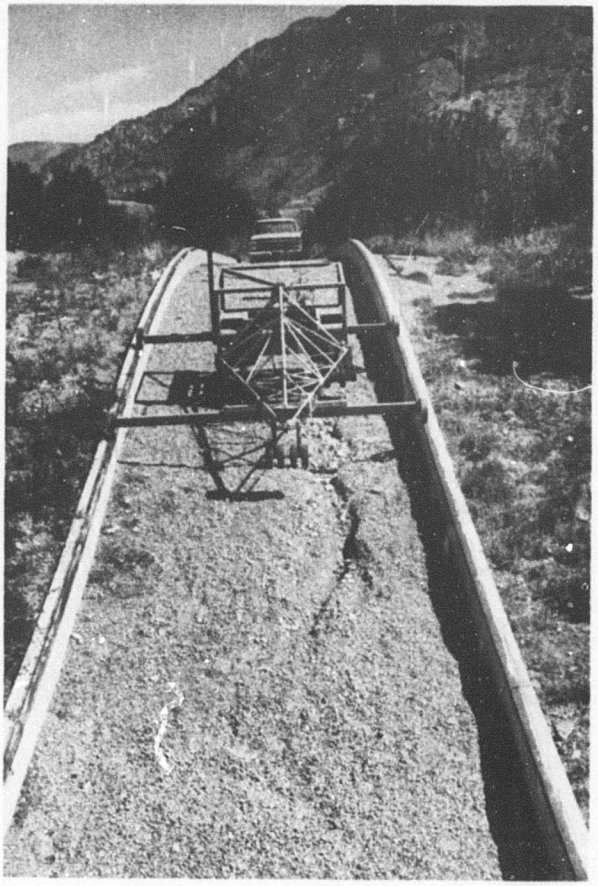

Figure 2.5. Acceleration Track.

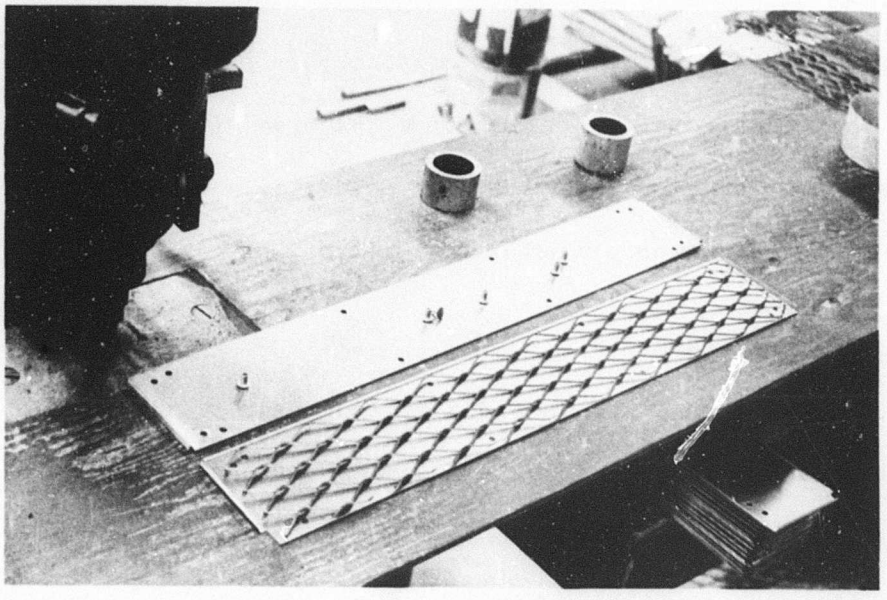

Figure 2.6. Model AM2 Landing Mat Parts Ready for Assembly.

slope of the C-5A at forward area airfields. Midway across the cantilevered rail the steel wheels leave the rail and the rubber tires come into contact with the runway surface simulating a landing.

The model attained a landing velocity of 28 ft/sec (50 mph in the prototype) by coasting down the 20-ft descent. Higher landing velocities were obtained by pushing the model with a truck. The maximum velocity attained in testing was 46 ft/sec (about 85 mph in the prototype).

## 2.5 The Model AM2 Landing Mat

The model AM2 landing mat units were constructed with an expanded metal core sandwiched between an upper and lower skin of 0.012-in. thick aluminum sheet metal (14H1100). The three parts were fastened together with eight aluminum semitubular rivets (Figure 2.6).

The assembled mat units correctly model the size and weight of the prototype. The proper stiffness in the longitudinal direction is also approximated. The longitudinal joint was designed so that when two units are connected they will separate if one unit is lifted up to an angle of 30 degrees. When rotated in the opposite direction (as in a bow wave), resistance to rotation is encountered at an angle of about 7 degrees. Thus, this action of the model mat closely resembles that of the prototype. Figure 2.7 shows the detail of the longitudinal joint.

The tensile strength of the longitudinal joint is about 12 lb/in. in the model compared with a value of 30 lb/in. scaled down from the prototype. The scaled-down value is based on a tensile strength of 1450 lb/in. joint tension test for the prototype and a scale factor of $n^2$ or 49. Strength of materials can be neglected in general. Joint strength

has nothing to do with initial stages of failure. However, for advanced stages of failure, overrunning of the bow wave is accompanied by tearing of the joints in tension behind the wheels. Joint stress does affect this failure somewhat.

The top surface of the mat was coated with a skid-resistant material of epoxy and fine sand providing a coefficient of friction of about 1.0. This is higher than required and permitted larger deceleration rates on the model mat than would be possible on the prototype mat.

The end joint of the model mat (Figure 2.8) resists transverse and tensile forces but has no moment resistance about an axis parallel to the joint whereas the end joint of the AM2 mat has a 2000 ft lb moment resistance about this axis (Ref. 5). However no adverse behavior was observed in the model mat as a result of this imperfection. About an axis perpendicular to the plane of the mat the end joint of the model mat does have some moment resistance as does the AM2 mat. This moment is of importance in resisting in-plane distortion (in-plane bow) of the runway.

## 2.6 The Model Runway

A runway about 120 ft long by about 14 ft wide was constructed of the model AM2 mat. This corresponds with a prototype field 97 ft wide and 840 ft long. By comparison, the test section of AM2 mat at Dyess AFB is 1200 ft long, but failure occurred 520 ft into the section. The model runway was restrained by weights at the ends to simulate additional length of runway.

The runway was prepared by subexcavating and then backfilling with 12 in. of blow sand. The moist sand was rolled lightly to provide a

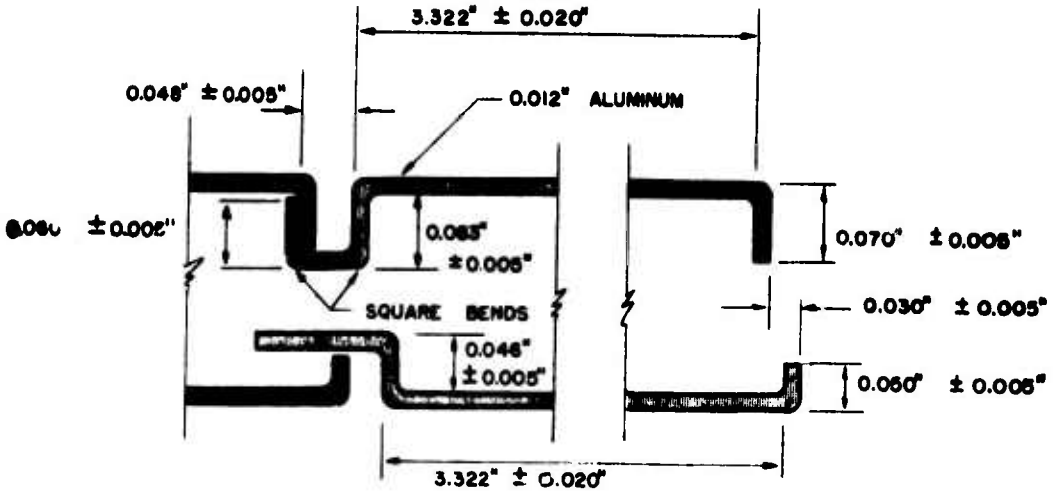


Figure 2.7. Longitudinal Joint Detail of Model AM2 Landing Mat.

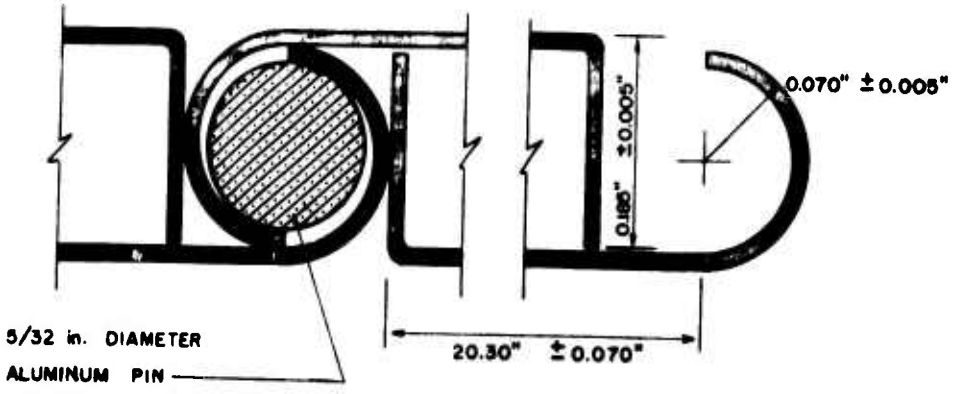


Figure 2.8. End Joint Detail of Model AM2 Landing Mat.

firm surface but was not compacted. The sand was, therefore, in a loose condition and tended to remain moist with the protection of the vinyl membrane. Static deflection tests with wheel loads of a 1440-lb model (495,000-lb prototype) averaged 0.050 in. The field was crowned at the center as was the Dyess airfield with a slope of 2½% down from the centerline to each side. A sheet of polyvinylchloride was spread over the sand to simulate the herculite membrane at Dyess and the landing mats were laid upon this.

The model runway was initially laid in the Dyess AFB pattern which had a 1-ft staggered centerline joint (Ref. 3). The offset in the model was 1/7 ft. Figure 2.9 shows the model runway.

The model mats were assembled by sliding the longitudinal joints together and inserting a 5/32-in. diameter aluminum pin at the edge joint (Figures 2.10, 2.11). When assembled, the longitudinal joints (transverse to the length of the runway) tended to be open.

The coefficient of friction between the bottom of the mat and the vinyl membrane was 0.5 as was reported for the prototype (Ref. 1). During the second series of tests, the mats were assembled in a diagonal pattern. The underside of the mat was coated with the skid-resistant surface for three other mat modification tests described in Section V.

## 2.7 Model Operation and Measurements

Measurements taken were of two kinds, those showing the behavior of the model aircraft and those showing the response of model landing field to forces imposed on it.

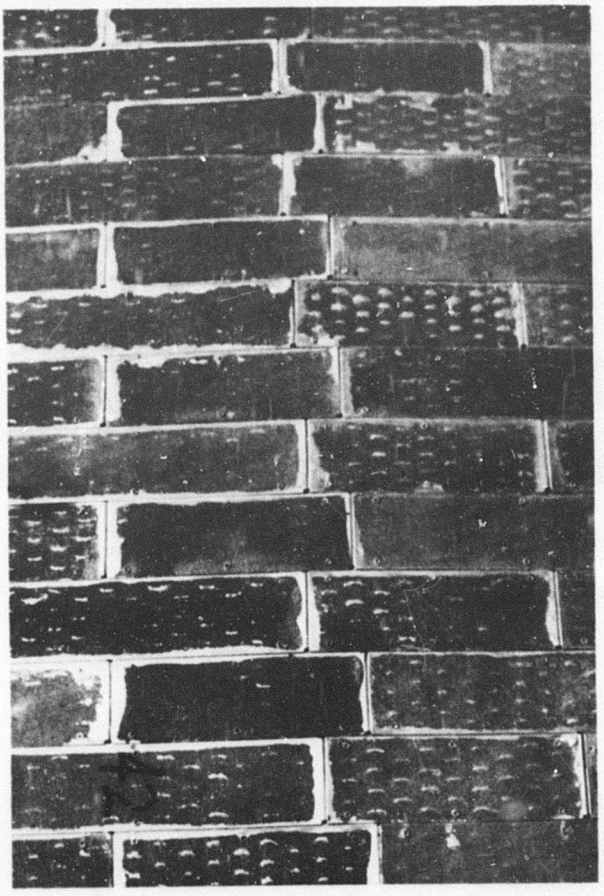

Figure 2.9. Centerline Joint of Assembled Model AM2 Mat Runway.

### 2.7.1 Operation of the Model Aircraft

The velocity and deceleration rate of the aircraft model were measured by using a series of switches which were tripped as the model passed. As each switch was opened, voltage was added to a circuit connected with a recorder. The velocity and acceleration were determined using the known position of switches and the voltage-time record obtained during the landing.

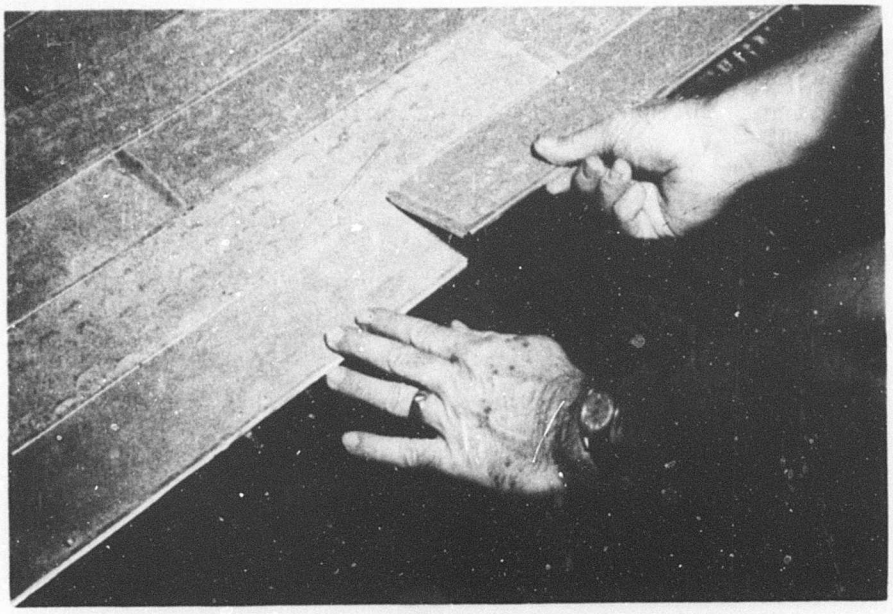

Figure 2.10. Assembly of Model AM2 Runway.

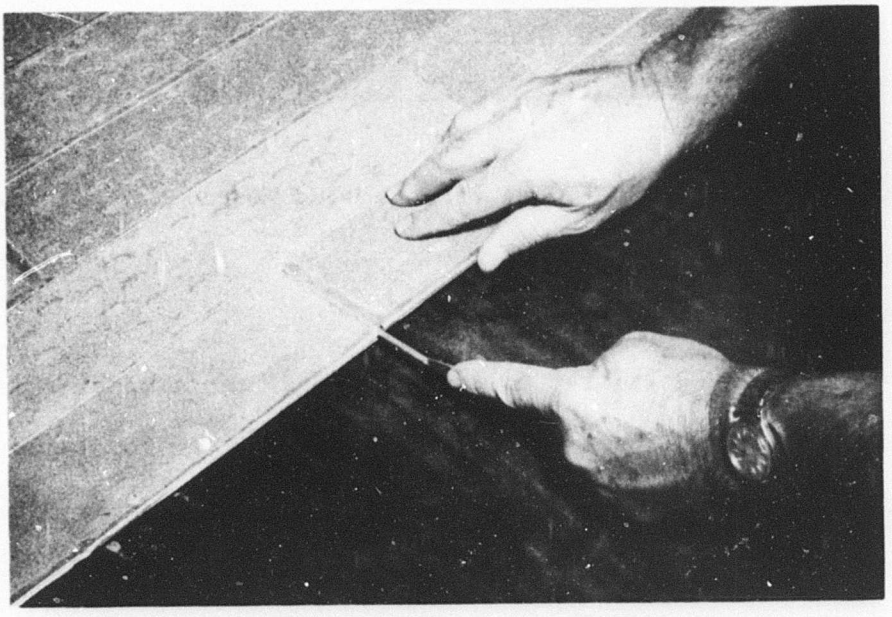

Figure 2.11. Inserting Pin in the Mat End Joint.

For many test landings the model was accelerated by allowing it to coast down the inclined track. The maximum velocity attained in this way was approximately 20 mph. Landing velocities up to 43 mph were reached in some tests by pushing the model with a truck. These velocities are equivalent to 53 mph and 84 mph in the prototype.

The deceleration rate of the model without applying the brakes varied from 4 ft/sec$^2$ to 6 ft/sec$^2$ as the temperature ranged from 50 degrees to 90 degrees Fahrenheit. This variation in deceleration is due to the normal drag of the wheel bearings. By applying the brakes, deceleration rates up to 17 ft/sec$^2$ (and in one extreme case 30 ft/sec$^2$) were achieved. For a few landings the braking was controlled by an air-activated piston. However for most landings the brake was applied directly by the ''pilot'' immediately after touchdown. The model was brought to rest with near-constant deceleration rates. Figure 2.12 shows the model during a landing.

For similitude, acceleration in the model must be the same as in the prototype. Records indicated a deceleration of about 10 ft/sec$^2$ for the C-5A at the Dyess failure (Ref. 3).

After the model was brought to a stop and the mat movement was determined, the model was pushed back to the end of the acceleration track and towed back up the ramp ready for another landing. Plywood panels were laid over the runway as a protective cover as the model was moved back over the mat runway. In this way mat movement was allowed to accumulate with additional landings. When the model was moved back over the mat without the use of the plywood cover, restoring movements occurred.

At the point of touchdown the mat sections tended to pull apart in tension failure. To prevent this, plywood panels were used to protect

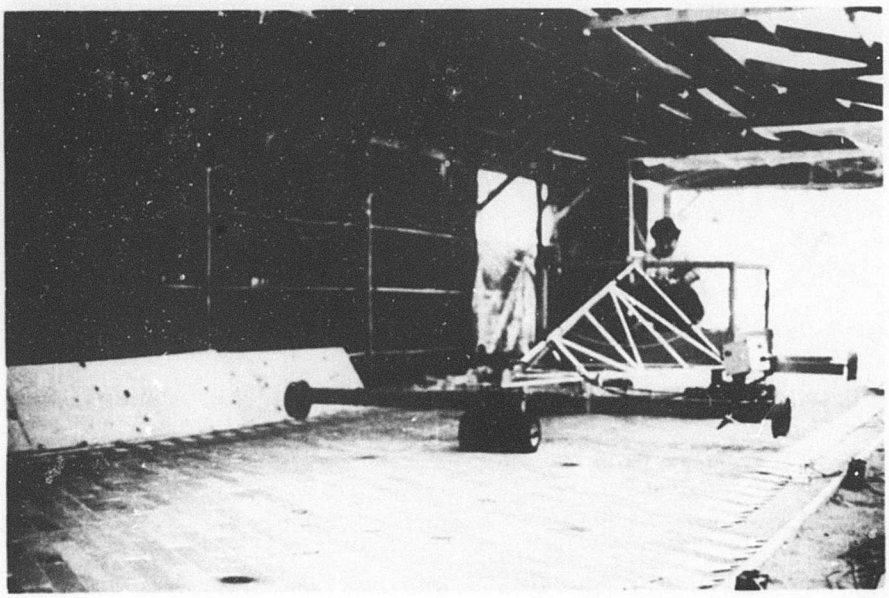

Figure 2.12. Model Landing Gear During a Test Landing.

the mat. The force on the mat at touchdown was high because of the stiff wheel bearings in the model. This is analogous to landing the prototype C-5A with partial braking at touchdown.

### 2.7.2 Measurement of Mat Movement

Mat movement is a critical indicator of overall behavior of the mat runway, therefore it was important to monitor the movement carefully. Two grid systems were used for reference. The first system, a series of stations located at 10-ft intervals along the edge of the runway, was used to determine absolute movement of the mat.

The second system consisted of four lines of gage points punched into the mat surface along the length of the runway at 33.5-in. intervals

(10 mat widths). One line was located 12 in. from each edge, a third line near the centerline and a fourth line 36 in. to the left of centerline and roughly in line with the path traversed by the left bogie of the model landing gear. The positions of these points established on the mat runway were recorded before and after each landing or series of landings. In the case of the diagonal mat pattern, four fixed longitudinal reference lines were also established to monitor movement of the mat in the transverse direction.

Relative movement between mat sections was monitored by measuring the change in distance between the gage points established along the mat sections. The purpose of the gage-point measurements was to record the opening or closing of the gap or spacing between adjacent mat sections. The mat sections were designed to have 0.036-in. movement in the longitudinal joint, which is 1/7 of the 0.25-in. movement of the prototype AM2 mat. Because of joint irregularities and presence of dirt or grit in the joints the actual movement was generally much less than 0.030 in. per joint. These gage measurements helped identify zones of compression or tension in the mat runway.

Electrolytic transducers located at 10-ft intervals for 60 ft to 70 ft down the left edge of the runway were used to measure the dynamic movement of the mat runway. The transducers were connected to an eight-track chart recorder on which movement was plotted against time on a chart moving at a rate of 10 cm per second. The position of the model landing gear moving down the runway was also recorded on the same chart. Figure 2.13 shows, as an example, the record made for test landing number 4. Data taken from Figure 2.13 was used to plot Figures 2.14 and 2.15.

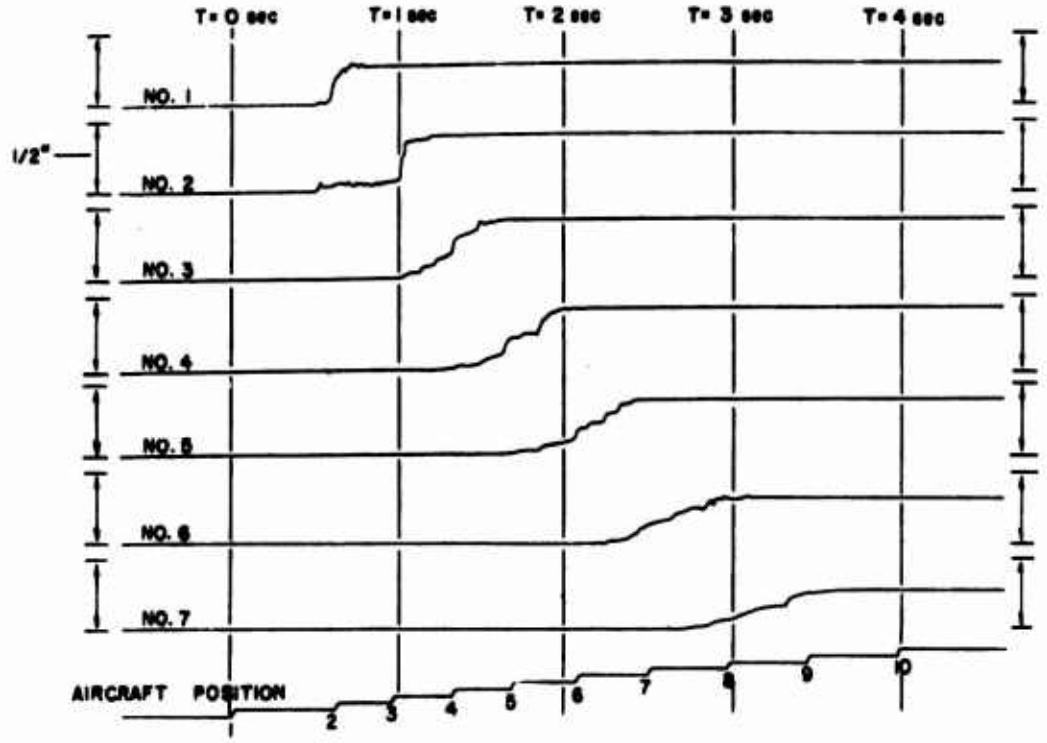


Figure 2.13. A Typical Record of Mat Displacement and Model Position Landing No. 4.

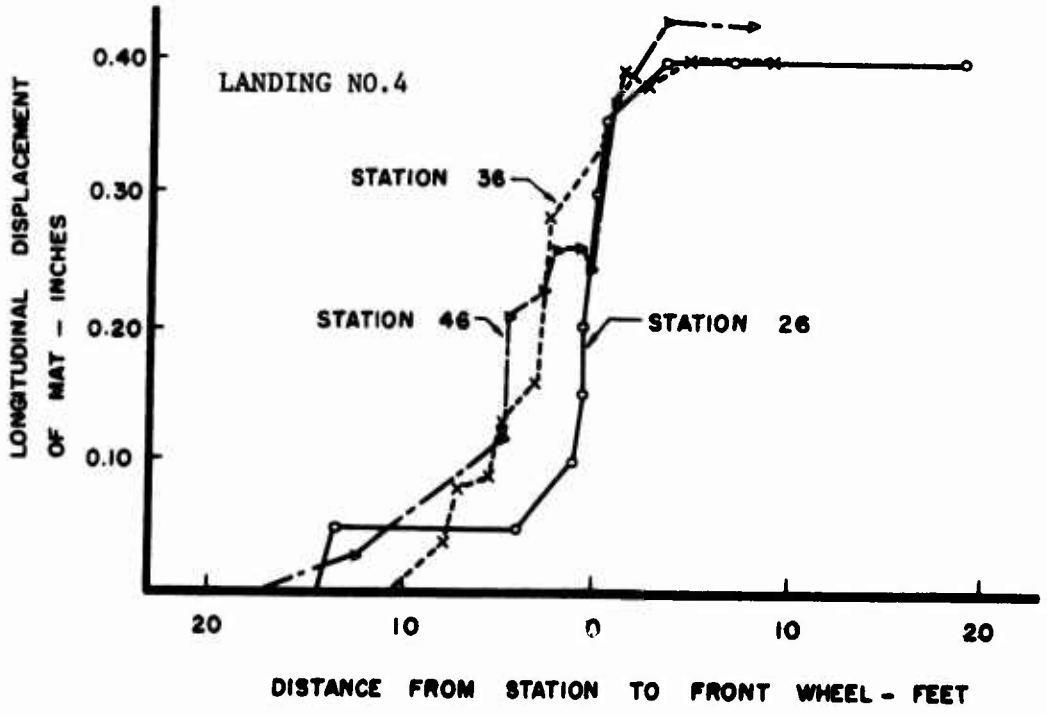


Figure 2.14. Displacement of Mat Versus Distance from Front Wheel of Main Bogie.

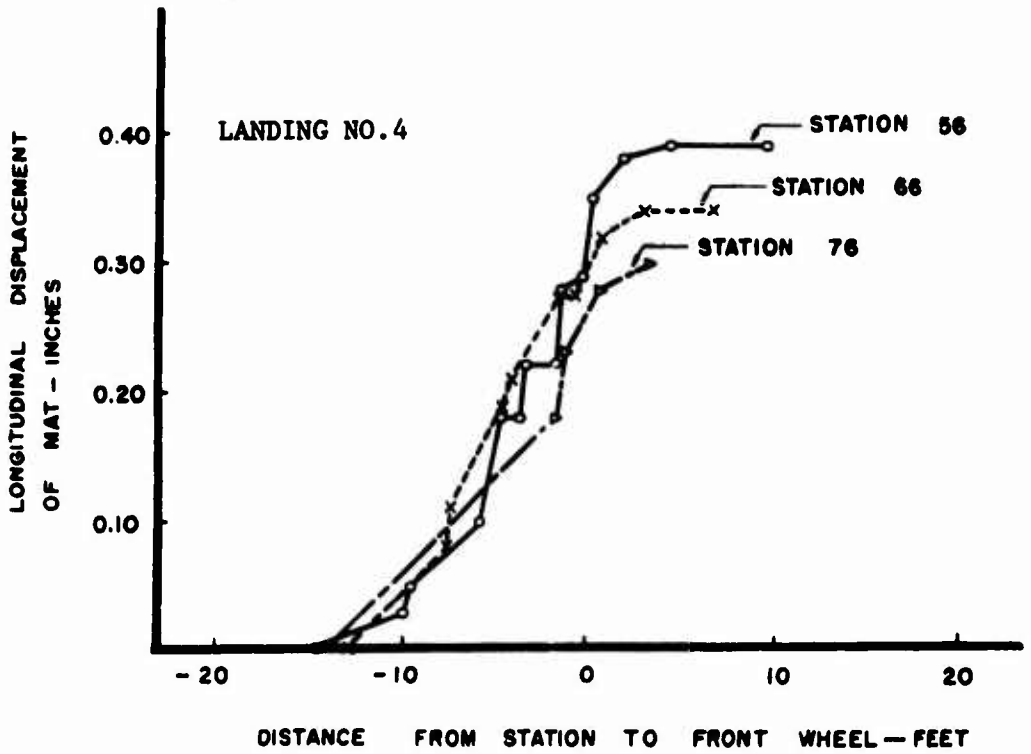


Figure 2.15. Displacement of Landing Mat Versus the Distance to the Front Wheel of the Main Bogie.

These show that the movement of the mat relative to the main bogie of the model landing gear began about 15 ft ahead of the main bogie, continued to increase as the bogie approached the point of measurement, and practically ceased as the model passed the station.

### 2.7.3 Film Records

Perhaps the best record of dynamic mat behavior was photographic. Sixteen-millimeter cameras, operating at 64 to 200 frames per second, were mounted on the model landing gear and focused on the mat area just ahead of the forward main bogies. During some test landings cameras were stationed along the edge of the runway. Mat behavior, including buckling action, was observable from the films taken. Photographs taken from these films are included in the discussions of mat behavior in Section IV.

### 2.7.4 Strain Gage Measurements

Pretensioned steel bands were riveted to the mat as one modification tested. Details are given in Section V. Strain gages were attached at several points along 120-ft long steel bands to measure the dynamic forces in the bands as the model aircraft moved down the runway. The signals obtained from the strain gages as the model aircraft moved down the runway were recorded on an eight-track chart recorder.

# SECTION III

# DEVELOPMENT OF THE ANALYTICAL MODEL

## 3.1 Model Description

### 3.1.1 Basic Assumptions

The analytical model consists of discrete rigid elements interconnected and suspended by springs and dashpots. External forcing functions are applied to the mat elements to simulate velocity independent forces, such as Coulomb friction and the action of the aircraft. Only mat influenced by the aircraft wheels is of primary importance; therefore, simplifying assumptions account for effects of mat outside this area of influence, but avoid the cumbersome equations that would result if all mat elements were considered, with each having six degrees of freedom. If each mat were considered to be an element in the model and no holonomic constraints were assumed, then in a general sense, 6N nonlinear second order differential equations (where there are N mats) would govern the motion of the system. Because the numerical methods reduce the second order differential equation to two first order equations, a system of 12N nonlinear equations would need to be solved. For example, a system of AM2 runway 8 mats wide and 100 mats long would require the solution of 9600 equations. As a matter of practicality, a limited number of mats, holonomic constraint equations and other engineering assumptions were used to develop a usable model. This simplification of the model was justified by observation of the experimental models and analysis of prior research as well as by engineering judgment.

In Figure 3.1, a typical arrangement of mat elements and the location of the aircraft wheels are shown at some arbitrary time during the landing. Section A-A is removed from the complete landing strip and includes the mass elements of the model. The number of mats behind or in front of the aircraft is arbitrary. An elevation view is shown in Figure 3.2.

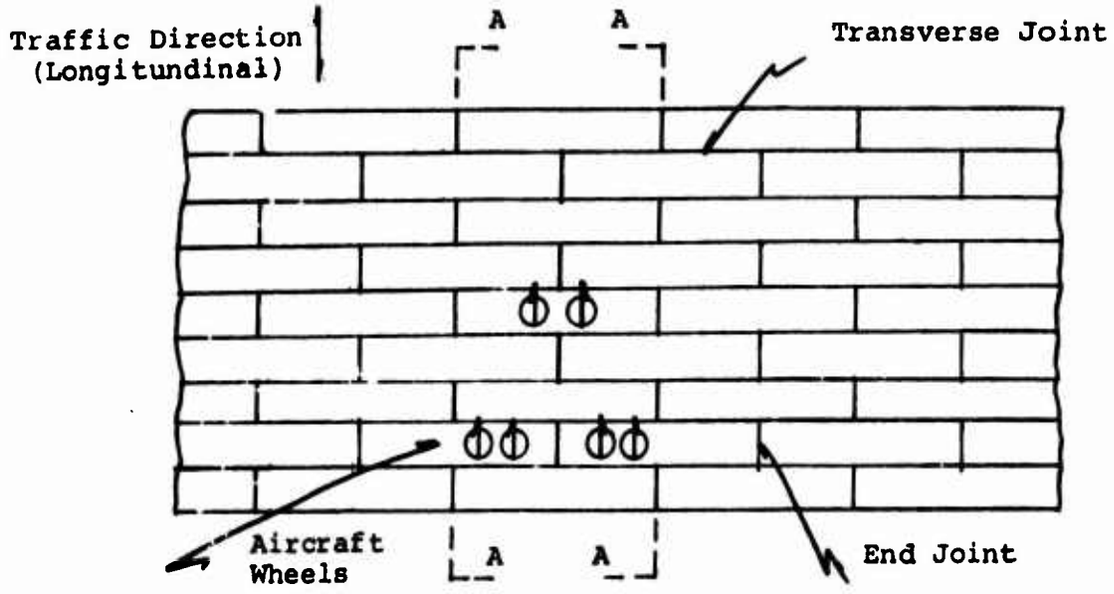


Figure 3.1. Typical Arrangement of Mat Elements in the Landing Strip.

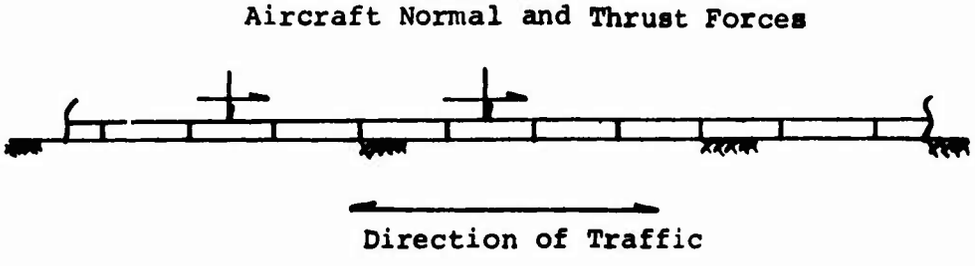


Figure 3.2. Elevation View of Model Section.

### 3.1.2 Degrees of Freedom, Assumed Motion

The generalized coordinates necessary to describe the possible motion of each mat element in the model are shown in Figure 3.3. Six degrees of freedom are associated with each mat, 3 translational and 3 rotational. Translation is described in terms of the xyz cartesian axes of a Newtonian system and rotations about the xyz axes are designated as $\theta_x$, $\theta_y$, and $\theta_z$, respectively. The model, however, does not necessarily need to account for motion in all six directions. Translation in the x direction is necessary to describe longitudinal displacement of the mass. Translation in the z direction was assumed to be negligible. Rotation about the transverse axis, $\theta_z$, was included. Rotation about the longitudinal axis, $\theta_x$, was assumed not essential to the formation of a bow wave. Rotation about the vertical axis $\theta_y$, is somewhat questionable, but was neglected

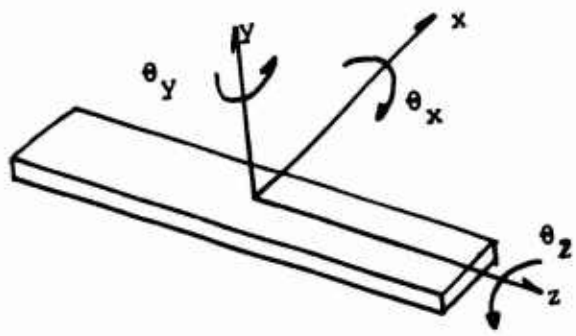


Figure 3.3. Degrees of Freedom for Each Mat Element.

in the model developed. Thus, translation in the x and y directions and rotation about the z axis, $\theta_z$, were considered to be essential.

### 3.1.3 Model Parameters

The complete theoretical model with springs, dashpots, and forcing functions is shown in Figure 3.4. Some parameters may be taken to be zero when this general model is used. The dependent variables are described as follows:

$q_1$ = vertical position of the mass center of the first mass, positive is downward (ft).

$q_n$ = horizontal position relative to the equilibrium position of the mass center of the $n^{th}$ mass, positive is to the right (ft).

$q_{n+1}$ = angular rotation with respect to the horizontal position of the $n^{th}$ mass, positive is clockwise (rad).

$Y_n$ = the vertical position of the left end of mass element n and is measured from the equilibrium position; positive is downward (ft).

The system parameters are defined as follows:

F = horizontal thrust force (lb).

Q = external vertical load (lb).

$V_n$ = vertical shear (lb). (Not shown in Figure 3.4)

f = dry friction coefficient between mat and subgrade.

CF = velocity independent forces such as Coulomb friction and shear (lb).

$KV_n$ = the equivalent elastic spring constant of the subgrade; one-half the total distributed force is concentrated at each end of the mat element. The value may vary from mat to mat (lb/ft).

$CV_n$ = viscous damping coefficient of the subgrade (lb-sec/ft).

$KL_n$ = elastic spring constant of the transverse joint at the left of the $n^{th}$ element (lb/ft).

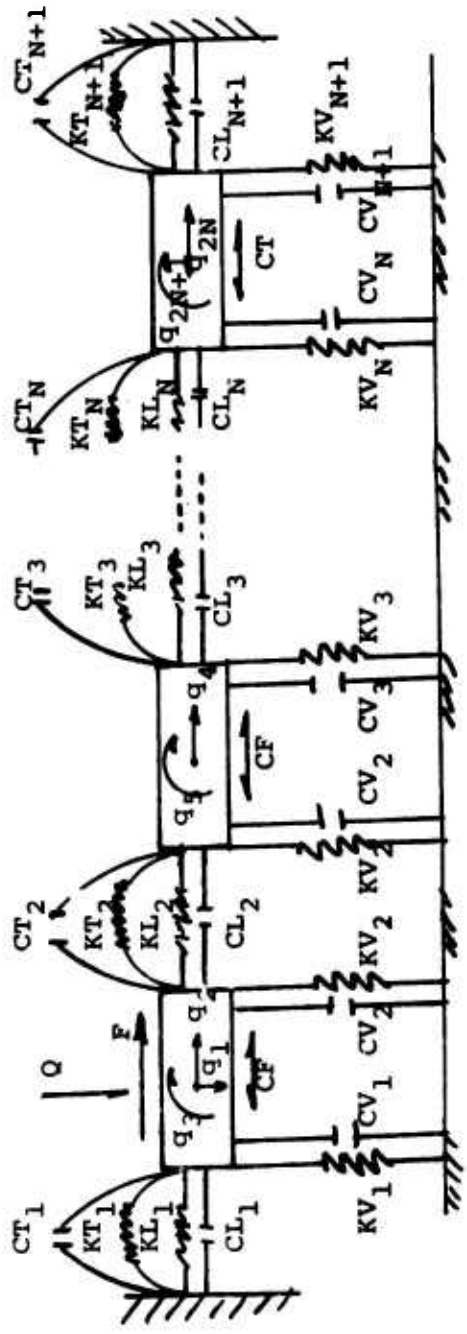


Figure 3.4 Theoretical Model of Landing Mat in the Neighborhood of the Aircraft.

$CL_n$ = viscous damping coefficient of the transverse joint at the left of the $n^{th}$ element (lb-sec/ft).

$KT_n$ = torsional spring constant of the transverse joint at the left end of the $n^{th}$ mass (ft-lb-sec/rad).

$CT_n$ = torsional damping coefficient of the transverse joint at the left of the $n^{th}$ element (ft-lb-sec/rad).

The end conditions can represent either fixed or free joints, or somewhere in between these two extremes. Consequently, open or closed joint conditions can be simulated at the first and last joints of the model.

## 3.2 Equations of Motion

The equations governing the motion of the discrete masses were derived using two different methods. The first method makes use of Newton's laws. The second method which was used to check results of the first method involves Lagrangian mechanics. Details of the development using Newtonian mechanics and an overview of the energy technique are given in Appendix A.

The equations governing the motion of the system as developed in Appendix A consider the transverse joints to be simulated by continuous springs and dashpots. In the actual mat, however, the joint is discontinuous during the transition from tension to compression and during relative rotation of adjacent mats. Attempts to model the available joint slack in passing from tension to compression or vice versa, were rather complicated and consequently avoided. Since the mat must be compressed in order for buckling to occur, it was assumed that the joints in front of the aircraft were closed. The magnitude of the initial compression in the closed joints is a variable and may consequently simulate various joint conditions.

In a compression region, longitudinal joint slack is available as a result of relative rotation of mats. Consider the extreme case where the mass centers of mat n and n + 1 are fixed as shown in Figure 3.5. Rotation of the mats will result in the end joints being displaced some distance d, even though the relative displacement of the mass centers is zero. Approximately 1/4 in. of resistance-free opening of the joint is available in the prototype. Once this gap has been exceeded, then a continuous spring and dashpot simulate the action. The theoretical model does account for this discontinuity in the early stages of bow wave formation by disregarding the bracketed terms in the equations of motion as derived in Appendix A. The later stages in the formation of a bow wave would require that the bracketed terms be included.

A second modification accounts for vertical lift or shear forces that occur at the transverse joints as a result of the horizontal thrust force, which propagates downfield and eventually lifts mat ahead of the aircraft. In order to describe the lifting mechanism, consider two mats which form an irregularity in the form of an inverted vee. Adjacent mats

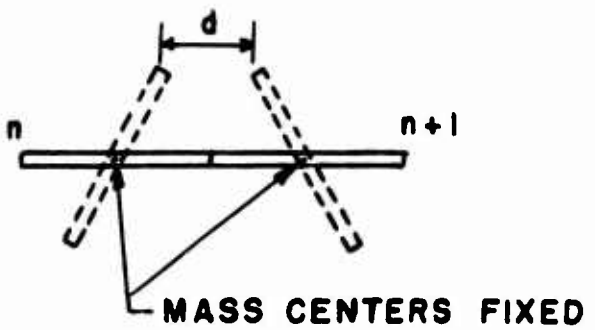


Figure 3.5. Joint Spacing Resulting from Relative Rotation.

on both sides are horizontal. The first mat is designated as n, and is rotated counterclockwise. The second mat is designated as n + 1 and is rotated clockwise to complete the vee shape. The next horizontal mat to the right of mat n + 1 is considered as mat number n + 2. When the aircraft approaches the vee shape from the left, mat n is the first subjected to horizontal joint forces which produce a counterclockwise moment. Mat n + 1 experiences a clockwise moment. Since the counterclockwise moment of mass n is greater than the clockwise moment of n + 1 the resulting angular accelerations are different. Consequently, the mat n + 1 is lifted vertically, which then lifts the left end of mat n + 2 and rotation of the mat occurs.

In the initial equilibrium position, the mat elements are supported by the subgrade and no appreciable vertical shear exists at the joints. When a mat element leaves the equilibrium position, however, the joints are subjected to a vertical force. The magnitude of the vertical force was determined by successive approximation to be approximately equal to the mat element weight and was applied only to mat elements that were subjected to the lifting mechanism described in the previous paragraph.

## 3.3 Solution of Equations of Motion

Using Newtonian mechanics, the constraint equations, and a change in variables, there result 2(2N + 1) first order differential equations, where N represents the total number of elements. Two different numerical methods, the quartic Runge-Kutta technique and Hamming's predictor-correction technique, were attempted as a means of solving the differential equations. The quartic Runge-Kutta method proved to be more efficient. An

IBM subroutine called RKGS was modified somewhat and used to solve the system of equations. The computer program listing provides a description of the general approach and includes alterations necessary to account for such things as springs and dashpots going to zero for certain values of displacement.

## 3.4 Determination of Model Parameters

In order to determine a numerical solution to the governing equations of motion, specific values or functional relationships need to be assigned to the system parameters. It is difficult to determine these values precisely; however, somewhat simple static and dynamic tests can be used to approximate parameter values. In addition to simulating an existing situation, the theoretical model is advantageous in predicting mat response under hypothetical conditions. This allows several variations in joints, subgrades, mat geometry, etc. to be evaluated rapidly and with little expense. Whether the model is used to study existing mat conditions or to predict response to mat modifications, reliable results are dependent upon proper model parameters.

The numerical values of system parameters used to simulate the landing of the C-5A on AM2 landing mat are given in Table 3.1. A brief description of the methods used to determine the less obvious results follows in the ensuing paragraphs.

The horizontal thrust force F was obtained by application of Newton's laws. The weight of the aircraft was taken as 480 kips suspended on 24 tires equally. If one assumes a deceleration of 10 ft/sec$^2$, a horizontal thrust force of approximately 6 kips is associated with each wheel.

Table 3.1. Analytical Model Parameters.

| PARAMETER | VALUE |
|---|---|
| MASS MOMENT OF INERTIA | 2 LB-FT-SEC$^2$ |
| MAT WEIGHT | 140-160 LB |
| MAT LENGTH | 12 FT |
| MAT WIDTH | 2 FT |
| TAD | 10° |
| F | 12000 LB |
| f | 0.5 |
| Q | 480,000 LB |
| KV | 1.1(10)$^6$ LB/FT |
| KL | 8(10)$^6$ LB/FT |
| KT | 1.0(10)$^5$ FT-LB/RAD |
| CT | 1.0 FT-LB-SEC/RAD |
| CL | 50.0 LB-SEC/FT |
| CV | 2.0(10)$^4$ LB-SEC/FT |

The coefficient of friction, f, between mat and subgrade was determined to be approximately 0.5 and was essentially velocity independent.

The force CF is the result of the product of the normal force and the coefficient of friction between the mat and subgrade. Shearing forces on the end joints could be included; however, observation of the physical model suggests that a complete row of transverse elements moves longitudinally when motion eventually takes place. Since the motion is somewhat uniform in front of the wheel, horizontal shear on element ends is not assumed to be critical in most cases.

The soil parameters $KV_n$ and $CV_n$ are equated to zero when the mat element leaves the ground surface. The elastic constant $KV_n$ was assumed to give slightly overdamped conditions. Although $KV_n$ and $CV_n$ may vary with each mass, the majority of tests were run with uniform soil conditions. No experimentation was conducted to determine soil parameters.

The elastic spring constant, $KL_n$, which multiplied by the relative displacement, models the horizontal force in the longitudinal direction at the joint, was determined experimentally. A 2-in. strip of AM2 mat running from the mid-point of adjacent mats and including the transverse joint was subjected to a tension test. A force versus deflection curve was plotted and $KL_n$ was found to be 9500 lb/in./in. Considering the mat to be 12 ft long, $KL_n$ for the total element was taken to be $1.6\ (10)^7$ lb/ft. This value is approximately equivalent to the same member subjected to uniaxial compression, and represents an upper limit. It was later found that $KL_n$ could best be determined by trial and error. A value of approximately $8\text{-}13(10)^7$ lb/ft better simulates the elastic action and allows for sufficient mat displacement when compared to the physical model. The viscous damping coefficient $CL_n$ multiplied by the relative velocity of adjacent mats n-1 and n accounts for dissipative forces that are velocity dependent. In addition, quantum losses of energy, such as kinetic energy lost upon impact of adjacent mats, may be converted to equivalent viscous damping terms by averaging over the period of vibration. In the case of AM2 landing mat, the friction force at the interface of the subgrade and mat was found to be velocity independent and the energy lost upon collision of the ''closed'' joints was assumed small. Consequently, the relative magnitude of the viscous damping forces was

relatively small compared to other forces.

The torsional stiffness and the torsional damping coefficient of the transverse joint are represented by $KT_n$ and $CT_n$, respectively. The product of $KT_n$ and the relative angular displacement of mats n and n-1 represent the elastic bending moment, while the product of $CT_n$ and the relative angular velocities of masses n and n-1 represent the damping moment. Both $KT_n$ and $CT_n$ are assumed zero until some relative angular displacement (referred to as TAD) is reached. This angle of free rotation (TAD) was specified as 10 degrees for AM2 mat, but could be assigned any arbitrary value. The value for $KT_n$ was $1.0(10)^5$ ft lb/rad for the 12-ft transverse joint and was obtained by applying a moment and measuring the angular deflection. The value of $KT_n$ was taken as the slope of the moment versus angular deflection curve, which was somewhat nonlinear. The value of $CT_n$ is assumed to be negligible.

The mass moment of inertia of each element about a long axis through the center of mass was found experimentally to be 2.0 $sec^2$-ft-lb. The experimental procedure involved hanging the mat element from two cords in a vertical plane. The element was then rotated and a steady state period of vibration was measured in seconds. Knowing the period, the length of the suspension cord, the weight and the horizontal distance between points of attachment of the cord to the element, the mass moment of inertia was determined.

In order to correlate results of the physical and analytical studies, the physical model parameters were determined. The mass moment of inertia of the physical model element was determined to be $1.0 \times (10)^{-4}$ ft-lb-$sec^2$/rad, whereas the prototype would scale down as $2/7^5 = 1.19 \times (10)^{-4}$

ft-lb·sec$^2$/rad. The longitudinal spring constant $KL_n$ was determined to be approximately 2.90 x $(10)^5$ lb/ft, where the tightly compressed condition in the prototype scaled down gives 1.8 x $(10)^7/7^2$ = 3.67 x $(10)^5$ lb/ft. This further suggests that the maximum $KL_n$ calculated from the prototype as 1.8 x $(10)^5$ lb/ft is an upper limit. The torsional stiffness constant for the model was calculated as 30 ft-lb/rad which is less than the scaled down stiffness from the prototype, i.e. $10^5 \div 7^4$ = 41.5 ft-lb/rad. The soil conditions and damping coefficients were not very significant in the comparison and were therefore not determined experimentally, but were simply scaled appropriately from the prototype.

## 3.5 Initial Conditions

In order to determine a solution to the equations of motion, initial displacements and velocities must be specified. In particular, the initial vertical, horizontal and rotational displacements and velocities of the first mass of the model, along with initial horizontal and rotational displacements and velocities for subsequent masses must be assigned. Since the analytical model removes an arbitrary number of elements from the complete runway, these initial conditions are somewhat difficult to evaluate. However, one can begin at touchdown and simply follow the aircraft along the mat if no other information is available. It was found that bow waves generally form where irregularities in the landing mat exist, consequently if sufficient elements were included in the model to allow the aircraft to pass over the mat before the influence propagated to the location of the irregularity, then initial conditions were approximately generated without beginning at touchdown.

Since the horizontal thrust force moves along the mat with the velocity of the aircraft, the solution was usually started sufficiently close to touchdown to allow initial relative displacements to be set equal to zero. If all the joints are closed, this implies that the compressive forces over the model elements are initially the same at each joint.

An initial mat velocity was specified at the location of the aircraft wheel on the runway. Other mat velocities were taken as zero. The value of this initial mat velocity is rather difficult to determine analytically. First approximations were 25 to 50 ft/sec. Upon later comparisons with the physical model, it was determined that the prototype mat velocity should be assumed to be approximately 2 ft/sec initially. This velocity difference is definitely significant.

The initial configuration of the landing mat is critical in regard to the formation of a bow wave. If the elements are completely flat, no standing wave is formed. However, if one mat is rotated only slightly, say 1/2 degree, a bow wave is possible under certain conditions. Since it is practically impossible to have landing mat completely flat in the field, small surface irregularities must be anticipated. The analytical model is capable of determining the dynamic results of surface non-uniformities that include one or several mats. Different initial configurations were assumed and are reported.

## 3.6 Analytical Results

The number of mat elements to include in the analytical model is primarily dependent upon the compressibility of the joints, the initial

conditions and the number of mats traversed by the moving horizontal thrust. Essentially, sufficient mats were included to allow some of the extreme elements to have zero displacement and velocity, i.e., they are outside the area of influence.

Both velocities and displacements were printed out as a function of time for each mat in the model. First attempts assumed initial mat velocities too high and both positive and negative horizontal velocities were recorded. However, initial velocities as determined from the physical model and scaled to simulate the prototype resulted in horizontal velocity changes, but negative relative velocities occurred only if insufficient mat elements were considered. Consequently, there is some flutter associated with the dynamic response, but this results from slight changes in the magnitude of velocity not the direction. The displacement is always cumulative in the positive direction. Flutter is also associated with angular kinematics, particularly when the free rotation angle is exceeded and the moment rigidity at the joint is first encountered.

In Figure 3.6, the landing of the C-5A aircraft on highly compressed mat is simulated. The compressed joint represents a maximum and the mat is essentially a rigid plate with hinged joints located every 2 ft. The parameters not identified on the figure are listed in Table 3.1, which follows also for subsequent figures. The initial irregularity in the surface involves four mats with the maximum joint height 0.0200 ft above the horizontal surface. The front two wheels of the front main bogie are initially located four joints from the first joint protruding above the horizontal surface 0.0099 ft. This does not mean that the mat irregularity is not influenced until the aircraft is located four joints ahead. Prior

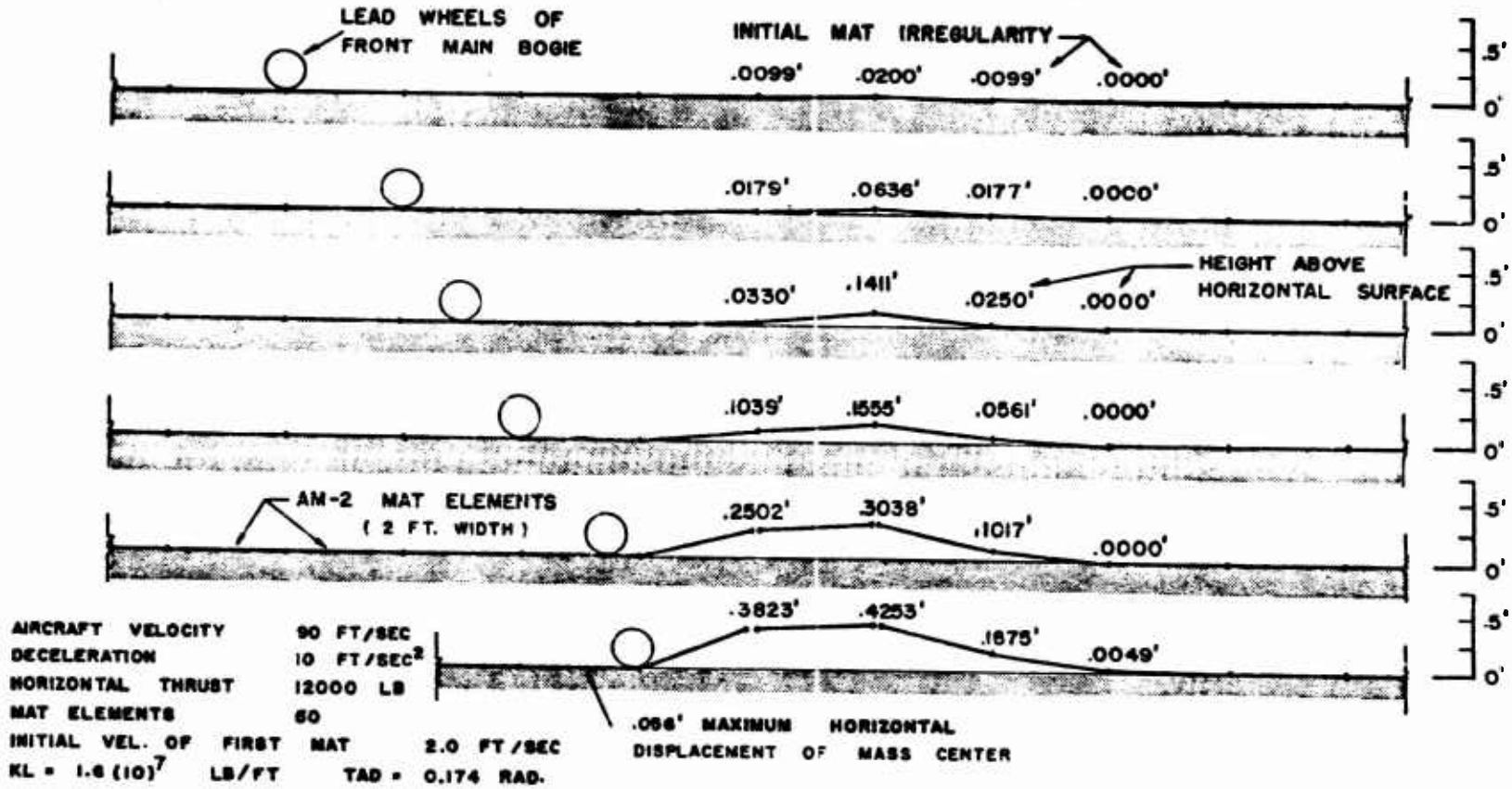


Figure 3.6 The Early Formation of a Bow Wave in AM2 Landing Mat that is Tightly Compressed as Predicted by the Analytical Model.

influence would give some additional horizontal mat displacement and some slight increase in the vertical displacements. As a result, the initial irregularities could have been less, but it is assumed that the cumulative discontinuity is as shown when the aircraft is located as shown. It should be noted that the bow wave flattens when the rotational rigidity is first encountered at about 10 degrees angle difference between adjacent mats. Also, the horizontal displacement is 0.056 ft after the aircraft has traversed three mats and indicates that the mat elasticity is probably assumed to be too stiff.

In Figure 3.7, the longitudinal spring constant $KL_n$ is reduced from $16 \times (10)^6$ lb/ft to $8 \times (10)^6$ lb/ft and the longitudinal displacement of mat 4 after the aircraft has travelled across 3 mats is 0.1036 ft. These results better simulate AM2 mat response. The bow wave does not form as rapidly when the joints are less rigid in the horizontal direction. In Figure 3.7, a flattening of the bow also takes place when the free-hinged joint conditions are exceeded and rotational rigidity is initiated. The reason for the maximum joint deflection in Figure 3.6 being less than in Figure 3.7 is related to flutter and the instantaneous value that was plotted. Also, the modification on the equations of motion that accounts for available longitudinal joint slack during relative rotation applies to bow waves in the early formation up to a height of about 0.5 ft. If the additional growth of a bow wave is desired, then the modification should be removed from the equations of motion. Both the solutions are currently programmed, but since the early formation of a bow is of primary importance, the low profile equations are considered and are given in this report.

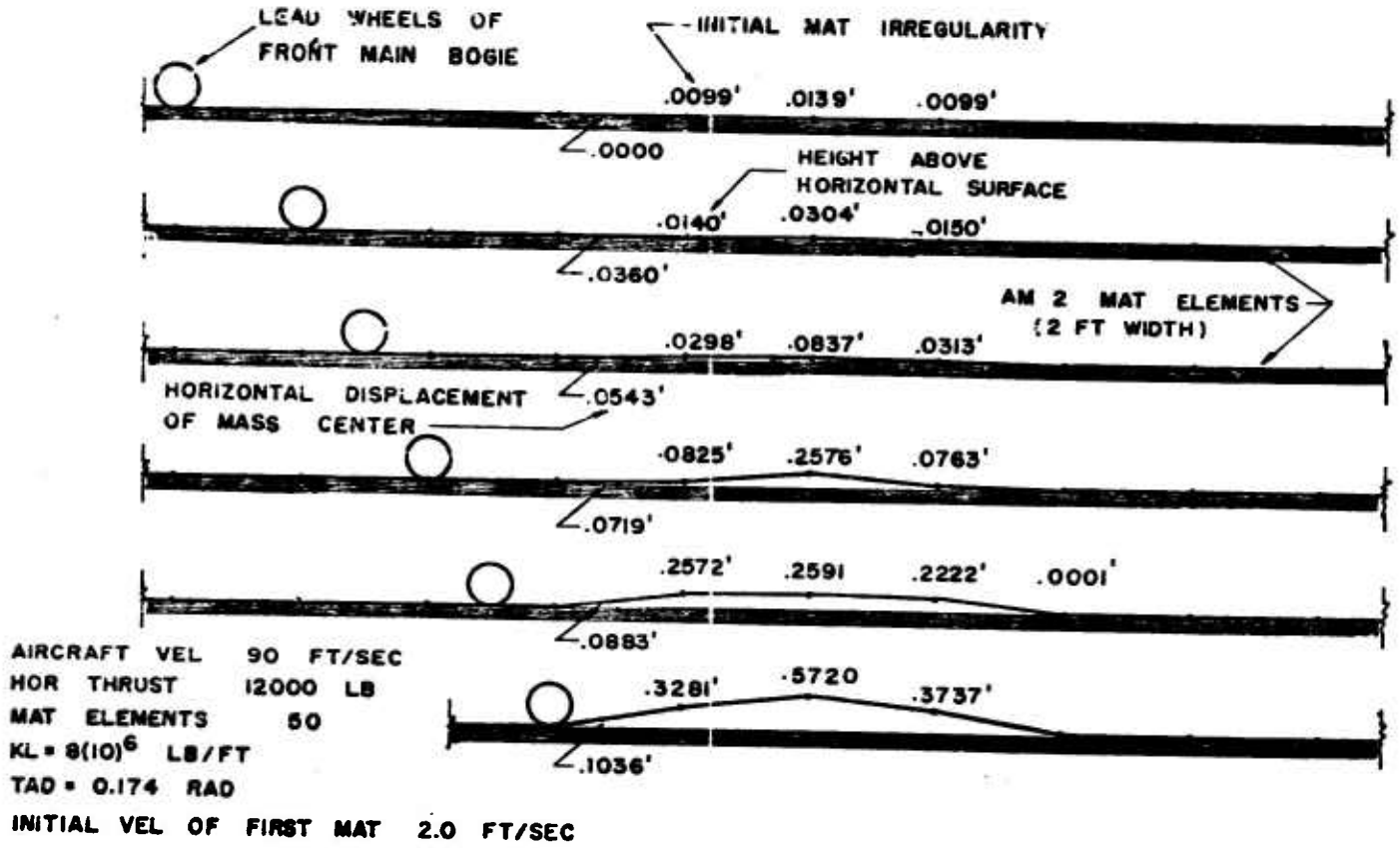


Figure 3.7 The Early Formation of a Bow Wave in Moderately Compressed AM2 Landing Mat as Predicted by the Analytical Model.

The longitudinal joint rigidity is critical to the formation of bow waves as shown in Figure 3.8. Initially, three joints are suspended slightly, with the maximum vertical height given as 0.0299 ft. The horizontal thrust is then initiated with a velocity of 90 ft/sec as shown. Since the irregularity was simply suspended and then released, the perturbed elements tend to settle back to the equilibrium or horizontal position until the influence of the thrust force is encountered. Although all three mats with different $KL_n$ values have been exposed to the same initial conditions, the mat having a $KL_n = 16 \times (10)^6$ forms a larger bow than the mat with a joint simulated by $KL_n = 16 \times (10)^4$, which restores itself to the horizontal position. This suggests that a bow wave will not form in flexible mat if sufficient relative displacement is provided. Also, note that the distance in front of the aircraft where the thrust force has any influence is related to the mat stiffness in the longitudinal direction, as indicated by the mat element experiencing no displacement. For example, in the landing strip having a $KL_n = 16 \times (10)^5$ lb/ft, all mats up to and including mat 16 are displaced as the aircraft crosses mat number 1. Beyond mat 12, however, the mat displacements are extremely small, e.g., mat 12 is displaced 0.0075 ft and mat 16 is displaced $.73 \times (10)^{-7}$ ft. The maximum vertical deflection initially is 0.0299 ft compared with 0.0200 ft in Figure 3.7. This larger "bump" initially results in a higher bow wave which is formed more quickly.

Several different initial configurations were studied in regards to the effect of friction between the mat surface and the subgrade. Figure 3.9 shows the early formation of a bow wave with an initial irregularity involving only three mats. The horizontal displacements of the mats with

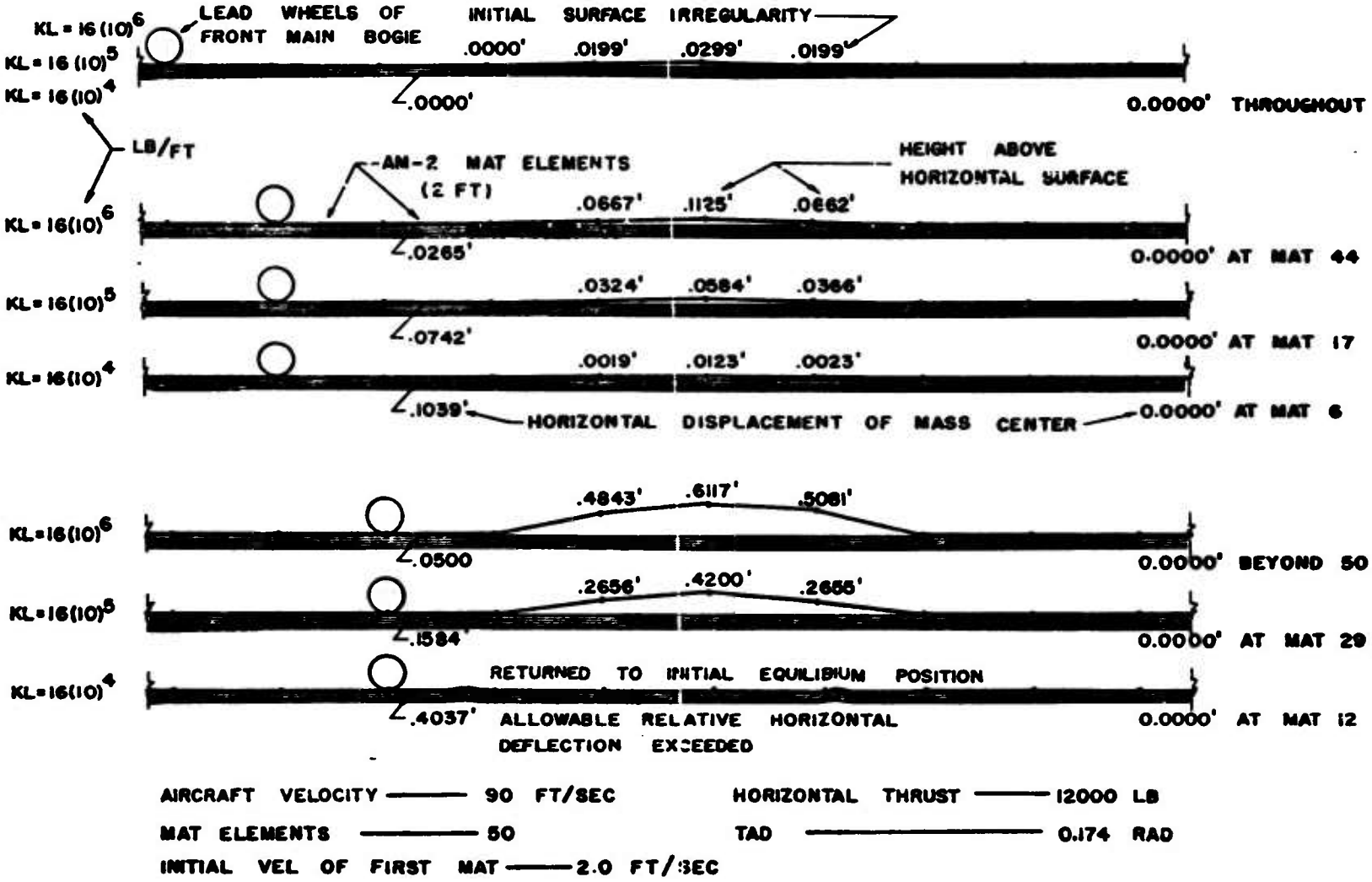


Figure 3.8 The Effect of Longitudinal Joint Elasticity on the Formation of a Bow Wave as Predicted by the Analytical Model.

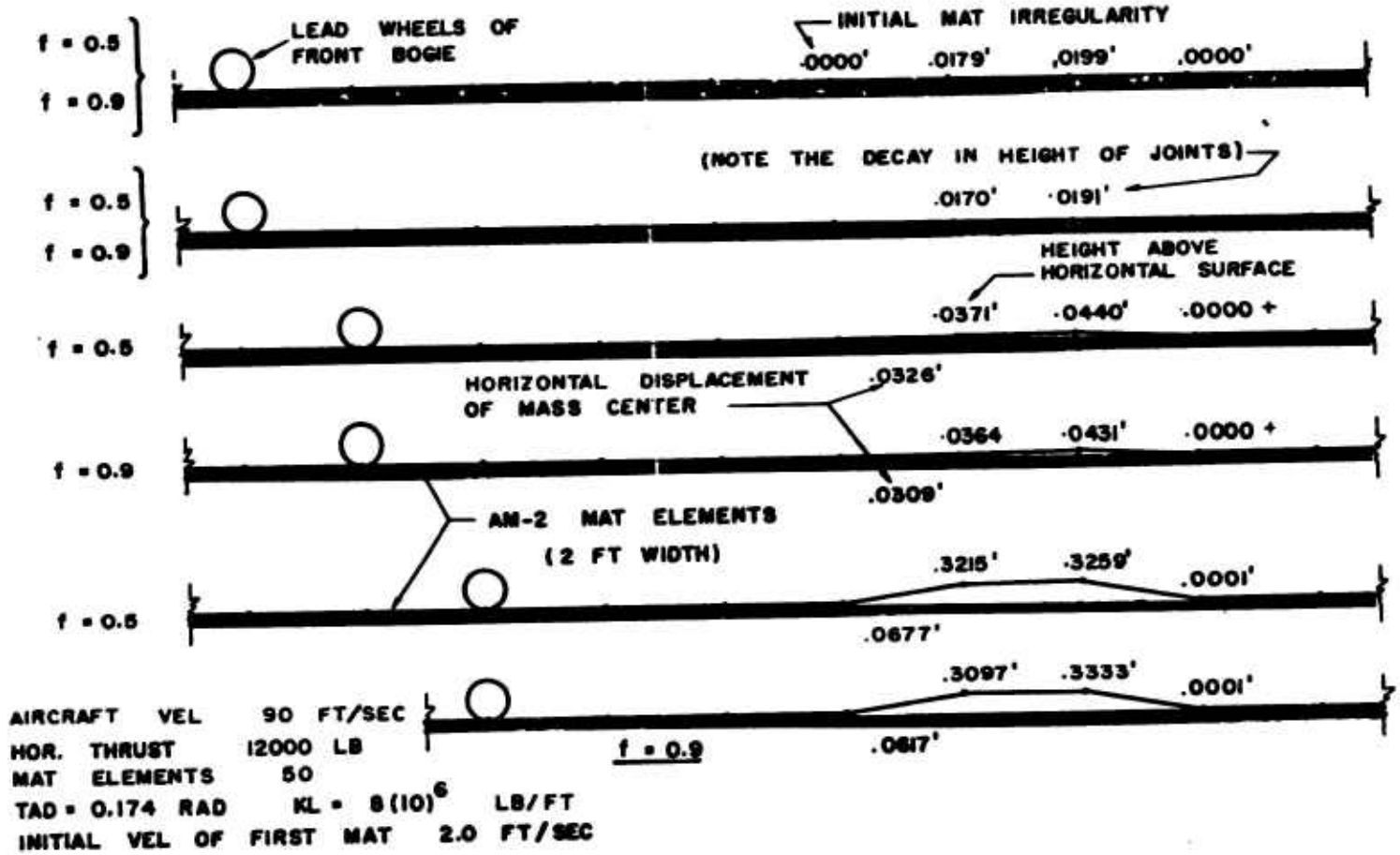


Figure 3.9. The Effect of Increased Friction Between the Mat and Subgrade on the Formation of a Bow Wave as Predicted by the Analytical Model. The Irregularity Involves Three Mats.

a coefficient of friction of 0.9 are slightly less than the mats having f = 0.5. The bow wave formation is almost identical. Figure 3.10 involves only two mats that are not perfectly flat initially and again friction is not significant.

The magnitude of the horizontal thrust is critical in the formation of standing waves. Figure 3.11 compares the bow waves developed by different thrust forces. The initial irregularity in the mat is very small as indicated. After the aircraft has crossed two and one-half panels, a horizontal thrust of 6000 lb produces no bow wave. Forces of 12,000 and 24,000 lb initiate waves as shown. This gives insight as to why the AM2 landing mat failed with the large C-5A, but not the lighter aircrafts. The magnitude of the horizontal thrust is assumed to be constant as the aircraft passes over four mats.

Another factor that was found to influence the dynamic response of landing mat is the relative rotation allowable between two adjacent mats before rotational rigidity begins. In Figure 3.12 the formation of a bow wave is followed as the aircraft traverses four mats. The AM2 mat now has a ''free'' rotation of 10 degrees (TAD = 10 degrees) and the vertical and horizontal displacements are compared with those of a mat allowing only 1 degree relative rotation before rotational rigidity is encountered. The results suggest that no bow wave would appear for a given horizontal thrust if sufficient moment rigidity were available. Other solutions with larger thrust forces and higher velocities indicate that the reduction of the free rotation would greatly reduce the bow wave potential.

Correlation between the analytical and physical models is also shown in Figure 3.12 by the mat with TAD = 10 degrees. The values of KT, KL, etc.

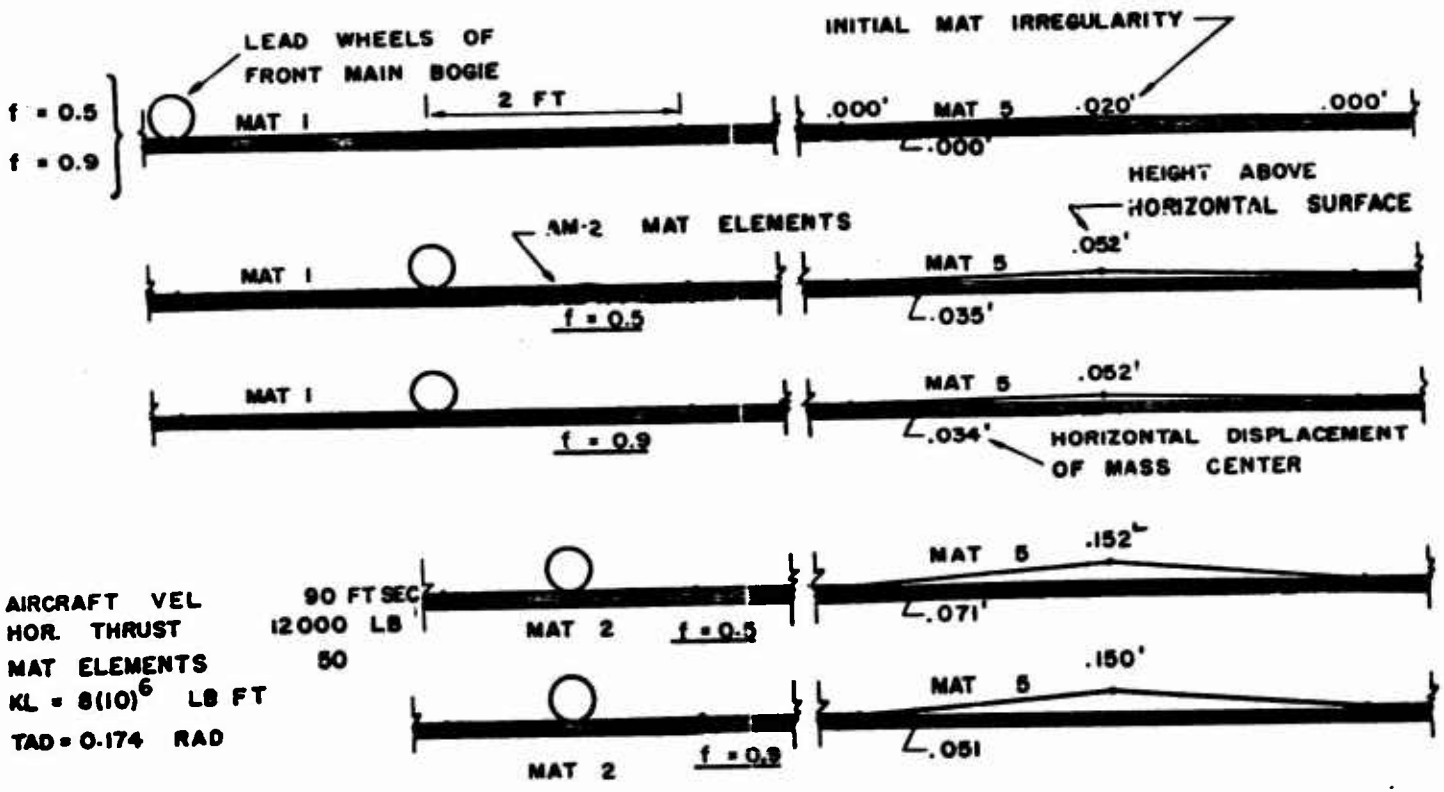


Figure 3.10 The Effect of Friction Between Mat and Subgrade on the Early Formation of a Bow Wave as Predicted by the Analytical Model. The Initial Irregularity Involves Only Two Mats.

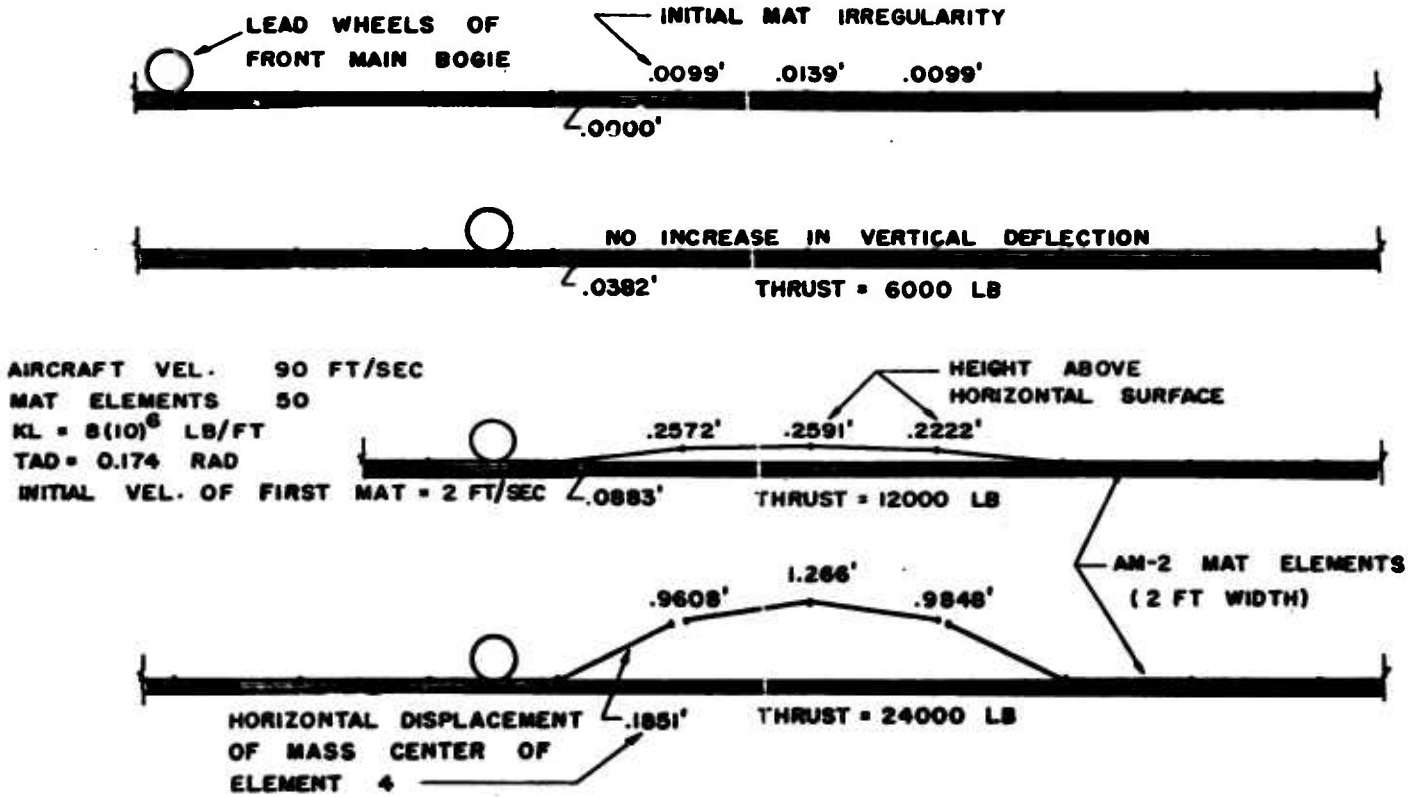


Figure 3.11 A Comparison of Standing Waves Predicted by the Analytical Model for Different Horizontal Thrust Forces.

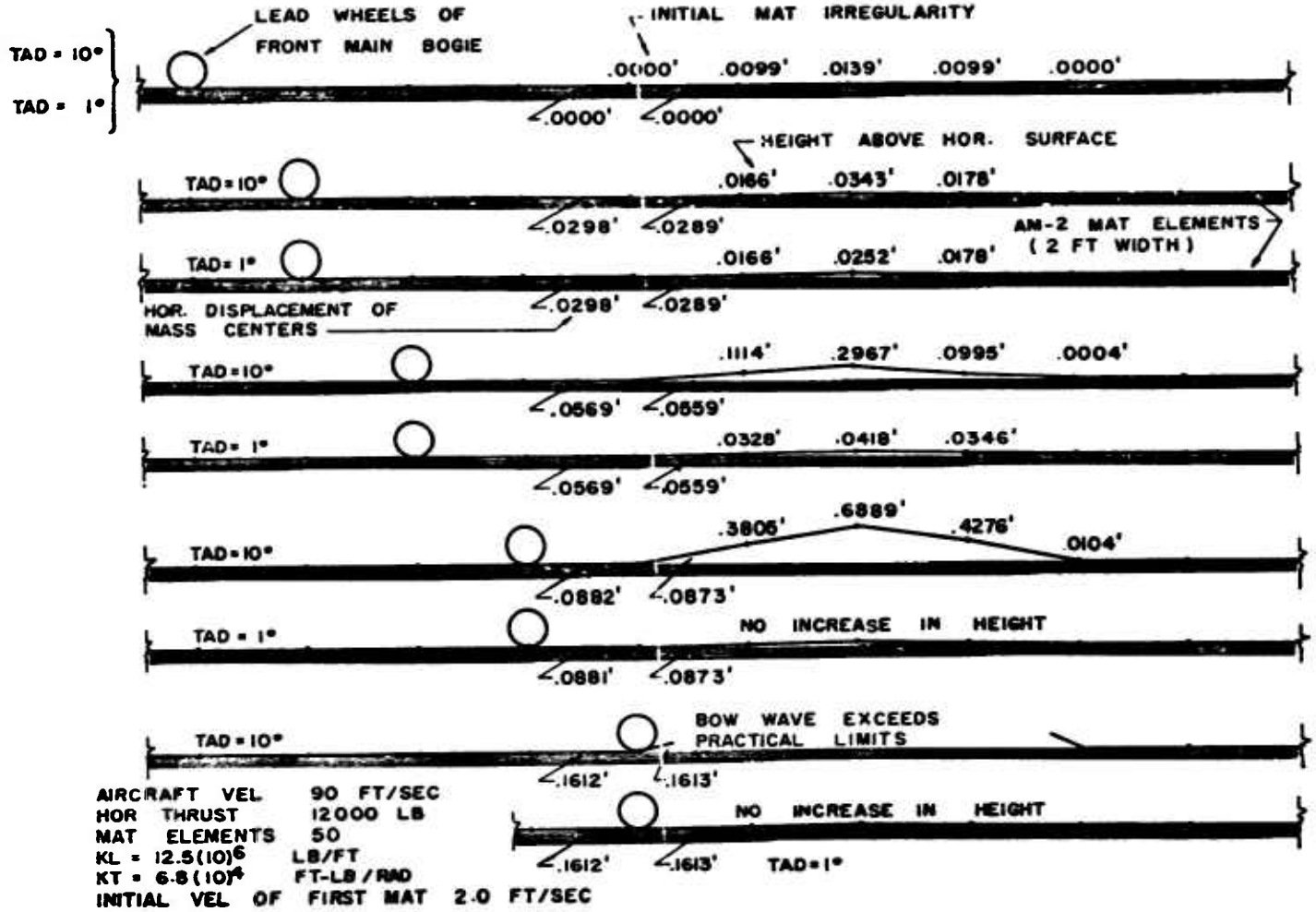


Figure 3.12 The Analytical Formation of a Bow Wave Using Parameters of the Physical Model. The Effect of Reducing the Allowable Relative Angle Before Rotational Rigidity is Encountered is also Compared.

as determined experimentally for the physical model are assigned to the analytical model. The displacements shown in Figure 3.12 should be divided by the scale factor 7 in order to compare results. For example, the longitudinal displacement in the neighborhood of the bow wave in the physical model is predicted by the analytical model to be 0.1612 ÷ 7 = .023 ft or between 1/4 and 1/3 in. This result agrees well with the physical model. The vertical displacement is difficult to compare, because it is dependent upon the initial irregularity. With the low profile modification on the equations of motion the horizontal displacement is not highly dependent upon the height of the bow wave. The validity of this comparison strengthens the reliability of both models.

The original intent of the analytical model was to remove a section one panel wide and several panels long from the interior of the landing surface immediately in front of the two leading wheels of a bogie. This strip was shown earlier in Figure 3.1. The amount of horizontal thrust applied to the model was then determined as the product of the thrust per wheel and the number of wheels influencing the model directly. In some situations, a large aircraft with several wheels may have a lower thrust per wheel than a lighter aircraft.

An alternative interpretation of the model was considered. The model was assumed to represent the complete width of the landing strip and the total horizontal thrust of the aircraft was considered, rather than thrust per wheel. The mat elements were taken to be 96 x 2 ft rather than 12 x 2 ft. Since mat geometry is a variable in the computer program, little difficulty is involved in correcting for the larger mass and moment of inertia.

A horizontal thrust of 144,000 lb, which is representative of the C-5A, was found to produce a bow wave in mat where the original irregularity involved two mats in an inverted vee with the apex 1/4 in. from the horizontal position. A thrust of 36,000 lb, representative of smaller aircraft, was found to produce no bow wave under the same surface conditions.

## 3.7 Analytical Conclusions

The analytical model suggests that several factors influence the stability of flexible landing surfaces. Horizontal thrust, rotational rigidity, joint elasticity, surface irregularities, and velocity affect the formation of bow waves. The analytical model can isolate the response of mat to changes in any of several parameters, or the combined effect of two or more modifications. Although several typical situations were investigated as part of this report, the program is still available for additional evaluations. Some general conclusions can be stated as follows:

1. Irregularities in the mat surface are potential locations for the formation of bow waves. The wave development is dependent upon the magnitude of the initial vertical deflection and the number of mats involved. A perfectly flat surface will not buckle under C-5A horizontal thrust forces.

2. Friction at the interface of the mat and subgrade is not critical in the formation of a wave.

3. Bow waves will not form if high compression in the joints can be avoided, even though the mat is subjected to large in-plane forces. A shock absorber that would maintain joint spacing would reduce the chances of a bow wave.

4. A reduction in the relative rotation allowable at a joint before rotational rigidity is encountered would greatly reduce the probability of bow waves forming.

5. Soil parameters have little influence on the dynamic response of mat in front of the wheels. This is perhaps not true directly beneath the wheel.

6. The development of a bow wave is highly dependent upon the magnitude of the horizontal thrust, and the aircraft velocity. Under similar mat conditions, lighter aircraft can land successfully, whereas the C-5A would cause failure.

7. The propagation of the dynamic response is dependent upon the longitudinal stiffness of the mat and travels much faster than the aircraft.

8. The analytical model simulated the response of the physical model when experimentally determined parameters for the physical model were programmed.

## SECTION IV

## DUPLICATION OF THE MAT FAILURE AT DYESS AFB

A major objective of the study was to establish the validity of the model by duplicating as nearly as possible the mat failure at Dyess AFB. With the validity of the model established the factors causing the failure and means of preventing failure could be studied.

### 4.1 Mat Failure at Dyess AFB

A series of C-5A support area landing tests were conducted on the 6000-ft long Tri-Service landing mat runway at Dyess AFB in August of 1970. The Tri-Service runway was constructed of 1140 ft of AM2 mat near the center with 2200 ft of XM19 mat on the north end and 2600 ft of XM18B and XM18C mat on the south end. The runway was 96 ft wide except near the ends where it had been widened. The subgrade soil is a heavy clay (CH) and was covered with a polypropylene-asphalt membrane overlaid with a herculite (vinyl-laminated nylon). No soil strength tests were made at the time of the C-5A test landings but earlier tests showed California Bearing Ratios from 11 to 36 percent for the surface soil (Ref. 2). Currin concluded that the soil strength was adequate and the subgrade weakness did not contribute to mat failure (Ref. 3).

Five takeoffs and three landings with the C-5A were completed without difficulty. On the fourth landing the mat buckled causing major damage to the AM2 mat portion of the runway at stations 27 + 12 and 27 + 34. The aircraft touched down at station 7 + 60, traveled 1440 ft on XM19 mat

before reaching the AM2 mat section at station 22 + 00, and stopped at station 29 + 40 still on AM2 mat. The connection between the XM19 and AM2 mat was broken. Thirteen panels were dislocated at station 27 + 12, and 40 panels were dislocated at station 27 + 34. The dislocated mat came mainly from the left side of the runway because the aircraft position was about 9 ft left of the runway centerline. At several other locations in the runway, panels were disconnected and end connectors were broken.

Detailed descriptions of the mat failure have been reported by Currin (Ref. 3) and Green (Ref. 4). The following conclusions have been reached largely from the reports of Currin and Green.

1. Large longitudinal mat movement occurred during the fourth landing. Because aircraft position was left of the runway centerline, movement was larger on the left edge of the runway. Little movement was observed on the right edge of the runway and, in fact, no measured values of such movement were reported for the right edge of the runway. The magnitude of longitudinal movement for the earlier C-5A test landings is not known.

2. In-plane bowing in the mat runway was much more severe during the failure than before or after. Evidence indicates that an in-plane bow in excess of 11 in. is necessary to cause weld breaks in the end connectors along the runway centerline. After the failure the measured bow varied from 6 in. to a maximum of 9 in. at a point immediately beyond the last failure area (Ref. 3). Therefore the mat rebounded relieving the high bow that existed during failure.

3. A plot of the longitudinal displacement (Figure 4.1) that occurred during the fourth landing along the left edge of the runway shows a tension

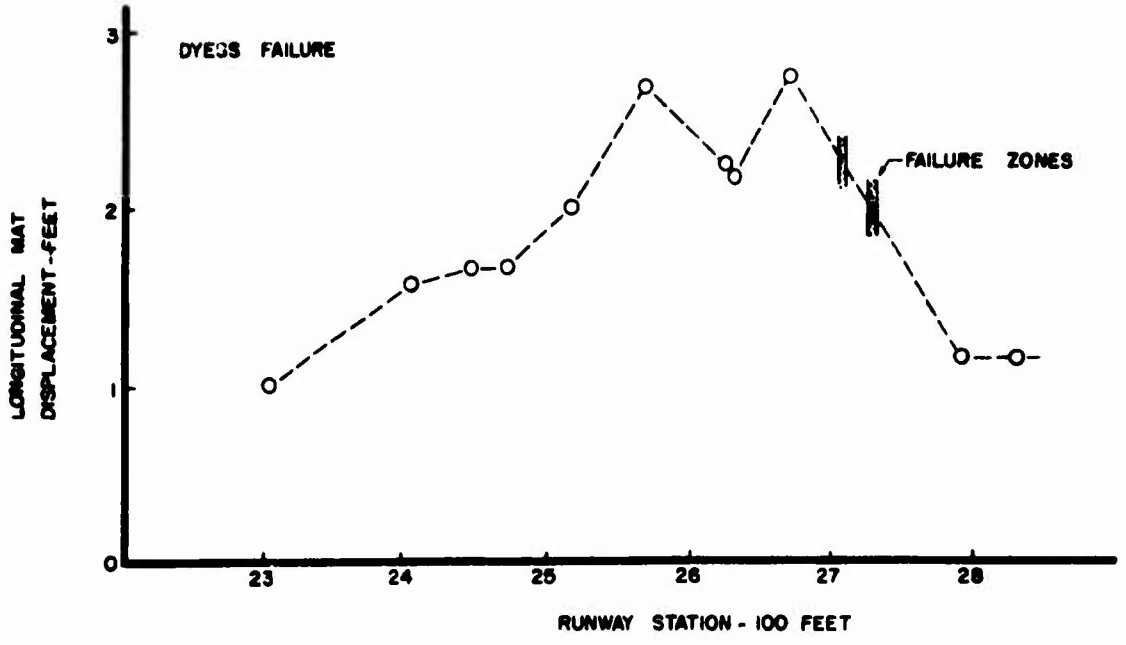


Figure 4.1 Mat Displacement During the Dyess AFB Mat Failure.

region from station 23 + 00 to station 25 + 60 where the mat joints must be open. This is the case since the mat at station 25 + 60 has moved further downfield than the mat at station 23 + 00. Beyond station 25 + 60 is a short compression region, then a short tension region followed by a much longer compression region where the two major mat failures occurred. In the first compression region at station 25 + 90 there was a minor failure involving unhinged panels and several broken end connections.

4. Photographs show the bow wave reached maximum height in front of the landing gear and tapered down to near zero height at the right edge.

5. Failure occurred as the height of the bow wave increased to such a height that the landing gear could not push the mats back down into the flat position as it rolled across. Photographs show the aircraft crossing small, probably two-panel, waves near station 25 + 90 where a row of

panels was unhinged (pages 72-73, Ref. 3). Two photographs later (pages 76, 77 Ref. 3) a larger wave is seen developing perhaps 40 ft ahead of the landing gear. The height of the wave increases as the aircraft approaches. In crossing the wave the right gear pushed the panels back down without tearing them apart, but the left gear tore 13 panels loose. Meanwhile a second and higher wave appeared at station 27 + 34. This second wave increased in height to nearly 4 ft (page 83, Ref. 3). Both the right and left gear pushed into this wave, tipping at least one row of panels over backwards and tearing loose 40 panels.

6. The break in the runway at station 27 + 12 extended from a position in line with the left gear to the left edge of the runway. At station 27 + 34, panels were torn loose from the left runway edge to about 18 ft to the right of center line, an area in line with the right landing gear. An approximately 30-ft width of intact mat remained along the right runway edge. These remaining mats were pushed up into a bow wave 1 to 1½ ft high, tapering down to zero height at the right edge (Ref. 4).

7. The mat upfield of the failure zone had moved downfield about one panel width with respect to the mat beyond the failure (Ref. 3).

## 4.2 Model Landing Tests

A buckling failure occurred in the model AM2 mat runway on the fifth test landing. For the first two landings the average deceleration rate was only 4 ft/sec$^2$ compared with 10 ft/sec$^2$ for the prototype landings. With the second landing several small two-panel waves appeared ahead of the model. This action was not evident on the first landing. On the fourth landing the average deceleration was 4.6 ft/sec$^2$. When the model

landing gear stopped, two small waves remained in the mat ahead of the front bogies at station 88. The deceleration on the fifth landing varied from 6.6 ft/sec$^2$ to 9.2 ft/sec$^2$ and the touch down velocity was 35.5 ft/sec. A buckling failure occurred at stations 85 and 91. The action of the mat was recorded by a high-speed camera (200 fps) mounted on the moving model. Study of the films shows a reasonable correlation between the action of the model runway and that of the prototype. Photographs taken from 16-mm movie film of the Dyess failure and the model failure are shown in Figure 4.2 for comparison. On all landings the model followed the same path, approximately 1.4 ft left of center. Photographs of the mat after the failure are shown in Figures 4.3 and 4.4. In this case the velocity of the model was not sufficient to run completely through the failure. When the model stopped, a three-panel wave remained in front of the wheels.

## 4.3 The Model Failure

The model runway behavior resembled that of the prototype in many ways. Action paralleling that of the Dyess failure is described as follows:

1. Large longitudinal movement occurred during the failure landing. Mat displacement was greater on the left side because the path followed by the model aircraft was always left of center. Little movement was measured on the right side of the runway. Longitudinal movements of at least 1/4 to 1/3 in. occurred along the left edge and center line of the runway with each passage of the model aircraft.

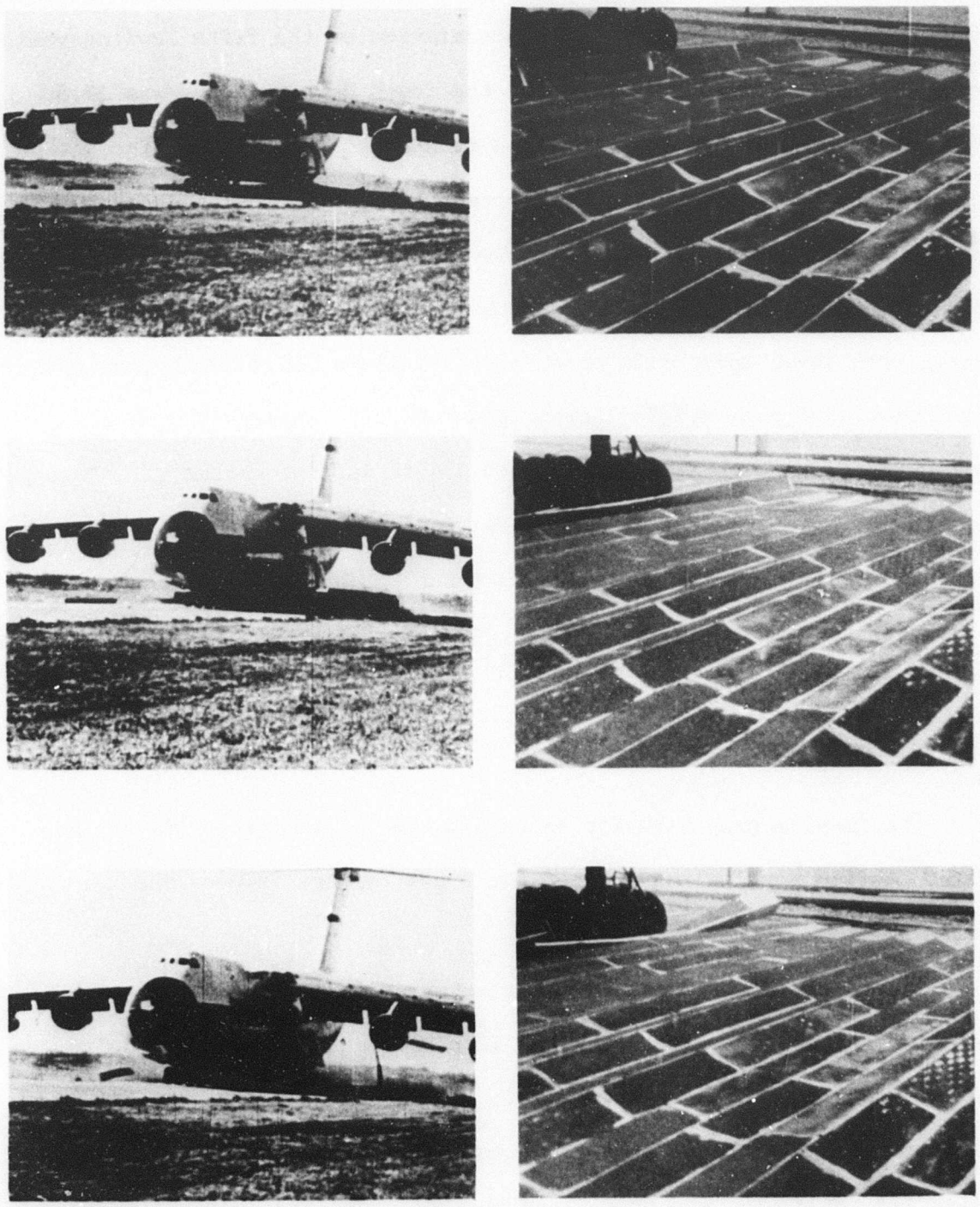

Figure 4.2. Sequence of Photographs from Movie Films of the Prototype and Model Landing Mat Failure.

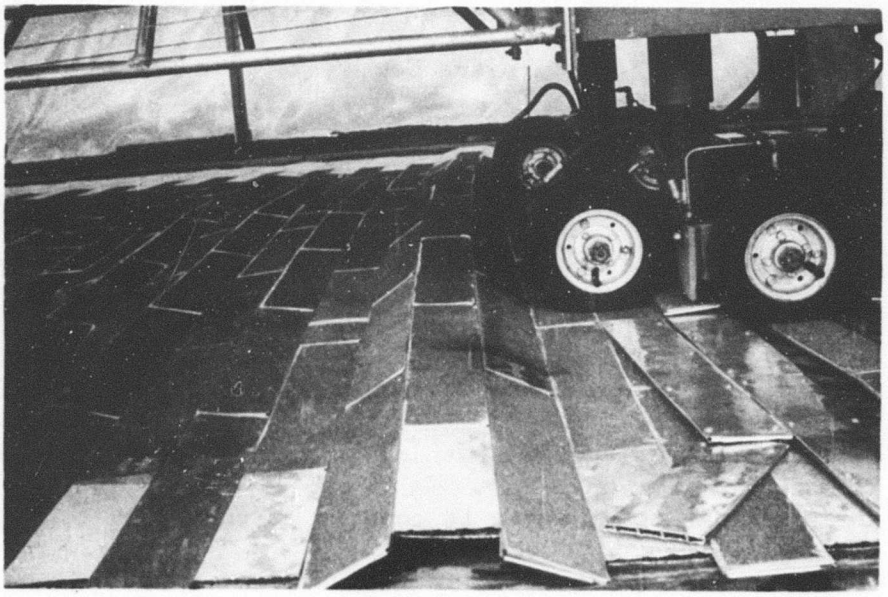

Figure 4.3. A Three Panel Wave Remaining Ahead of the Forward Main Gear After the Mat Failure.

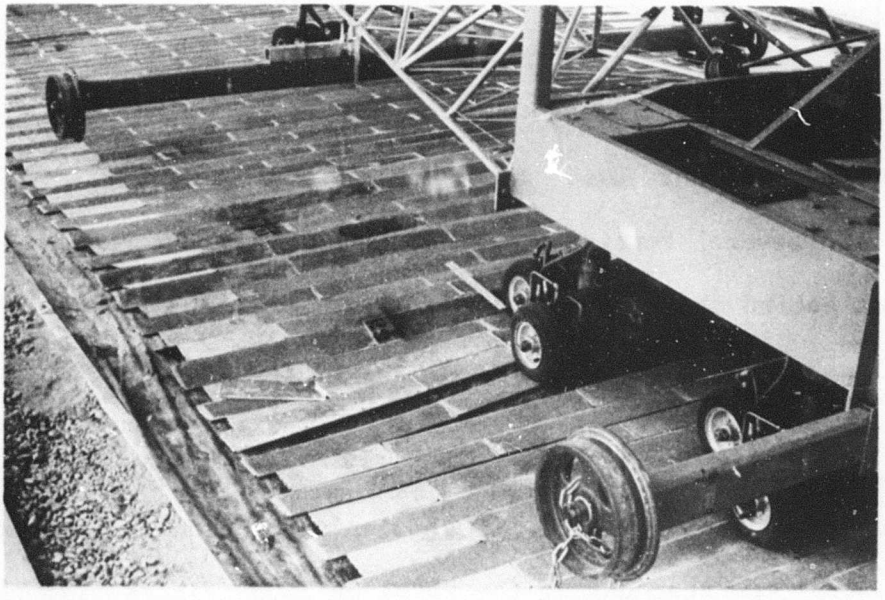

Figure 4.4. A View of the Broken Runway After Failure.

2. An in-plane bow developed in the mat which increased with each landing. Panel end joints along the staggered center line joint showed some distress as a result of the in-plane bow.

3. A plot of the longitudinal displacement (Figure 4.5) that occurred during the model failure landing shows a tension region from station 10 to 80. Beyond station 80 the mat is in a compressed state. Failure occurred a few feet inside the compressed region.

4. Failure occurred when the bow wave increased to a critical height and was overrun by the model. Smaller two-panel waves were pushed down by the model causing higher waves to come up further down the runway. When several panels were involved in the wave the passing wheels broke a longitudinal joint leaving two panels in a vertical position. The forward-moving wheels pushed the vertical panel over backward, flipping adjacent panels. See Figure 4.2.

5. Breaks in the model runway were near the center line and left side and did not extend across to the right side of the runway. After the failure a small bow wave remained in the mat on the right side but tapered off toward the right edge. The break occurred at two stations along the mat with several tension breaks in the mat further back.

6. The mat behind the failure moved forward about one panel width during the failure, with respect to the mat beyond the failure.

## 4.4 Graphical Comparisons

The similarity of the longitudinal mat displacement during the Dyess failure (Figure 4.1) and that during the model failure (Figure 4.5) is evident.

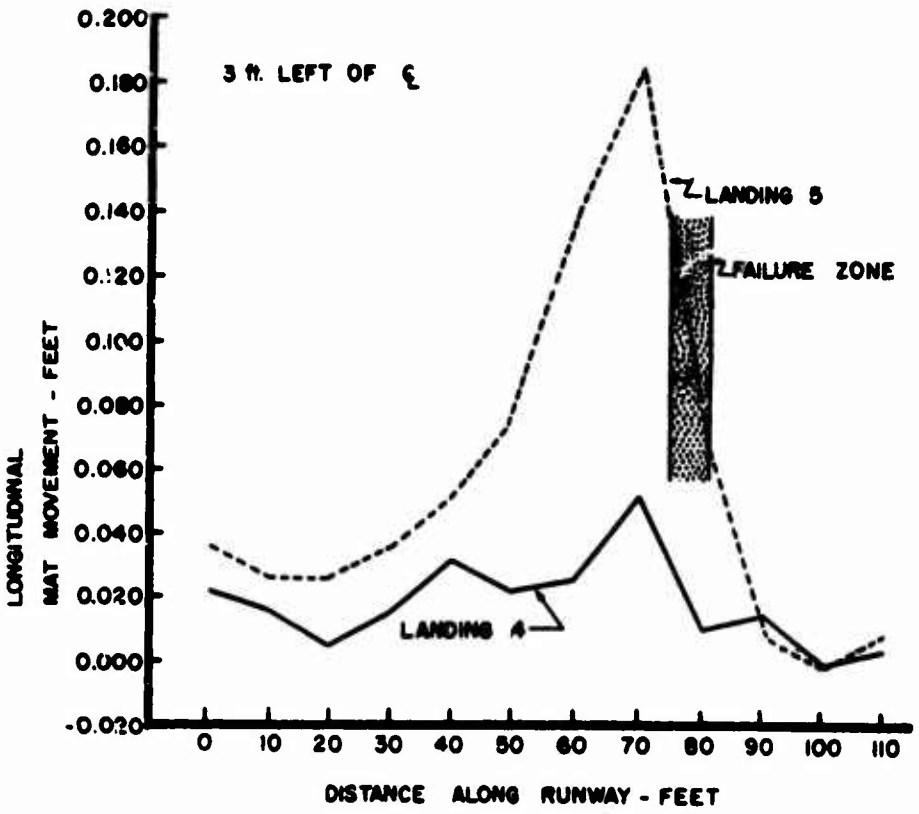


Figure 4.5. Longitudinal Displacement of Model Mat, Landings 4 and 5.

In both cases the buckling failure occurred within a region of compressed mats. The number of mats sections involved in the longer compressed region of the Dyess failure is about 60. In the model, about 70 mats are included in the compressed region. The exact length of the compressed zone cannot be accurately determined for either the model or prototype.

In the prototype no longitudinal measurements were made on the earlier landings. The lower curve in Figure 4.5 shows the displacement that occurred for the model landing previous to the failure landing and indicates the build-up of the compression region between stations 80 and

90. It will be noted that the points of maximum displacement coincide on landings four and five, identifying the point at which buckling occurs. The appearance of small two-panel waves in the same area on the previous landing also indicated that buckling was impending.

The number of landings required to produce the failure is not considered to be of great significance because several factors leading to failure are not properly simulated in the model. There is no assurance that the joint openings between mats had the same magnitude and distribution in the model runway as existed in the Dyess runway when the C-5A test landings began. The Dyess runway had been subject to numerous landings of lighter aircraft and although most of the C-5A test landings and takeoffs were in the southward direction, there was at least one takeoff in the northward direction (Ref. 4). The lengths of runway traversed and the magnitude of braking forces applied at any point are unknown. In the model the deceleration for three landings was less than 5 $ft/sec^2$, much less than the 10 $ft/sec^2$ deceleration of the prototype aircraft when failure occurred. All the above factors make it unlikely that the model failure would occur after the same number of landings as for the Dyess failure.

## 4.5 Second Model Failure

The build-up of the compression zone prior to a buckling failure was also demonstrated in tests on mat with increased bottom friction. These tests are described in Section 5.4, but they have been included here because they demonstrate more clearly the build-up of the compression region in the mat prior to the buckling failure. As indicated in Section 5.4, increasing the friction between the mat and subgrade did

not change the mat behavior appreciably except to reduce the longitudinal movements slightly. Figure 4.6 shows the cumulative longitudinal displacement after each of three landings. The point of maximum displacement after the third landing is at station 90. Movements at station 100 and 110 are much smaller indicating that the mats between these stations were in a compressed state (joints closed). On the fourth landing a buckling failure occurred at station 93.

## 4.6 Discussion

In the two series of model tests described, buckling failures occurred in regions of compressed mat. The zone of compressed mat was identified in each case from a plot of longitudinal displacement versus position along the runway. Displacements of the Dyess runway were measured only after the failure landing (Figure 4.1), but can be compared with the model data in Figure 4.5. The similarity between model and prototype data is apparent.

The behavior of the model mat was shown with reasonable clarity in the films taken during most test landings. Although the mat action cannot be seen clearly in the film of the Dyess failure, the action during the Dyess failure appears to be closely duplicated in the model. All other evidence such as mat displacement, location of breaks in the runway, and bow wave formation support the conclusion that the model does correctly represent the prototype.

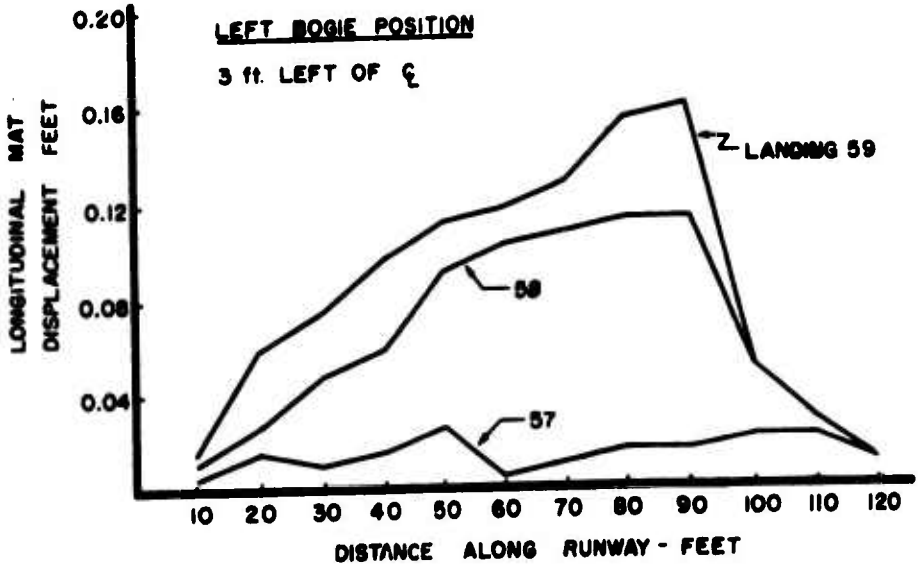


Figure 4.6. Displacement During Three Landings Prior to Failure (Mat With Increased Bottom Friction).

## SECTION V

## MODIFICATION OF AM2 RUNWAY

A major objective of the model study was to evaluate various alterations of the AM2 mat runway to permit the safe operation of C-5A aircraft. These alterations must be practical for inexpensive field implementation.

Five alterations were studied: (1) mat restraint by pretensioned bands, (2) diagonal laying pattern, (3) increased friction coefficient, (4) cleats beneath the runway, and (5) longitudinal stiffeners.

### 5.1 Pretensioned Bands

#### 5.1.1 Fundamental Purpose of Bands

The large horizontal force produced by the braking C-5A led to the buckling failure of the AM2 mat at Dyess. Initial design of the mat placed greater importance on vertical load-carrying ability than on resistance to horizontal forces. During C-141 operations, buckling of AM2 mat was not recognized as a potential failure mode since the C-141 satisfactorily performed the test program. Despite the higher flotation capability of the C-5A the AM2 mat buckled. This indicates that the horizontal force normally produced by the C-141 is less than the critical buckling load of the mat, whereas with the C-5A it is greater than the critical buckling load.

Longitudinal tension bands were conceived as a means of transferring the horizontal force among all mat panels back to anchors, thus reducing the horizontal force carried by the mat and preventing the closure of

joints. This would place most of the horizontal loads on the bands and the vertical loads on the mat as originally designed. Pretensioning the bands would restrict movement in the band at the point of load application.

### 5.1.2 Preliminary Tests of Banded Runway

#### 5.1.2.1 Test Conditions

In the initial tests, two steel bands 3/8 in. wide by 0.020 in. thick were stretched the length of the runway. The two bands were 26 in. apart and located astride the runway centerline. After receiving an initial tension of 100 to 150 lb, the bands were riveted to every 10th mat by two 1/8 in. diameter pop rivets. Only mats in the first 50 ft of the runway were riveted to the band and tests were conducted to restrict the model movement primarily to the riveted length of the runway. The section of banded mats is shown in Figure 5.1.

After three landings on the banded mat, a third band was added in line with the left bogie of the model. The pretensioning force was about 60 lb and every 40th mat was riveted to the band.

#### 5.1.2.2 Results and Conclusions of Preliminary Tests

The first landings on the banded runway showed that the bands restricted the mat movement to about 1/16 in. despite higher deceleration of the model aircraft (up to 9 ft/sec$^2$). No waves were evident in he area of the restrained mat. The portion of runway in line with the left bogie of the model was not initially restrained by bands. As a result, mat movement at the left edge was 1/4 in. to 7/16 in. during each landing and small two-panel waves were evident ahead of the moving bogies. To restrain this movement, the third band was installed.

Figure 5.1. Longitudinal Tension Bands Attached to Model AM2 Mat Runway.

During the next five landings, with the third band installed, the accumulated movement of the restrained mat was less than 1/4 in. More movement was noted on the left side where the band had lower tension and greater spacing between riveted mats. Figure 5.2 compares cumulative displacement of the banded mat with the cumulative displacement that occurred in the two landings after the bands were removed. Displacements of the unbanded runway during two landings were several times larger than those of the banded mat during five landings.

This preliminary series of seven test landings demonstrated the effectiveness of the band in controlling mat movement and buckling. As a result, a second series of more detailed tests was planned to better

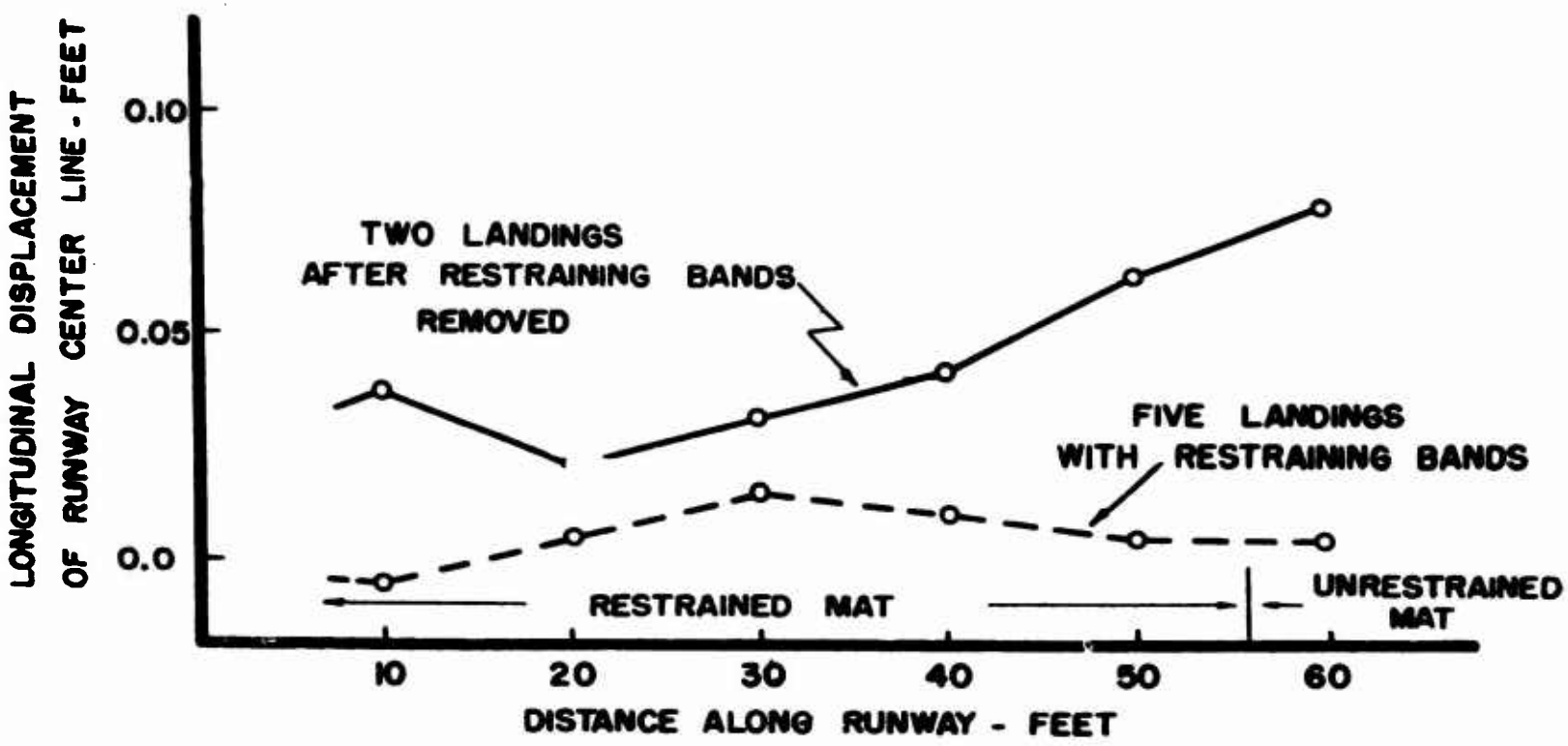


Figure 5.2. Comparison of Mat Displacement at Runway Centerline with and without Tension Bands.

evaluate the required band tension and number of free mats between points of attachment.

### 5.1.3 Detailed Tests of Banded Runway

#### 5.1.3.1 Band Construction and Instrumentation

For the second series of tests, four steel bands were stretched the length of the runway and pretensioned to 100 lb. At each end of the runway the bands were attached to springs which were anchored. The springs were used to adjust the tension in each band and to serve as shock absorbers.

Strain gages were attached to the bands at 14 locations to monitor force changes. Figure 5.3 shows the location of bands with respect to the model landing gear. Every 20th row of mats was riveted to the bands.

#### 5.1.3.2 Test Details and Results

Twenty-six test landings were made on the banded runway. Movement was definitely restricted by the bands. No major buckling failure occurred. The cumulative mat movement on the left edge of the runway did reach values of about 1 in. However, this is believed to be mainly the result of loss of tension in the left band during the third landing of the series, when the band connection slipped at the upper end. The resultant loss of restraint allowed the mat to move during the next landings. Although the tension in the left band was restored, the band did not behave as well thereafter because the tension could not be made uniform throughout the band.

The displacements during any one landing averaged 1/16 in. with a few values up to 3/16 in. The displacements were not cumulative because

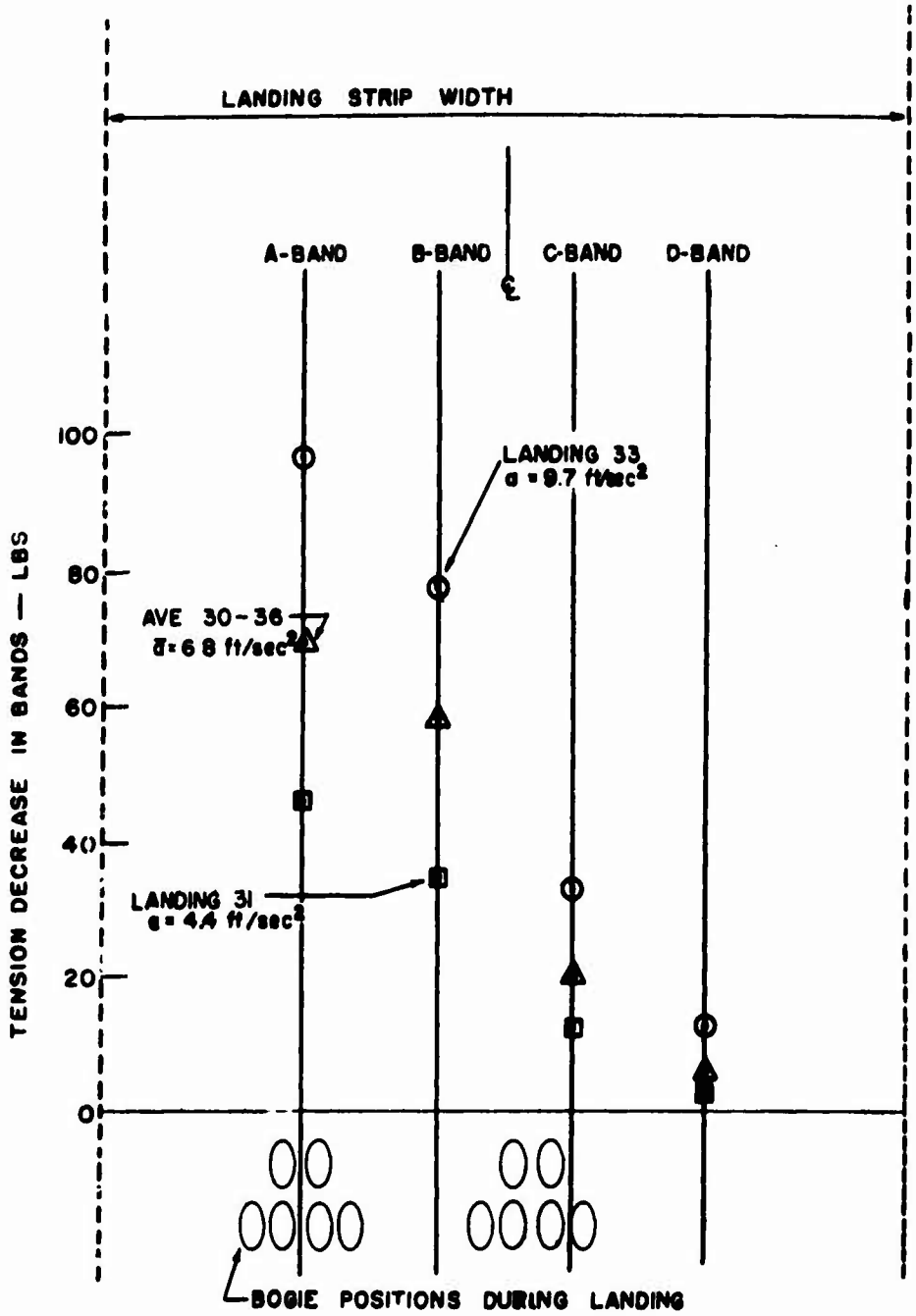


Figure 5.3. Average Change in Band Tension as a Function of the Deceleration of the Model.

the band acted to restore the mat to its initial position. Measurements at some locations showed that the band had pulled the mat back 3/16 in. overnight, because of temperature changes.

In later tests some of the rivets were pulled out of the mat. The rivet connection to the mat was resistant to shear but could not withstand a vertical force. The rivets were easily pulled through the 0.012-in. thick aluminum mat surface, and tended to pull out as the passing model depressed the riveted mat or rotated the mat, thus producing a normal component of force. This pull-out problem became more severe during the last few tests.

Strain gage data showed that the tension in the band decreased at a given location as the C-5A model approached, then equalled or exceeded its original value as the model passed. Figure 5.3 shows the average change in band tension as related to the deceleration of the model.

After thirteen tests it was concluded that 100 lb initial tension in the bands was inadequate, because the band ahead of the model was observed to slacken and small waves formed in the mat. The bands were then tensioned to between 130 lb and 150 lb, but the force was not uniformly distributed over the length of the band because attachment had taken place before tensioning.

As the tests continued, more rivets began to pull out because of enlarged or worn rivet holes. Other bands appeared to go slack and small buckling waves were observed. Despite this action no mat buckling failure occurred. The deceleration rate varied between 6 $ft/sec^2$ and 11 $ft/sec^2$ for most tests. In general, the mat behavior was good. Most of the difficulties were observed during final tests in areas of the runway where rivets had pulled out.

### 5.1.4 Conclusions

It was concluded that the pretensioning force is essential if the band system is to work properly. For the model, a force greater than 150 lb (51,000 ib for the prototype), is recommended for each band to provide some factor of safety. If a band is broken, it may be difficult to obtain proper tension in the repaired band. The 20-mat spacing between points of attachment to the band appeared satisfactory. However, the mat behavior with 10-mat spacing was better, in that less movement was observed, connecting rivets showed less distress, and the small buckling waves were less obvious.

## 5.2 Design of Restraining Bands

Test results on the banded mat indicated the need for a high initial tension force in the band. For better model performance the force in the active tension bands was approximately equal to the total force required to brake the aircraft. This suggests that the bands assume the braking force, and any force generated by friction between mat and sub-grade should be neglected. Based on the above assumption and assuming a uniform distribution of the force among N active bands, the initial tension, $T_o$, required in the bands and the number of bands, N, may be obtained from

$$T_{o\ min.} \geq nF' + R/2 \tag{5.1}$$

$$T_{o\ max.} \leq Af_y - R/2 \tag{5.2}$$

and

$$N = \frac{Wa}{gR} \tag{5.3}$$

in which nF' is the total friction force acting on the mats and as a holding force on the bands, A is the cross-sectional area of the band, $f_y$ is the yield stress of the band material, R is the force transmitted by the landing strip into a single band as the aircraft friction acts on the landing strip, W is the weight of the aircraft, a is the deceleration rate of the aircraft, and g is the acceleration of gravity. Details of the development of these equations are given in Appendix C.

## 5.3 Diagonal Laying Pattern

A frequently suggested solution is an altered laying pattern. A 45-degree pattern is one which can readily be placed without any modification of either the model or prototype mat sections. In placing this runway, the joint along the centerline of the model runway was similar to that used at Dyess except that the offset was about 40% greater as a result of the 45-degree angle (see Figure 5.4).

In addition to the transverse reference lines, four longitudinal reference lines were established to monitor possible transverse movement. Seven 45-degree lines of gage points were established at right angles to the mat joints to monitor movement of the joint spacing.

Mat performance was superior for this pattern compared to that of the transverse pattern. The mat was much more stable and showed little tendency for the occurrence of the two-panel waves so evident with the Dyess pattern. The model landing gear landed to the left of center as on previous tests. On an early landing a few two-panel waves were formed on the right side of the runway to the right of the area crossed by the model landing gear. These waves tended to remain through several landings. For the last five landings the model landing gear was adjusted to land on

Figure 5.4. Centerline Joint of Model AM2 Mat Placed in 45 Degree Pattern.

the right side of the runway. On the first landing right of center, the two-panel waves were worked out along the right edge leaving the mat flat. No additional waves were evident on following landings.

A total of sixteen landings were made on the diagonal mat. For several of the later landings the deceleration reached values of 15 ft/sec$^2$ to 17 ft/sec$^2$. No failure occurred except for tearing of joints in tension

at four or five points. This was primarily due to the weakness of the model mat in tension.

For the sixteenth landing on the diagonal mat full braking was applied, which locked the wheels and produced a deceleration of 32 ft/sec$^2$. This extreme loading caused a tension failure across the runway behind the model and allowed mat and landing gear to slide together along with parts of the torn vinyl water barrier. This severe loading, possible because of the high coefficient of friction between the wheels and mat surface, represents about twice the loading possible in the prototype, in which friction and brake pressures do not permit this high deceleration rate.

Longitudinal movement continued to occur with each landing. The total movement recorded for 15 landings is shown in Figure 5.5. At the 20-ft station nearly 7 in. of movement was recorded without any distress being observed on the mat. This large movement is possible because of sliding along the 45-degree joint as well as by adjustment of joint spacing. Sliding along the longitudinal mat joint is not correctly modeled since sliding would be greater in the prototype mat than was observed in the model. The thin material used in the model could not be formed into a joint which would remain straight enough to correctly model lateral sliding. The resistance to this sliding would have to be increased for a satisfactory prototype installation.

## 5.4 Dyess Pattern with Modified Friction

In the prototype the coefficient of friction between the AM2 mat and the herculite-covered subgrade is about 0.5 while the coefficient of friction between the tires and mat is about 0.6 (Ref. 1). This suggests

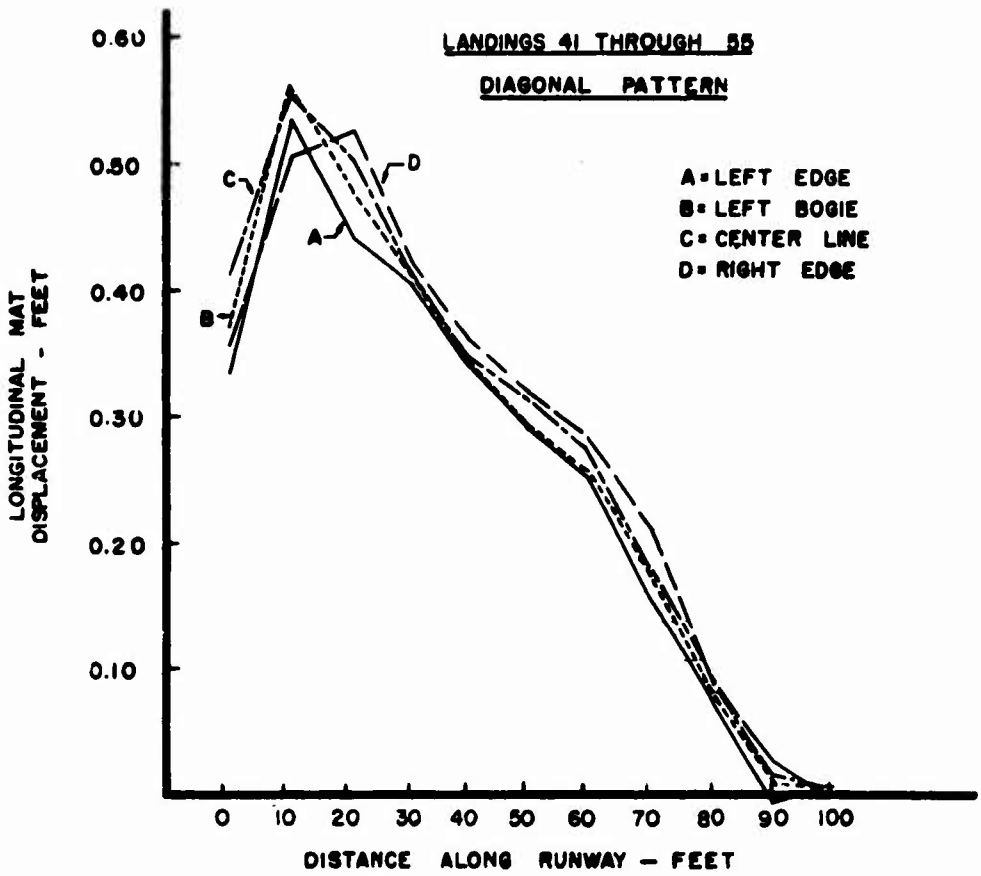


Figure 5.5. Longitudinal Displacement of Mat Placed in 45 Degree Diagonal Pattern.

that improvement in mat behavior could be obtained by increasing the coefficient of friction of the underside of the mat. To test this hypothesis the bottom surfaces of the model AM2 mat were coated with epoxy and a fine sand, similar to the coating on the top surface. The resulting coefficient of friction tested on a vinyl surface was about 0.85, an increase of 70%.

The mat was assembled using the Dyess-type pattern. The model was adjusted to land left of the runway centerline. A grid system of gage

points was established on the runway to monitor changes in joint spacing. Transducers were located along the left edge of the mat to record mat movement. Absolute movement at four positions across the mat was measured from 10-ft reference points (a fixed grid system) along each side of the runway.

Failure of this runway occurred on the fourth landing. General behavior of the mat was like that of the mat without increased friction (see Figure 5.6). The plot of mat displacements is also in Section IV (Figure 4.6) because these results are similar to those of mats without increased bottom friction. Results of these tests give a clearer picture of the compression zone build up and eventual failure of the mat. Approximately 40 rows of mats were in the tightly compressed zone just before failure. The mat showed increased resistance to sliding but this was not enough to prevent the development of a compression zone in the mat and an eventual buckling failure. One difference noted was that the mat behind the failure zone did not slide as far as the mats in the first series of tests without the increased bottom friction. This made the break relatively easy to repair.

It should be noted that the average deceleration for these runs was not higher than 7.5 ft/sec$^2$, much less than the 10 ft/sec$^2$ to 17 ft/sec$^2$ deceleration applied to the runway restrained with bands or the diagonal lay pattern.

## 5.5 Cleated Mats

Cleats attached to the bottom of the mat sections are a means of greatly increasing resistance to longitudinal movement. Since the cleat

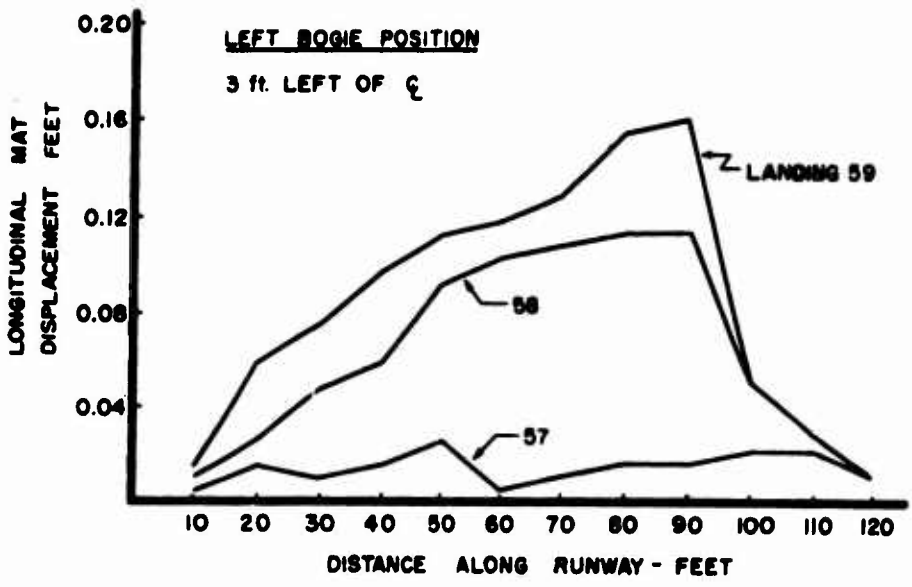


Figure 5.6. Displacement During Three Landings Prior to Failure (Mat With Increased Bottom Friction).

penetrates into the subgrade soil, this device would present problems in maintaining a waterproof barrier to protect the subgrade soil.

A model runway was constructed using the Dyess pattern, but with a 3/4-in. cleat attached to the bottom of every sixth row of mats. The cleats were made of 0.012-in. thick aluminum bent into a T shape. The

stem of the T consisted of two thicknesses of aluminum. The cleats extended the full length of the mat and were attached by 8 rivets (Figure 5.7).

A series of tests on a line of mats of only one mat width were used to select the spacing for the cleated mats. A small model representing one of the main gears of the C-5A was towed slowly down the line of mats with wheels locked. When the cleated mats were spaced further than every tenth row there was an increasing tendency to buckle or lift the mat from the surface. With a five-mat spacing there was no buckling tendency evident and mats remained in contact with the surface. The six-mat spacing was selected for constructing the model runway.

The soil surface was covered with a piece of 6-mil polyethylene to simulate the herculite covering of the prototype. When placing a row of cleated mats, a knife was used to cut through the plastic and form a groove in the soil to receive the cleat. The bottom of all mats used in this test were coated with the epoxy and sand high friction surface.

The runway failed by buckling on the eighth test landing. Figure 5.8 is a photograph of the damaged runway. The cumulative displacement for these tests is plotted in Figure 5.9. For the first two landings the longitudinal displacement was very small, demonstrating the effectiveness of the cleats. With successive landings small movements developed causing the cleated mats to be lifted slightly and then pushed back down as the wheels of the model passed. The weight of the model pushing the cleats into the soil gradually bent the cleats till they were flat against the bottom of the mat (Figure 5.10). Portions of the cleats not directly under the wheels were not bent, however they had been partially lifted out of the ground and their resistance to sliding was small.

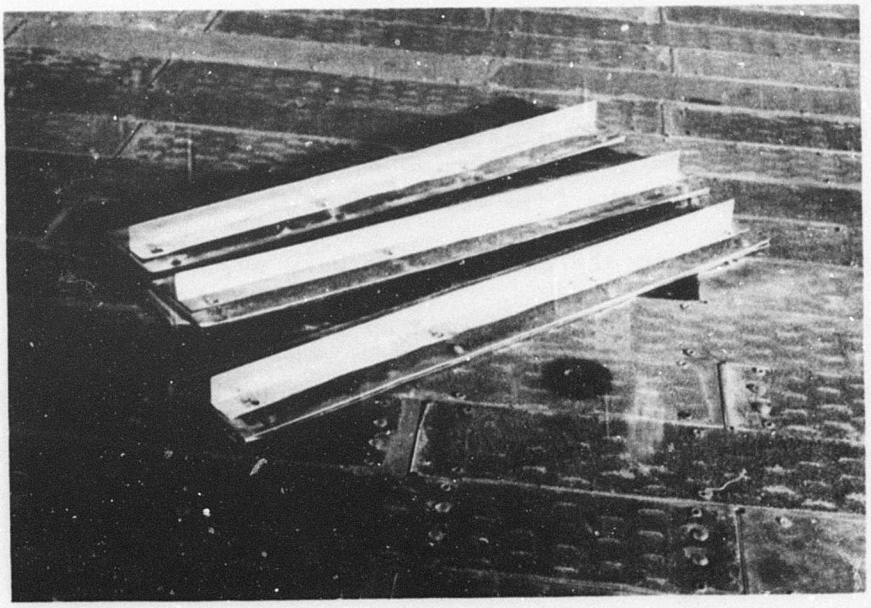

Figure 5.7. Mat Sections with Cleats Attached.

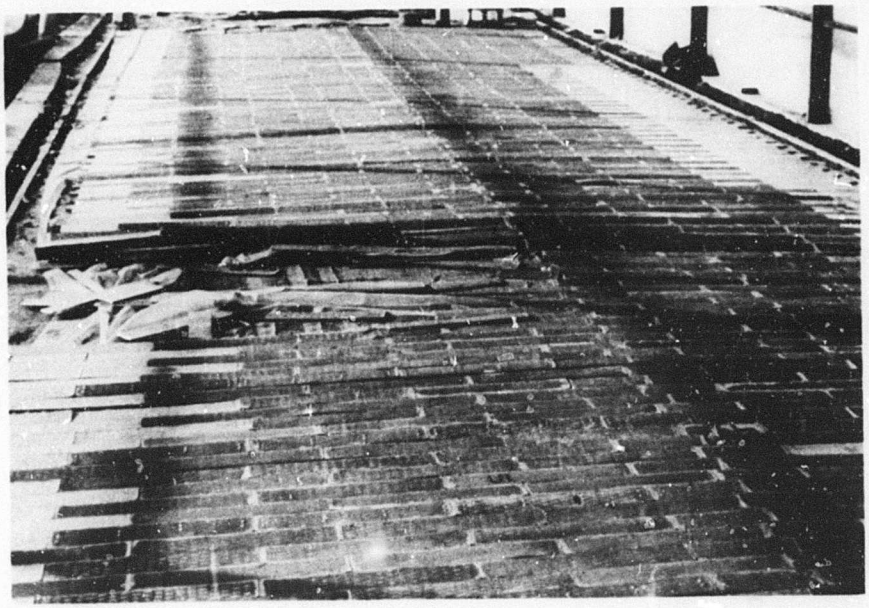

Figure 5.8. View of the Failure of the Cleated Mat Runway.

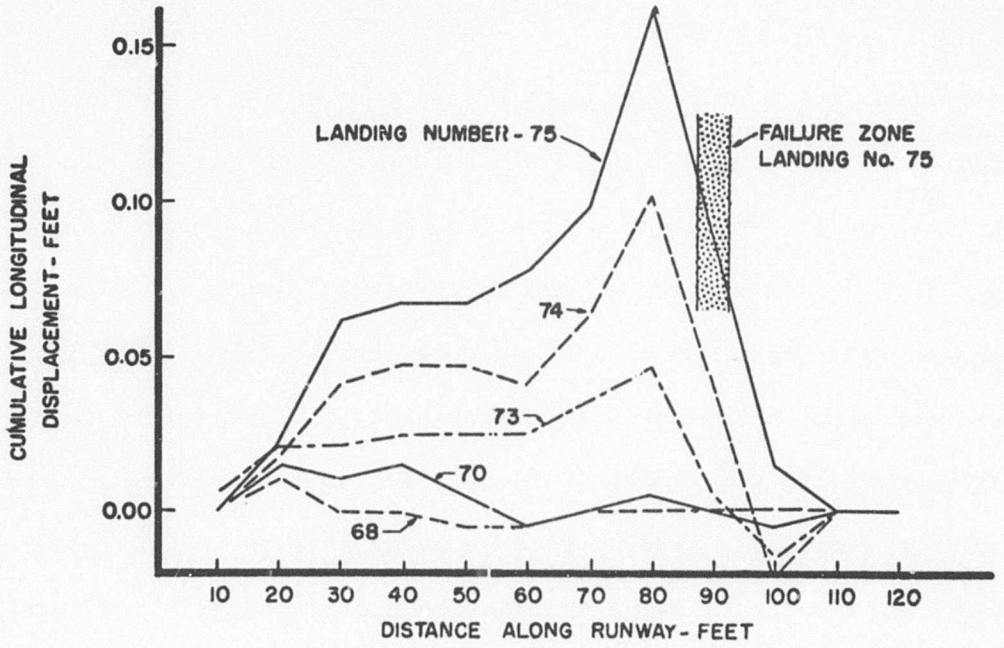


Figure 5.9. Cumulative Displacement of the Cleated Mat Runway.

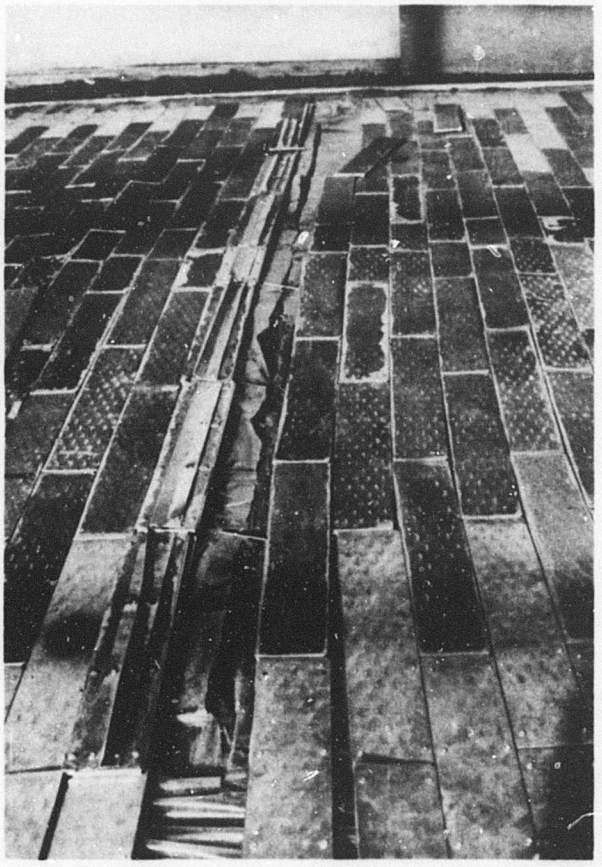

Figure 5.10. Row of Cleated Mats Turned Over to Show Bent Cleats Under the Wheel Path.

The path of the model landing gear was left of center as for the other test landings. The rates of deceleration ranged from 5 ft/sec$^2$ to 10 ft/sec$^2$. The longitudinal displacement was greatest on the left side of the runway. On the right side of the runway small cumulative displacements opposite the direction of landing were observed (up to 1/4 in.).

A stiffer cleat which could be pushed back into the soil without bending would be more effective, but it is believed that longitudinal movement would continue eventually leading to a buckling failure. Other possible improvements in the cleat design include the use of longer cleats or the use of tie-downs to hold the cleats in tight contact with the soil.

## 5.6 Longitudinal Stiffeners

Since rotation about the hinged joints is one factor leading to the buckling failures, stiffening of these joints was suggested as a means of preventing runway buckling. The analytical model shows that increasing the rigidity of the individual transverse joints would decrease the possibility of bow wave formation. Also, the use of stiffeners would tie groups of mats together and thereby increase the moment of inertia of the runway, further reducing the buckling tendency.

For this series of tests the runway joints were stiffened by riveting three parallel rows of mat units longitudinally over the length of the runway (Figure 5.11). The runway was assembled in the Dyess pattern. The stiffening rows of mat were located so the model wheels positioned left of the runway centerline would travel between the rows of stiffeners. Each longitudinal stiffener crossed six transverse joints but still left one or two joints between sections relatively free to rotate. However

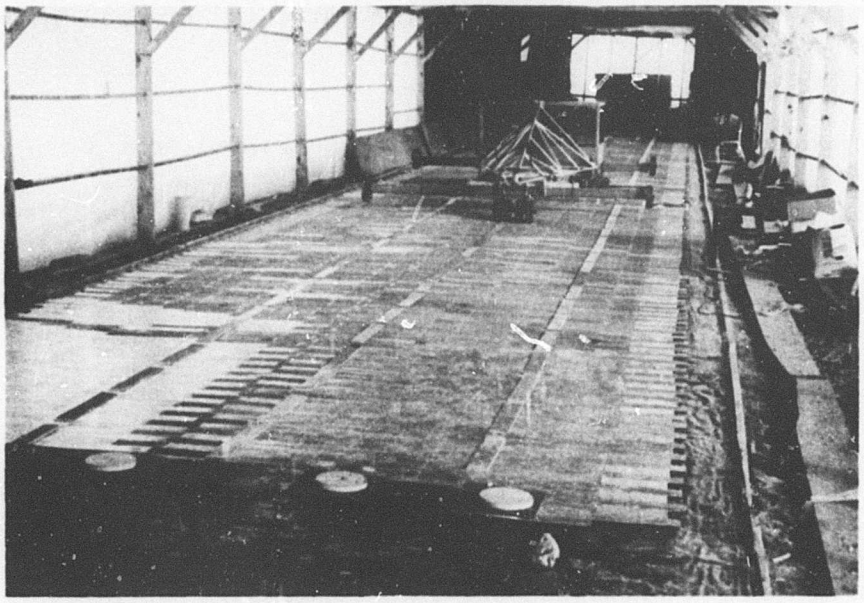

Figure 5.11. View of the Runway with Three Rows of Stiffeners.

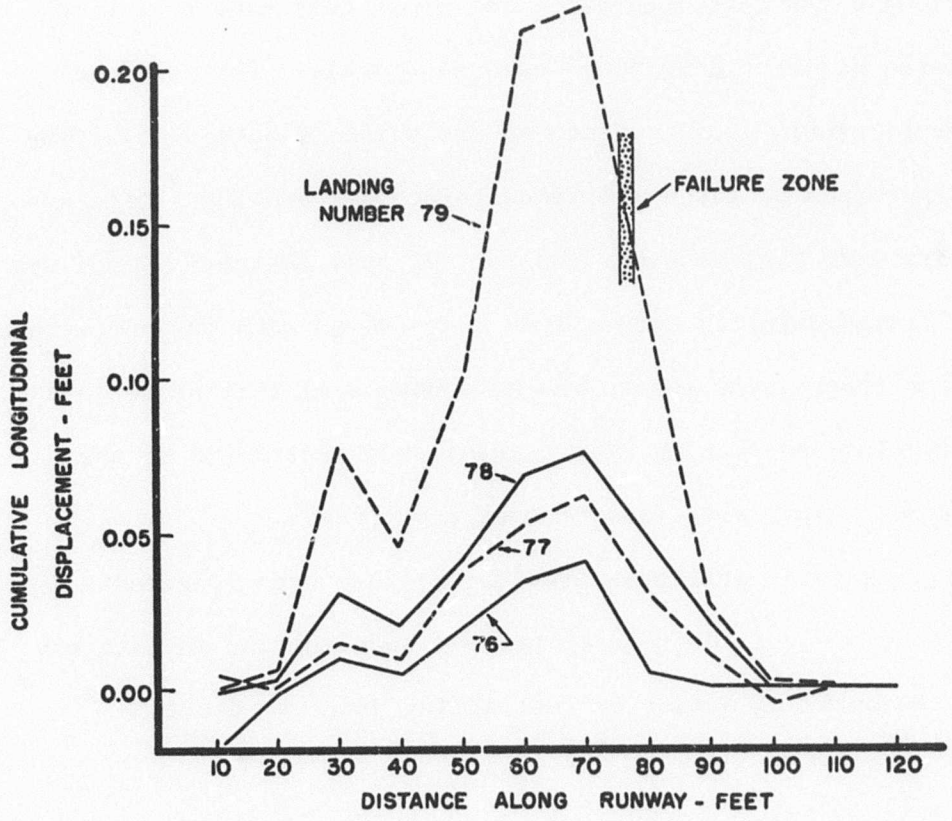


Figure 5.12. Cumulative Displacement of Stiffened Mat Runway.

by staggering the stiffeners each transverse joint was crossed by at least two stiffeners.

Deceleration rates for this series of tests varied from 5 ft/sec$^2$ to 8 ft/sec$^2$. A buckling failure occurred on the fourth landing of this test series. Longitudinal movement and a build-up of the compression region was observed on the first landing (landing 76 on Figure 5.12). The potential failure zone was identified by the compressed mats between stations 70 and 90 after the third landing (landing number 78 on Figure 5.12). Numerous joints were pulled apart in tension and at each of four locations five or six mat sections were torn loose and displaced. Photographs of the damaged runway are shown in Figures 5.13 and 5.14. The number of displaced panels was less than for previous failures because the stiffeners held the mats together. The model gear came to a stop against the large bow wave involving seven mat panels. The stiffener holding the seven panels was bent into an arc shape (Figure 5.15). The initial buckling began at the unstiffened joints between the stiffeners. Because the mats were tied together the initial wave action involved six or seven mats lifted together rather than just two as with the unrestrained mat runway. The compression region may have developed earlier because longitudinal opening and closing of mat joints was restricted by the stiffeners. Fewer joints were free to open and close.

The additional joint stiffness provided by the three longitudinal stiffeners was obviously inadequate to prevent buckling and in fact may have hastened the buckling action by restricting joint movement.

Figure 5.13. View of Damaged Stiffened Mat Runway.

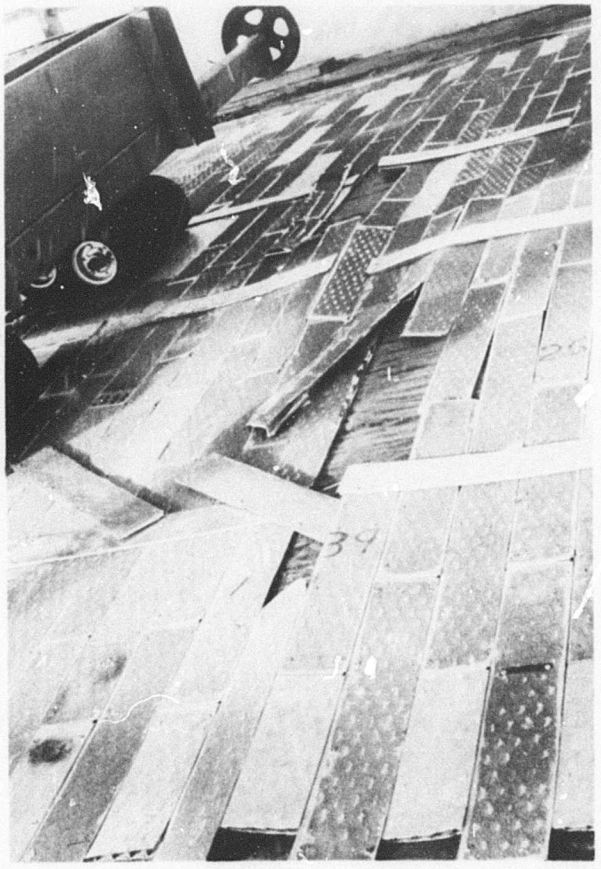

Figure 5.14. Close Up of Damaged Stiffened Mat Runway.

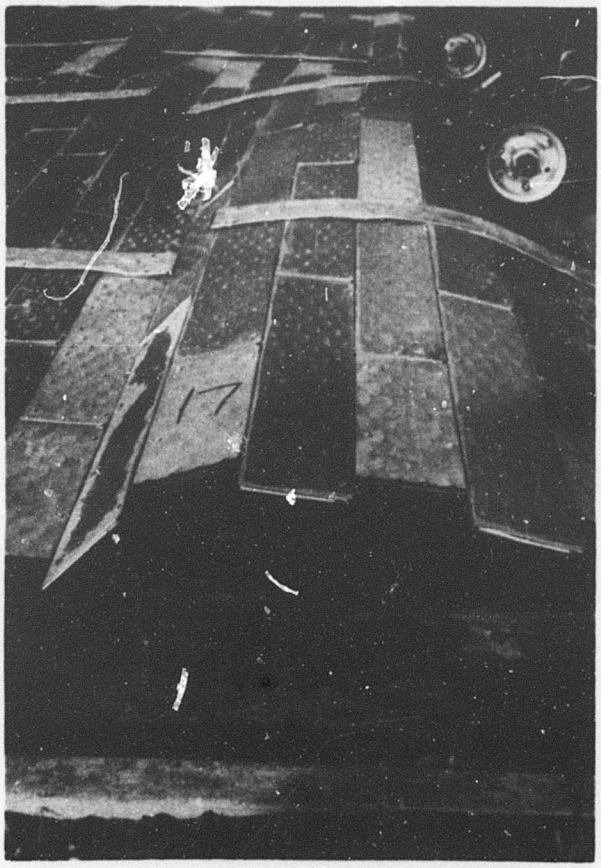

**Figure 5.15.** Bow Wave Left in the Runway After Failure of the Stiffened Mat.

SECTION VI

DISCUSSION AND CONCLUSIONS

## 6.1 Discussion

### 6.1.1 Problem

Runways constructed of AM2 landing mat placed in the standard brick-type laying pattern (the Tri-Service runway at Dyess AFB) have served adequately for aircraft much lighter than the C-5A. However, the large horizontal braking force of the C-5A caused the mat to buckle.

### 6.1.2 Models Developed

An analytical model and a 1/7 scale physical model were developed to study the behavior of the mat under dynamic loading and evaluate means of preventing the buckling failure. Test landings of the model C-5A landing gear on a runway constructed of model AM2 landing mat demonstrated that the model simulated the behavior of the prototype landing at Dyess AFB. The analytical model also demonstrated the mat buckling phenomena and was used to evaluate changes in mat parameters.

### 6.1.3 Analytical Model

The analytical model represents an expedient and inexpensive method by which the dynamic mat response as related to mat modifications and surface conditions can be evaluated. Several such mat conditions and loadings were analyzed by applying the 12,000 lb horizontal thrust produced by the two lead wheels of a bogie to a single column of mat in front of the wheels. The point of application of the thrust was

moved from mat to mat with the velocity of the aircraft. It was found that if the AM2 mat joints were sufficiently compressed longitudinally to approximate the elasticity of a continuous solid plate, then surface irregularities involving one or more mats with a maximum vertical displacement of 3/16 in. from the horizontal would produce buckling. Relative displacement between adjacent joints was critical.

An elastic compressibility constant at the joint in the longitudinal direction of $8(10)^6$ lb/ft seemed to best simulate the longitudinal displacement of the AM2 mat as compared to the physical model when buckling did occur. Again in the less compressed mat under similar conditions it was found that a surface irregularity of 3/16 in. would eventually result in buckling, although the rate of bow wave formation was slower. If the joint compressibility is only $16(10)^4$ lb/ft, which would allow for considerable relative longitudinal displacement, buckling did not occur.

The analytical model shows the effect of moment rigidity at the joint. The apex of an inverted vee involving two mats initially, will continue to move vertically when subjected to horizontal thrust until the relative angle of free rotation (approximately 10 degrees) is exceeded. At that time, the moment rigidity at the joint is initiated and the vertical motion of the apex is slowed down while additional mats are being lifted. The result is a bulge rather than a sharp vee. It was shown that if the free rotation angle of the joint were reduced from approximately 10 degrees to 1 degree, then surface irregularities of 3/16 in. which normally produce buckling in AM2 mat would not produce a bow wave. It is noted, however, that stiffeners along the mat surface would increase the moment rigidity, but would not allow for relative longitudinal displacement of the joint. Some physical

arrangement to decrease the angular freedom, yet allow relative longitudinal displacement would be recommended. It was also found that by increasing the width of the mat the moment of inertia increases and the mat rotation is decreased significantly.

The analytical model determined that the bow wave formation is essentially independent of the coefficient of friction between mat and subgrade. This does not imply that total mat migration is independent of friction, nor the compressibility at the joint after repeated landings.

The horizontal thrust is definitely significant in bow wave formation. There is some difficulty in estimating the magnitude of thrust passed from a bogie to a single column of mat in front of the two lead wheels. The analytical model showed, for example, that an initial bump of approximately 3/16 in. would result in a bow wave of approximately 3 in. in height when subjected to 12,000 lb thrust, but a wave over 1 ft in height resulted when the mat was subjected to 24,000 lb thrust. These vertical displacements were taken at the same time increment after touchdown of the aircraft.

In addition to the results obtained for a single column of mat taken in front of the lead wheels of a bogie, mat elements were considered that extended the complete width of the landing strip. The total thrust of 144,000 lb was applied to the series of 96 x 2 ft elements. The model parameters were assigned values to simulate AM2 mat response and the surface irregularity was specified as 1/4 in. The model showed a bow wave formation for the 144,000 lb thrust, but no buckling occurred when the same mat was subjected to only 40,000 lb thrust, which is that produced by a C-130.

The analytical model does have limitations. The determination of model parameters requires some approximations. As mentioned, the exact description of the thrust per wheel and the particular number of mats influenced by each wheel is difficult. The initial velocity experienced by the mat upon touchdown of the aircraft is not readily calculated, even though it appears as a simple impulse-momentum problem. The initial velocity is best determined by measurement of the prototype. The joint discontinuity and the free translation and rotation are also difficult to simulate. Nevertheless, the analytical model predicted results that were experienced by the physical model and the prototype. It provides a supplemental tool along with the physical model. The computer program is available and could be used to help predict the mat response as a result of additional modifications, surface conditions and other situations that might arise.

### 6.1.4 Physical Model Mat Response

The major weaknesses of the AM2 mat placed in the standard pattern are its short dimension normal to the direction of traffic (2 ft) and the transverse hinges provided by the joints. For a buckling failure to occur there must be sufficient longitudinal displacement in the runway to create a region of compressed mats where the joints are tightly closed. Displacements of 1/16 in. to 1/4 in. were measured with each model landing on unrestrained mat runway. Comparable data for prototype mat displacement is not known.

Model data show that a compression wave moves down the mat ahead of the aircraft. When the aircraft stops or the brakes are released, the compression wave remains at that point in the runway. If other compression

waves are pushed to the same area a longer section of compressed mat develops. Small two-panel waves were observed to increase in number and height with successive model landings. The weight of the aircraft pushing down a small two-panel wave exerts a large longitudinal force in the runway. The weight of the aircraft on the mat behind as well as the impact of the wheels on the raised panel would force movement of the panels ahead. If the joints ahead are closed, waves are produced down field. The impact of the wheels on the raised panels increases the horizontal force on the mat causing more displacement and higher waves down field. The impact of the wheels on these high waves provides the force necessary to cause the large displacement measured in both the prototype and model runways during buckling failures.

The mat action described was observed in several model failures. Measurements of each failure showed that buckling failure occurred 10 to 15 panel widths inside a zone of 50 to 60 compressed mats. Measurements of displacements during the Dyess failure suggest a similar type action.

It is the horizontal braking force of the aircraft that causes the longitudinal movement leading to the potential buckling condition. Experience with lighter aircraft (C-141A and C-130) on the Dyess test runway suggests that they do not produce a horizontal force large enough to buckle the mat. It is also possible that critical lengths of compressed mats did not develop in the runway during the tests. Without prototype displacement measurements the condition of Dyess test runway is not known.

The critical force required to produce buckling in the AM2 mat is therefore less than the braking force of the C-5A and may be greater than that of the C-141A. The analytical study shows that the critical buckling

force is dependent upon the mat size and weight, joint stiffness, the magnitude of an initial mat irregularity or misalignment and the number of mat panels in compression.

### 6.1.5 Mat Runway Modificiations

For an AM2 mat runway to safely permit landing of heavier aircraft like the C-5A, one or more of the factors leading to failure must be controlled. Longitudinal movement and joint rotation are two factors which can be reasonably controlled without involving a complete redesign of the mat sections.

Three mat modifications tested in this study restricted longitudinal movement: (1) longitudinal pretensioned bands, (2) cleats attached to the bottom of mat panels, (3) increased friction on the bottom of the mat.

Two modifications were studied which restricted joint rotation: (1) the mat in a 45-degree pattern, (2) longitudinal stiffeners attached to the top of the mat.

### 6.1.6 Pretensioned Bands

Model tests demonstrated that the longitudinal movement was controlled by attaching the mats to pretensioned bands stretched the length of the runway. The bands transferred the horizontal braking force to anchors at the end of the runway behind the aircraft. No buckling failures occurred during the 34 test landings on banded runway despite deceleration rates up to 13 $ft/sec^2$.

Tests indicated that the bands should be designed to take the full braking force of the aircraft. Attaching the band to every $10^{th}$ to $20^{th}$ mat was determined to be satisfactory.

The length of bands between anchor points is limited by build-up of residual friction in the mat which could reduce the force in a band to zero at one end. If the band were to go slack, longitudinal movements large enough to produce buckling could occur. A detailed analytical study is required before specific values or limits for a prototype band system can be established. However, a design example based on simplifying assumptions is given in Appendix C.

In the model mat the tension bands were placed on top of the mat but could have been placed beneath the mat.

### 6.1.7 Modified Friction

Tests on model AM2 mat with increased bottom friction showed there was no significant improvement in the stability of the runway with the Dyess-type pattern. Longitudinal mat movement was slightly reduced but still allowed the development of a compression region and a buckling failure. Results from the analytical model also bear out this conclusion.

### 6.1.8 Cleated Mat Runway

Three-quarter-in. long cleats attached to the bottom of every sixth row of mat runway provided additional sliding resistance. Longitudinal movement was small on the initial landings, but increased with each landing till a buckling failure occurred. The cleats were raised then pushed down and finally bent flat against the mat. Although the portions of the cleats to either side of the wheel path were not bent, they were lifted out of the ground and were not effective.

### 6.1.9 Diagonal Mat Pattern

The model runway constructed of panels in a 45-degree diagonal pattern was definitely more stable than the standard brick-type pattern. Deceleration rates up to 17 ft/sec$^2$ caused no buckling. However longitudinal displacement and distortion of the runway occurred with each landing. With higher deceleration rates there was some tendency for the mats to slip along the 45-degree joint. This problem would be more severe in a prototype runway because the prototype mat has a lower sliding resistance along this joint than is represented by behavior of the model mat.

### 6.1.10 Runway with Longitudinal Stiffeners

Three lines of mat units were riveted to a model runway assembled in the standard brick-type pattern. The mat units were staggered so that each transverse joint was crossed by at least two stiffeners. This additional joint stiffness was not sufficient to prevent a buckling failure. A zone of compressed mat developed and buckled on the fourth landing.

## 6.2 Conclusions

1. Both the physical model and the analytical model are useful in studying dynamic behavior of landing mats. The analytical model simulated the response of the physical model when experimentally determined parameters for the physical model were programmed.
2. The physical model demonstrated that on unrestrained AM2 mat runways longitudinal displacement occurs for braking forces as low as 40% the normal C-5A braking force.

3. The buckling potential exists in zones of compressed mat formed by accumulative displacements.
4. The critical force required to buckle the AM2 mat in the standard brick-type pattern depends upon the initial mat irregularities and the number of mats in a compressed state. Irregularities in the mat surface are potential locations for the formation of bow waves. The wave development is dependent upon the magnitude of the initial vertical deflection and the number of mats involved.
5. Physical model tests demonstrated that the use of pretensioned bands was an effective means of preventing buckling failure of AM2 landing mat runways with C-5A landings.
6. Both the analytical and physical model demonstrated that increasing the coefficient of friction on the bottom of the mat does not prevent longitudinal displacement or buckling failure of the runway.
7. Cleated mats offer a practical means of preventing longitudinal mat movement if tied down by anchors. This idea merits further study.
8. Physical model tests demonstrated that an AM2 mat runway placed in a 45-degree pattern will not buckle with C-5A landings. However, severe maintenance problems would be expected with repeated landings because of longitudinal displacement and displacement due to sliding along the 45-degree joint.
9. Model tests with longitudinal stiffeners that restricted both rotation and relative translation were not effective in preventing mat failure. However, other patterns for stiffeners that would allow some relative longitudinal displacement should be investigated further. A reduction

in the relative rotation allowable at a joint before rotational rigidity is encountered would greatly inhibit the formation of bow waves.

## APPENDIX A

### A.1 Development and Details of the Mathematical Model

A free body diagram of the first mass is shown in Figure A.1.

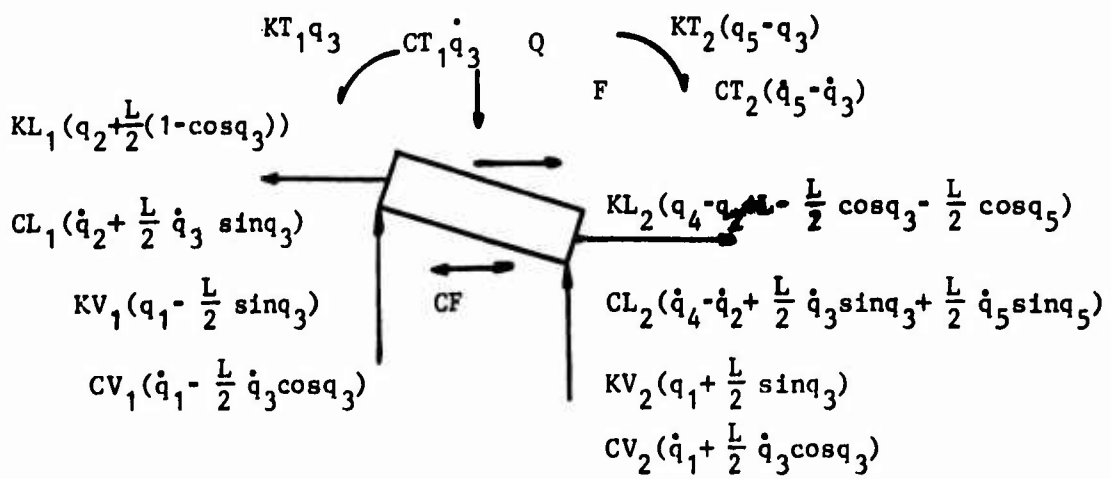


Figure A.1. Free Body Diagram of the First Mass.

Summation of vertical forces results in the equation

$$m_1\ddot{q}_1 = -[KV_1(q_1 - \tfrac{L}{2}\sin q_3) + KV_2(q_1 + \tfrac{L}{2}\sin q_3)$$

$$+ CV_2(\dot{q}_1 + \tfrac{L}{2}\dot{q}_3\cos q_3)] + Q + CV_1(\dot{q}_1 - \tfrac{L}{2}\dot{q}_3\cos q_3) \qquad \text{(A-1)}$$

where the notation for time derivatives is used throughout as

$$\frac{dq_1}{dt} = \dot{q}_1 \,, \quad \frac{d^2q_1}{dt^2} = \ddot{q}_1$$

and L is the length of the element. The mat thickness is assumed small. Summation of horizontal forces in the longitudinal direction yields

$$m_1\ddot{q}_2 = -KL_1q_2 - CL_1\dot{q}_2 - CL_2(\dot{q}_2-\dot{q}_4) - KL_2(q_2-q_4) - CF(\text{sign } \dot{q}_2) + F$$

$$+\frac{L}{2}\left[-KL_1(1-\cos q_3) - CL_1\dot{q}_3\sin q_3 + KL_2(1-\cos q_3) + KL_2(1-\cos q_5)\right.$$

$$\left. + CL_2(\dot{q}_3\sin q_3 + \dot{q}_5\sin q_5)\right] \qquad \text{(A-2)}$$

The terms included within the dotted brackets show the effect of rotation on the horizontal springs and dashpots. These terms will eventually be neglected in order to simulate the free longitudinal displacement allowable at the joint. Equating moments about the center of mass to the time rate of change of angular momentum one obtains:

$$I_1\ddot{q}_3 = -CT_1\dot{q}_3 - CT_2(\dot{q}_3-\dot{q}_5) - CL_1\dot{q}_2\frac{L}{2}\sin q_3 + CL_2(\dot{q}_2-\dot{q}_4)\frac{L}{2}\sin q_3$$

$$+ CV_1(\dot{q}_1 - \frac{L}{2}\dot{q}_3\cos q_3)\frac{L}{2}\cos q_3 - CV_2(\dot{q}_1+\dot{q}_3\frac{L}{2}\cos q_3)\frac{L}{2}\cos q_3$$

$$- KT_1q_3 - KT_2(q_3-q_5) - KL_1q_2\frac{L}{2}\sin q_3 + KL_2(q_2-q_4)\frac{L}{2}\sin q_3$$

$$+ KV_1(q_1 - \frac{L}{2}\sin q_3)\frac{L}{2}\cos q_3 - KV_2(q_1 + \frac{L}{2}\sin q_3)\frac{L}{2}\cos q_3$$

$$-(\frac{L}{2})^2\sin q_3\left[KL_1(1-\cos q_3) + CL_1\dot{q}_3\sin q_3 + KL_2(1-\cos q_3)\right.$$

$$\left. + KL_2(1-\cos q_5) + CL_2(\dot{q}_3\sin q_3 + \dot{q}_5\sin q_5)\right]$$

(A-3)

The moment contribution of the Coulomb friction force was neglected in this equation.

Obviously, the free body diagrams of mass elements other than masses on the ends are essentially identical. This does not imply, however, that the so-called intermediate system parameters are equal, nor are the forces involved by any means equal. A typical sketch of the forces acting on the $n^{th}$ mass is shown in Figure A.2. Since each mat element is rigid and adjoining mat elements are connected, a system of holonomic constraint equations may be written, viz.,

$$Y_1 = q_1 - \frac{L}{2}\sin q_3 \qquad Y_2 = q_1 + \frac{L}{2}\sin q_3$$

$$Y_n = q_1 + \frac{L}{2}\sin q_3 + \sum_{k=3}^{n} L \sin q_{2k-1} \tag{A-4}$$

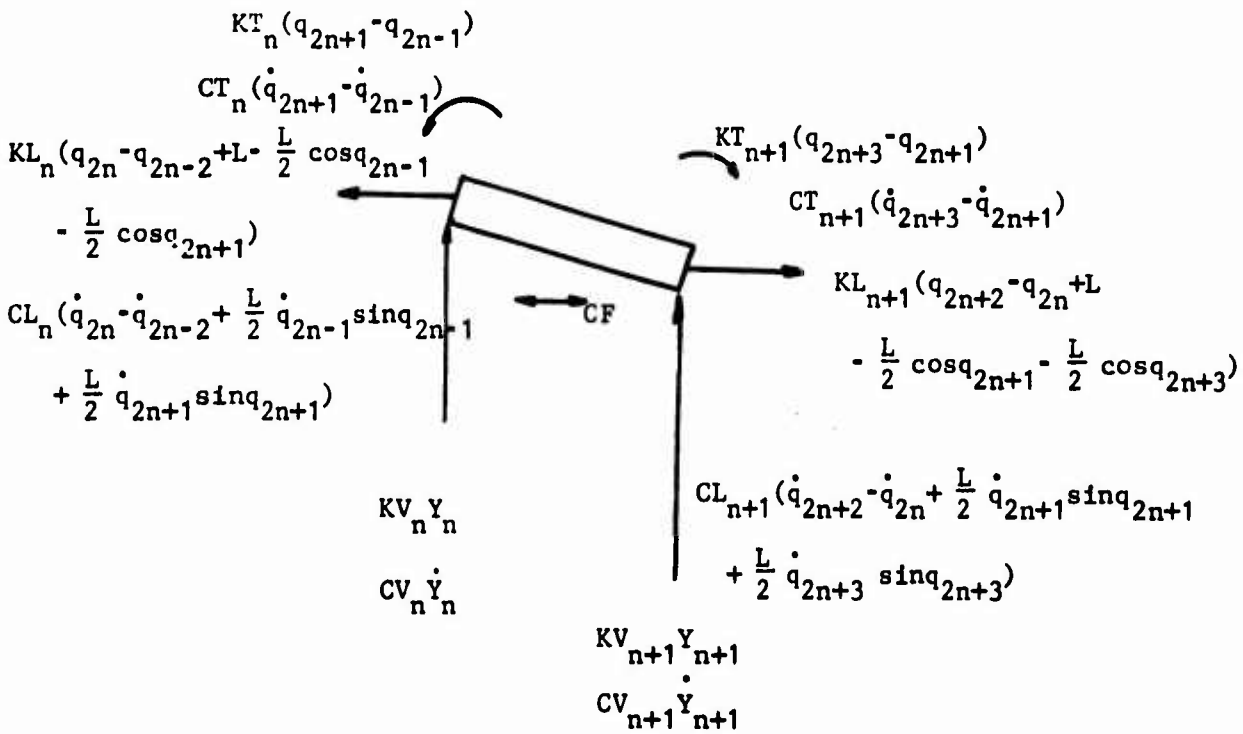


Figure A.2. Free Body Diagram of $n^{th}$ Mass.

where $Y_n$ is the vertical deflection of the left end of the $n^{th}$ mass and N is the total number of mass elements. This constraint condition reduces the number of independent differential equations required to specify the motion.

Summation of forces in the longitudinal direction on the $n^{th}$ mass yields:

$$
\begin{aligned}
m_n\ddot{q}_{2n} = &- KL_n(q_{2n}-q_{2n-2}) - CL_n(\dot{q}_{2n}-\dot{q}_{2n-2}) - KL_{n+1}(q_{2n}-q_{2n+2}) \\
&- CL_{n+1}(\dot{q}_{2n}-\dot{q}_{2n+2}) - CF(\text{sign } \dot{q}_{2n}) \\
&- KL_n\left(L - \tfrac{L}{2}\cos q_{2n-1} - \tfrac{L}{2}\cos q_{2n+1}\right) \\
&- CL_n\left(\tfrac{L}{2}\dot{q}_{2n-1}\sin q_{2n-1} + \tfrac{L}{2}\dot{q}_{2n+1}\sin q_{2n+1}\right) - KL_{n+1}\left(-L + \tfrac{L}{2}\cos q_{2n+1}\right. \\
&\left. + \tfrac{L}{2}\cos q_{2n+3}\right) + CL_{n+1}\left(\tfrac{L}{2}\dot{q}_{2n+1}\sin q_{2n+1} + \tfrac{L}{2}\dot{q}_{2n+3}\sin q_{2n+3}\right) \qquad \text{(A-5)}
\end{aligned}
$$

By equating moments to angular momentum change on the $n^{th}$ mass, one obtains:

$$
\begin{aligned}
I_n\ddot{q}_{2n+1} = &- \tfrac{L}{2}\sin q_{2n+1}\left[KL_n(q_{2n}-q_{2n-2}) + CL_n(\dot{q}_{2n}-\dot{q}_{2n-2}) + KL_{n+1}(q_{2n+2}-q_{2n})\right. \\
&\left. + CL_{n+1}(\dot{q}_{2n+2}-\dot{q}_{2n})\right] + \tfrac{L}{2}\cos q_{2n+1}(KV_nY_n + CV_n\dot{Y}_n) - \tfrac{L}{2}\cos q_{2n+1}\,(KV_{n+1}Y_{n+1} \\
&+ CV_{n+1}\dot{Y}_{n+1}) - KT_n(q_{2n+1}-q_{2n-1}) - CT_n(\dot{q}_{2n+1}-\dot{q}_{2n-1}) + KT_{n+1}(q_{2n+3}-q_{2n+1}) \\
&+ CT_{n+1}(\dot{q}_{2n+3}-\dot{q}_{2n+1}) \\
&- \tfrac{L}{2}\sin q_{2n+1}\left[KL_n\left(1 - \tfrac{L}{2}\cos q_{2n-1} - \tfrac{L}{2}\cos q_{2n+1}\right) + CL_n\left(\tfrac{L}{2}\dot{q}_{2n-1}\sin q_{2n-1}\right.\right. \\
&\left. + \tfrac{L}{2}\dot{q}_{2n+1}\sin q_{2n+1}\right) + KL_{n+1}\left(L - \tfrac{L}{2}\cos q_{2n+1} - \tfrac{L}{2}\cos q_{2n+3}\right) \\
&\left. + CL_{n+1}\left(\tfrac{L}{2}\dot{q}_{2n+1}\sin q_{2n+1} + \tfrac{L}{2}\dot{q}_{2n+3}\sin q_{2n+3}\right)\right] \qquad \text{(A-6)}
\end{aligned}
$$

Again it is noted that no moment is contributed by the Coulomb friction force.

The free body diagram for the last mass is shown in Figure A.3.

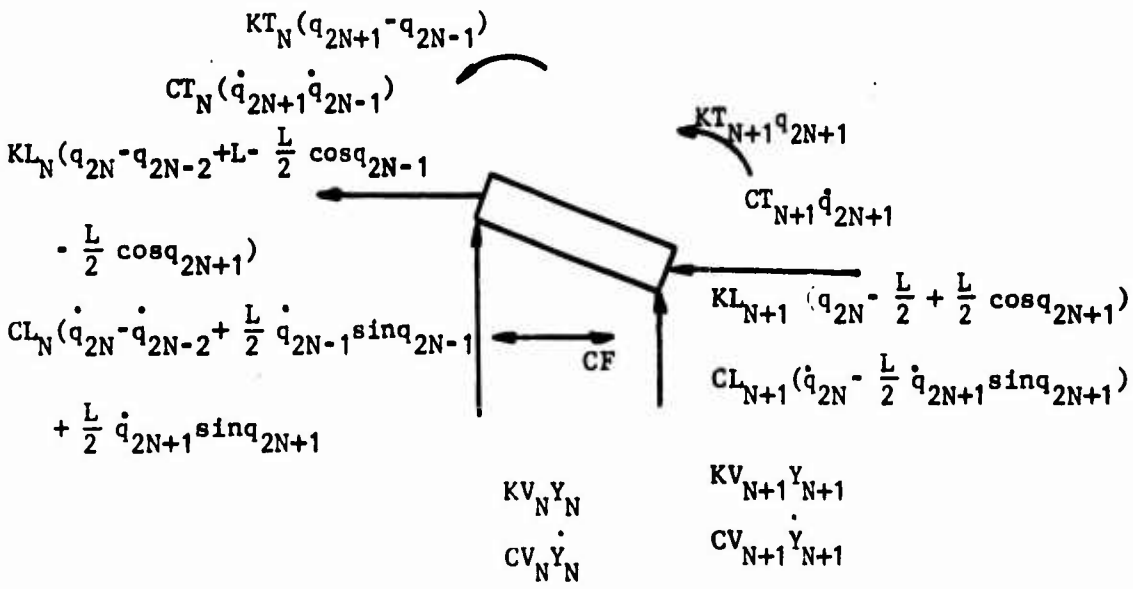


Figure A.3. Free Body Diagram of the Last Mass.

Equating the summation of forces in the horizontal direction to the product of mass and acceleration gives:

$$m_N\ddot{q}_{2N} = -CL_N(\dot{q}_{2N}-\dot{q}_{2N-2}) - CL_{N+1}\dot{q}_{2N} - KL_N(q_{2N}-q_{2N-2}) - KL_{N+1}q_{2N} - CF(\text{sign}\ \dot{q}_{2N})$$
$$+ \frac{L}{2}[-KL_N(1-\cos q_{2N-1}) - KL_N(1-\cos q_{2N+1}) - CL_N(\dot{q}_{2N-1}\sin q_{2N-1}$$
$$+ \dot{q}_{2N+1}\sin q_{2N-1}) + KL_{N+1}(1-\cos q_{2N+1}) + CL_{N+1}(\dot{q}_{2N+1}\sin q_{2N+1})] \quad \text{(A-7)}$$

Using the equation $\Sigma M_N = I_N \ddot{q}_{2N+1}$ on the last mass N, one obtains

$$I_N\ddot{q}_{2N+1} = -\frac{L}{2}\sin q_{2N+1}\left[KL_N(q_{2N}-q_{2N-2})+CL_N(\dot{q}_{2N}-\dot{q}_{2N-2}) - KL_{N+1}q_{2N} - CL_{N+1}\dot{q}_{2N}\right]$$

$$+\frac{L}{2}\cos q_{2N+1}\left[KV_N Y_N + CV_N\dot{Y}_N - KV_{N+1}Y_{N+1} - CV_{N+1}\dot{Y}_{N+1}\right] - KT_N(q_{2N+1}-q_{2N-1})$$

$$- CT_N(\dot{q}_{2N+1}-\dot{q}_{2N-1}) - KT_{N+1}q_{2N+1} - CT_{N+1}\dot{q}_{2N+1} \quad \boxed{- \frac{L}{2}\sin q_{2N+1}\left[KL_N\left(L\right.\right.}$$

$$\boxed{\left. - \frac{L}{2}\cos q_{2N-1} - \frac{L}{2}\cos q_{2N+1}\right) + CL_N\left(\frac{L}{2}\dot{q}_{2N-1}\sin q_{2N-1} + \frac{L}{2}\dot{q}_{2N+1}\sin q_{2N+1}\right)}$$

$$\boxed{\left. + KL_{N+1}\left(\frac{L}{2} - \frac{L}{2}\cos q_{2N+1}\right) + CL_{N+1}\left(\frac{L}{2}\dot{q}_{2N+1}\sin q_{2N+1}\right)\right]} \qquad \text{(A-8)}$$

Using the constraint equations, for the system of N discrete masses, each of which has 3 degrees of freedom, there are 2N + 1 nonlinear second order differential equations. The equations are coupled.

The 2N + 1 nonlinear differential equations of motion were also derived using Lagrange's equation in the form

$$\frac{d}{dt}\left(\frac{\partial T}{\partial q_i}\right) - \frac{\partial T}{\partial q_i} + \frac{\partial D}{\partial q_i} + \frac{\partial V}{\partial q_i} = Q_i \qquad \text{(A-9)}$$

where

$q_i$ ≡ Generalized coordinate

T ≡ Kinetic energy of the system

D ≡ Dissipative function associated with damping

V ≡ Potential function associated with elastic springs

$Q_i$ ≡ All generalized forces excluding those included in D and V

A four mass system was considered and the equations were in agreement with those equations derived using Newton's laws. This energy method was cumbersome and involved numerous routine calculations, therefore it will not be presented in detail.

## A.2 Reduction of Equations of Motion to First Order

A change of variables was required to reduce the 2N + 1 second order differential equations to 2 x (2N + 1) first order differential equations in order to obtain a numerical solution. The generalized coordinates $q_n$ and the time derivatives $\dot{q}_n$ were changed as follows:

$$
\begin{aligned}
q_1 &= \bar{Y}_1 \\
\dot{q}_1 &= \bar{Y}_2 \\
q_2 &= \bar{Y}_3 \\
\dot{q}_2 &= \bar{Y}_4 \\
&\vdots \\
q_n &= \bar{Y}_{2n-1} \\
\dot{q}_n &= \bar{Y}_{2n} \\
&\vdots \\
q_N &= \bar{Y}_{2N-1} \\
\dot{q}_N &= \bar{Y}_{2N}
\end{aligned}
\qquad \text{(A-10)}
$$

Since the substitution of the above variables into the second order equations of motion is straightforward, the procedure will be demonstrated by reducing only equation A.2 to a first order equation. The other equations follow in a similar manner, but will not be written.

$$
\begin{aligned}
m_n \dot{\bar{Y}}_{4n} = &- KL_n(\bar{Y}_{4n-1} - \bar{Y}_{4n-5}) - CL_n(\bar{Y}_{4n} - \bar{Y}_{4n-4}) - KL_{n+1}(\bar{Y}_{4n-1} - \bar{Y}_{4n+3}) - CL_{n+1}(\bar{Y}_{4n} \\
&- \bar{Y}_{4n+4}) - CF(\operatorname{sign} \bar{Y}_{4n}) \\
&- KL_n\left(L - \frac{L}{2}\cos \bar{Y}_{4n-3} - \frac{L}{2}\cos \bar{Y}_{4n+1}\right) \\
&- CL_n\left(\frac{L}{2}\bar{Y}_{4n-2}\sin \bar{Y}_{4n-3} + \frac{L}{2}\bar{Y}_{4n+2}\sin \bar{Y}_{4n+1}\right) - KL_{n+1}\left(-L + \frac{L}{2}\cos \bar{Y}_{4n+1}\right.
\end{aligned}
$$

$$+ \frac{L}{2}\cos\bar{Y}_{4n+5}) + CL_{n+1}\left(\frac{L}{2}\bar{Y}_{4n+2}\sin\bar{Y}_{4n+1} + \frac{L}{2}\bar{Y}_{4n+6}\sin\bar{Y}_{4n+5}\right)\Bigg] \qquad \text{(A-11)}$$

If $n = 2$, then $\dot{\bar{Y}}_{4n} = \dot{\bar{Y}}_8$ and corresponds to $\ddot{q}_4$, which is the horizontal acceleration of the second mass as expected. As mentioned earlier, the second order differential equation associated with the horizontal motion of the second mass is replaced by two first order differential equations. The second first order equation for mass 2 follows readily from the variable transformation as

$$\bar{Y}_{4n} = \bar{Y}_{4n-1}$$

Consequently, $2(2N + 1)$ nonlinear first order differential equations are obtained.

## APPENDIX B

## PILOT STUDY

Preliminary to design of the detailed physical model, a pilot model was constructed and tested. The purpose of the pilot model was to obtain some initial insight into the problem of modeling the landing mat using a simple and inexpensive model.

### B.1 Dimensional Analysis and Similitude

For the pilot model the variables shown in Table 1 were considered.

Table B.1. Fundamental Variables Considered in Pilot Study.

| Symbol | Definition | Dimensions FLT |
|---|---|---|
| $\psi$ | performance (bow wave, failure, etc.) | — |
| N | number of runs to form or overrun the bow wave | — |
| f | coefficients of friction | — |
| $\lambda$ | linear distances | L |
| W | weight of aircraft or mat | F |
| $\rho$ | density of materials | $FT^2L^{-4}$ |
| E | stiffness of materials | $FL^{-2}$ |
| g | acceleration of gravity | $LT^{-2}$ |
| v | velocity | $LT^{-1}$ |
| p | tire pressure or material stress | $FL^{-2}$ |

If $\lambda$, $\rho$, and $g$ are selected as repeating variables the following set of dimensionless pi-parameters results.

$$(\psi),\ (N),\ \left(\frac{W}{E\lambda^2}\right),\left(\frac{\rho g\lambda}{E}\right),(f),\left(\frac{v^2}{g\lambda}\right),\left(\frac{p}{E}\right)$$

Expressing $\psi$ as the dependent variable,

$$\psi = \text{function}\left[\left(\frac{W}{E\lambda^2}\right)\ \left(\frac{\rho g\lambda}{E}\right)\left(\frac{v^2}{g\lambda}\right)\ (f)\ \left(\frac{p}{E}\right)\quad (N)\right]$$

To establish pertinent similitude design conditions between model and prototype the three set conditions shown in Table B.1 were considered important. The subscript m refers to the model, no subscript indicates the prototype and the subscript r indicates the prototype to model ratio. For example:

$$\frac{g}{g_m} = g_r = 1$$

The requirement that the density of materials in the model be n times that in the prototype would be difficult to achieve. For the purpose of the pilot model, however, similitude was only approximated for most of the above variables.

## B.2 Pilot Model Construction

A simple model, built to a scale factor of approximately 6.6, was constructed for the pilot study (Figure B.1). The landing mat panels were 24-in. lengths of 1 x 4 lumber, drilled and strung on nylon cords, the cords acting as a flexible hinge between panels. The leading duals of one bogie of the landing aircraft was simulated by two pneumatic tires 8 in. in diameter, mounted on wheels attached to an angle iron frame. Two trailing wheels were attached to the frame for stability. The two

Table B.2. Similitude Conditions for the Pilot Model.

| | Variable and Scale Factor | | Comment |
|---|---|---|---|
| set conditions | $g_r = 1$ | | model and prototype operating in the same gravitational field |
| | $\lambda_r = n$ | | linear scale ratio-geometric similitude |
| | $E_r = 1$ | | materials of same stiffness in model and prototype |
| resulting conditions | $W_r = n^2$ | $\left(\frac{W}{E\lambda^2}\right) = \left(\frac{W}{E\lambda^2}\right)_m$ | results in relatively heavy model |
| | $\rho_r = 1/n$ | $\left(\frac{\rho g \lambda}{E}\right) = \left(\frac{\rho g \lambda}{E}\right)_m$ | difficult to achieve |
| | $f_r = 1$ | $(f) = (f)_m$ | |
| | $v_r = \sqrt{n}$ | $\left(\frac{v^2}{g\lambda}\right) = \left(\frac{v^2}{g\lambda}\right)_m$ | |
| | $p_r = 1$ | $\left(\frac{p}{E}\right) = \left(\frac{p}{E}\right)_m$ | same pressure and stress in model and prototype difficult to achieve |

lead wheels were controlled by an electric brake mechanism which operated either full on or off.

To correctly model a load of 40 kip on the bogie (480 kip aircraft) the weight should be about 900 lb ($40{,}000/6.6^2 = 920$ lb). However, the weight used was about 500 lb.

The 1 x 4 lumber correctly represented one row of 12 ft by 2 ft AM2 mat as to length and width, but was about 3 times too thick and 3.5 times too light to model the thickness and weight of the AM2 mat. The coefficient of friction on the top and bottom of the wooden panels were varied using

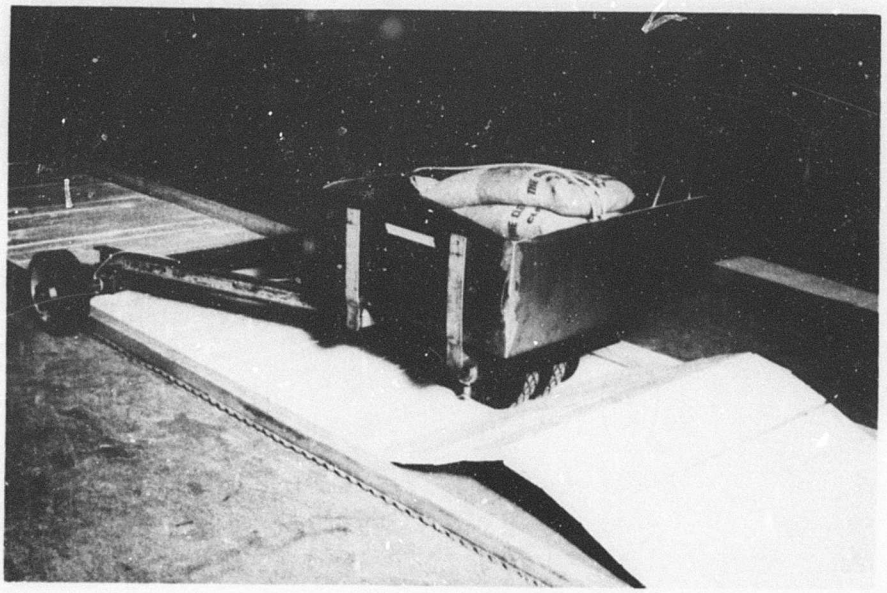

Figure B.1. Pilot Model AM2 Mat.

different adhesives. The joint spacing was varied by loosening the nylon cord and inserting spacers between panels. The compressibility of the support was varied by using rubber carpet pad as well as a concrete floor.

## B.3 Results of Pilot Model Tests

(1) The failure phenomenon of the C-5A braking on AM2 landing mat (bow waves) was duplicated in the small scale model.

(2) With the model mats resting on a concrete sub-base and the coefficient of friction between the wheels and the top of the mat greater than the coefficient of friction between the mat and the sub-base the bow wave and buckling failure occurred at various locations down the runway.

(3) When the landing mat model was placed on a compressible base (rubber carpet pad), the bow wave normally formed in front of and close to the landing gear. The crest of the bow wave was usually within five to eight panel widths from the landing gear (see Figure B.1). Buckling tended to occur at places of instability such as at a high spot under a panel or at a warped panel.

(4) Failure did not appear to be overrunning or intersecting of the bow wave by the landing gear as much as it was the disconnecting of panels and subsequent collapse of the bow wave ahead of the wheels. The forming of breakers in ocean waves is an approximate analogy.

(5) When the coefficient of friction between the bottom of the landing mat and the floor was increased to a value greater than the coefficient of friction between the top and the wheels, the buckling or bow wave did not develop.

(6) Velocity of the vehicle made no significant difference at low speeds (up to 10 mph).

## APPENDIX C

## DESIGN THEORY FOR RESTRAINING BANDS

If N bands are assumed to act together to support the horizontal braking force of the airplane, after receiving it from the landing mats through band-to-mat connections, it may be observed that

$$NR = \frac{W}{g} a \qquad (C.1)$$

in which R is the force transmitted to each band, and W/g is the mass of the aircraft which is decelerating at rate a.

If b equals the width of influence of the landing gear then the band spacing s is:

$$s = \frac{b}{N} \qquad (C.2)$$

Combining equations (C.1) and (C.2)

$$R = \frac{Wa}{g} \left(\frac{s}{b}\right) \qquad (C.3)$$

or

$$s = \frac{b}{\frac{Wa}{gR}} \qquad (C.4)$$

The force R transmitted to the band will decrease the band tension ahead of and increase the band tension behind the aircraft. The magnitude of the force change can be estimated by considering a simplified section of mat as in Figure C.1. A length of band L is assumed held between two springs of equal stiffness K (which may be other sections of band). The band stiffness is AE/L where A is the cross-sectional area of the band

and E is the modulus of elasticity of the material. The force R may be applied at any general distance aL from the left end. Part of the braking force, R, of the aircraft would be transmitted directly into the ground. This effect (conservatively) is neglected, as is the resistance to movement because of inertia of the mats.

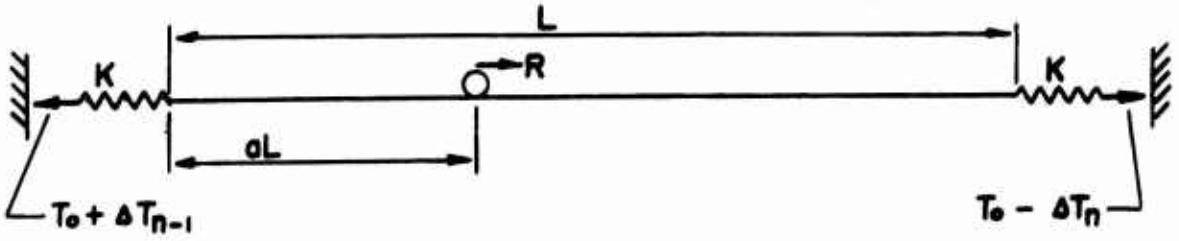


Figure C.1. Free Body of Band Segment Acted Upon by Force R.

Assuming that the ends of the system are fixed and that the system remains in tension, the length changes caused by R are equal to zero, thus

$$\frac{\Delta T_n}{K} + \frac{(1-a)\ L\Delta T_n}{AE} + \frac{aL(\Delta T_{n-1})}{AE} + \frac{\Delta T_{n-1}}{K} \qquad (C.5)$$

The letter n here represents the number of mat segments attached to the band in length L. Using $\Delta T_n + R - \Delta T_{n-1} = 0$ (which neglects friction between the mats and subgrade) and simplifying,

$$\Delta T_n = \frac{-R\left[a\frac{KL}{AE} + 1\right]}{\frac{KL}{AE} + 2} \qquad (C.6)$$

and

$$\Delta T_{n-1} = \frac{R\left[(1-a)\frac{KL}{AE} + 1\right]}{\frac{KL}{AE} + 2} \qquad (C.7)$$

For a = 1/2 the change in tension is always R/2 regardless of the value of KL/AE. For a = 0 or a = L and values of KL/AE less than one, T is still approximately R/2. Thus, as an approximation, the change in tension, $\Delta T$, can be assumed equal to R/2.

In a long airfield, however, the tension in the band could be greatly influenced by residual friction of the mat on the subgrade. A free body of an initially tensioned band with attached mats is shown in Figure C.2(a). The mats are assumed to have open joints and no initial frictional reaction on the subgrade. After several passages of aircraft to the right, friction forces will be as in Figure C.2(b).


(a)


(b)

Figure C.2. Free Bodies of a Single Band-Mat System.

The tension in the mat will be altered by the number of mats displaced and held by friction forces due to the weight of the mats.

A single band-to-mat connection may be isolated and analyzed during passage of an airplane. Figure C.3 shows this connection.

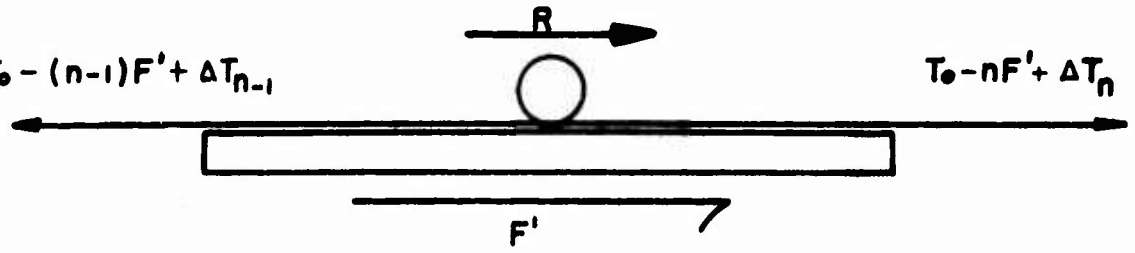


Figure C.3. Free Body of the $n^{th}$ Connection During Aircraft Passage.

Minimum band tension occurs where n, the number of mat connections acted upon by friction forces, is a maximum, and

$$T_{min} = T_o - nF' + \Delta T_n \geq 0$$

Since the band must remain in tension and $\Delta T_n \approx - R/2$ the minimum initial tension is:

$$T_{o\ min} \geq nF' + \frac{R}{2} \qquad (C.8)$$

Maximum band tension is limited by the yield strength $Af_y$ or other limiting strength, and where n approaches zero is expressed as

$$T_{max} = T_o - (n-1)F' + \Delta T_{n-1} = T_o + \frac{R}{2} \leq Af_y$$

Thus the maximum initial tension is

$$T_{o\ max} \leq Af_y - \frac{R}{2} \qquad (C.9)$$

The maximum and minimum initial tensions can be equated, to yield the following equations for the maximum number of mat connections acted upon by friction.

$$n = Af_y - R \qquad (C.10)$$

The cross-sectional area of a band and its yield stress will be known and the force R can be conservatively obtained. The maximum mat friction force nF' may be determined and used to complete the design of the band.

Suppose, for example, that a band 6 in. wide by 3/8 in. thick having $f_y$ = 50 ksi is used, that the deceleration rate of a 480-kip airplane is g/2 maximum and that four bands spaced 12 ft apart respond equally in preventing mat movement. Then R = 480(½)(¼) = 60 kips. Thus

$$nF' = (6)(3/8)(50) - 60 = 112.5 - 60 = 52.5 \text{ kip}$$

$$T_o = 82.5 \text{ kip}$$

Assume that at each connection point, four mats act against the connection of band to mat so that, for mats weighing 160 lb apiece and coefficient of friction of 0.5, F' = 320 lb. Then

$$n = \frac{52500}{320} = 164$$

This is the number of connections permitted. If there is a connection to every 10th mat, considering mats to be two feet wide, the band length may be 164(20) = 3280 ft long between shock-absorbing springs.

The above analysis is simplified but illustrates the band behavior. The results are conservative, since direct friction from plane to mat to subgrade and the inertia of the mats are neglected. The band system may be designed to serve equally well under the mat, although the model test was conducted with the band system on top.

## REFERENCES


1. Barker, Walter R. Memorandum For Record; AM2 Landing Mat Performance under C-5A Traffic at Dyess AFB, Texas, Waterways Experiment Station, Vicksburg, Mississippi, 3 November 1970.

2. Burns, C.D. and Grau, R. W. Reconstruction of Landing-Mat Test Facility and Its Performance During C-141A Flight Test Program, Dyess Air Force Base, Texas, Miscellaneous Paper S-69-50, U.S. Army Engineer, Waterways Experiment Station, Vicksburg, Mississippi, December, 1969.

3. Currin, David D. C-5A Ground-Flotation Test on a Landing Mat Runway, Technical Report No. AFWL-TR-71-45, Air Force Weapons Laboratory, Kirtland AFB, Kirtland, Nex Mexico, July 1971.

4. Green, H.L. Observation of C-5A Operations on Landing Mat Test Facility, Dyess Air Force Base, Texas, Miscellaneous Paper S-72-10, U.S. Army Engineer Waterways Experiment Station, Vicksburg, Mississippi, March 1972.

5. Naval Air Engineering Laboratory Task Progress Reports of AM2, Report NAEL 3960.4, 17 January 1968.


## BIBLIOGRAPHY


Airplane Landing Mat Investigation Engineering Tests on Steel, Pierced Type, M8, and Aluminum, Pierced Type, M9, Technical Memorandum No. 3-324, U.S. Army Engineer Waterways Experiment Station, CE, Vicksburg, Miss., May 1951.

Aircraft Ground-Flotation Investigation, Technical Documentary Report AFFDL-TDR-66-43, Parts I, II, III, IV, V, VII, X, XI, and XIII, U.S. Air Force Flight Dynamics Laboratory, Wright-Patterson AFB, Ohio, 1966.

Brabston, W.N., Evaluation of Three-Piece AM2 Aluminum Landing Mat, Miscellaneous Paper No. 4-886, U.S. Army Engineer Waterways Experiment Station, CE, Vicksburg, Miss., April 1967.

Burns, C.D., Fenwick, W.B., Development of CBR Design Curves for Runways to be Surfaced with M8A1 (Formerly T10) Steel Landing Mat, Miscellaneous Paper No. 4-817, U.S. Army Engineer Waterways Experiment Station, CE, Vicksburg, Miss., May 1966.

Criteria for Designing Runways to be Surfaced with Landing Mat and Membrane Type Materials, Technical Report No. 3-539, U.S. Army Engineer Waterways Experiment Station, CE, Vicksburg, Miss., April 1960.

Development of Tentative CBR Design Curves for Landing Mats, Miscellaneous Paper No. 4-29, U.S. Army Engineer Waterways Experiment Station, CE, Vicksburg, Miss., December 1952.

Dorr, J., Der Unendliche, Federnd Gebettete Balken Unter Dem Einfluss Einer Gleichformig Bewegten Last, Ing. Arch., Vol. 14, 1943, pp. 167-192.

Engineering Tests of Experimental T11 Aluminum Airplane Landing Mat, Technical Report No. 3-634, U.S. Army Engineer Waterways Experiment Station, CE, Vicksburg, Miss., September 1963.

Harr, M. E., Rosner, J.C., Theoretical Study of Landing Mat Behavior, Contract Report S-69-7, July 1969; prepared by Purdue Research Foundation under Contract No. DACA 39-67-C-0044, for the U.S. Army Engineer Waterways Experiment Station, CE, Vicksburg, Miss.

Hetenyi, M., and Izadi-Vahedi, M., Traveling Loads on Plates on Elastic Foundation, Research Report Air Force Special Weapons Center (SWMKR-2), Kirtland AFB, New Mexico.

Holl, D.L., Dynamic Loads on Thin Plates on Elastic Foundations, Proc. of Symposia in Appl. Mech., Vol. 3, 1950.

Kenney, J.T., Jr., Steady State Vibration of Beam on Elastic Foundation for Moving Load, J. Appl. Mech., Vol. 21, 1954, pp. 359-364, Trans. ASME, Vol. 76.

Ladd, D.M., Development of Landing Mat Ground Flotation Evaluation Criteria, AFWL-TR-70-79, U.S. Army Engineer Waterways Experiment Station, CE, Vicksburg, Miss., September 1970.

Lenzner, L.R., Evaluation of Dow Chemical Extruded Aluminum Landing Mat (Modified (MX18-B), Miscellaneous Paper No. S-69-4, U.S. Army Engineer Waterways Experiment Station, CE, Vicksburg, Miss., February 1969.

Ludwig, K., Die Verformung Eines Beiderseits Unbergrenzten Elastisch Gebetteten Geleises Durch Lasten Mit Konstanter Horizontal Geschwindigkeit, Proc. 5th Int. Cong. Appl. Mech., Cambridge, Mass., 1938, pp. 650-655.

Mathews, P.M., Vibration of a Beam on Elastic Foundation, Z. Agnew. Math. Mech., Vol. 38, 1958, pp. 105-115.

Mathews, P.M., Vibration of a Beam on Elastic Foundation, Z. Agnew. Math. Mech., Vol. 39, 1958, pp. 13-19.

Meirovitch, L., Analytical Methods in Vibrations, The MacMillian Co., New York, 1967.

Pickett, Gerald, Deflections, Moments and Reactive Pressures for Concrete Pavements, Kansas State College Bulletin No. 65, October 1951.

Ralston/Wilf, Mathematical Methods for Digital Computers, Wiley, New York/London, 1960, pp. 110-120.

Rosner, J.C., Theoretical Study of Landing Mat Behavior, Ph.D. Thesis, Purdue University, Lafayette, Ind., August 1969.

Theoretical Landing Mat Studies, U.S. Army Engineer Waterways Experiment Station, Technical Memorandum No. 3-418, Vicksburg, Miss., October 1955.

Timoshenko, S., Method of Analysis of Statical and Dynamical Stress in Rail, Proc. 2nd Int. Cong. Appl. Mech., Zurich, 1926, pp. 407-418.

Tse, F.S., Morse, I.E., Hinkle, R.T., Mechanical Vibration, Allyn and Bacon, Inc., Boston, 1963.

Turner, R., Carr, G.L., Evaluation of Kaiser Aluminum Honeycomb Landing Mat, Miscellaneous Paper No. 4-897, U.S. Army Engineer Waterways Experiment Station, CE, Vicksburg, Miss., August 1967.

Wang, M.C., Mitchell, J.K., Monismith, C.L., Stress and Deflection in Cement-Stabilized Pavements, July 1970. Prepared by University of California, Berkeley, under Contract No. DA-22-079-eng-414, for the U.S. Army Engineer Waterways Experiment Station, CE, Vicksburg, Miss.

White, T.D., Theoretical Landing Mat Analysis, Sponsored by U.S. Air Force, Conducted by U.S. Army Engineers Waterways Experiment Station, CE, Vicksburg, Miss., August 1970.

Winkler, E., Die Lehre von der Elasticitaet und Festigkeit, Prag. Dominicus, 1867.